

FUNCTIONAL BACTERIAL AMYLOID NANOMATERIALS

A THESIS SUBMITTED TO
THE GRADUATE SCHOOL OF ENGINEERING AND SCIENCE
OF BILKENT UNIVERSITY
IN PARTIAL FULFILLMENT OF THE REQUIREMENTS FOR
THE DEGREE OF
MASTER OF SCIENCE
IN
MATERIALS SCIENCE AND NANOTECHNOLOGY

By

Tuğçe ÖNÜR

September 2016

FUNCTIONAL BACTERIAL AMYLOID NANOMATERIALS

By Tuğçe Önür

September 2016

We certify that we have read this thesis and that in our opinion it is fully adequate, in scope and in quality, as a thesis of the degree of Master of Science.

Urartu Özgür Şafak Şeker (Advisor)

Devrim Pesen Okvur

Serkan İsmail Göktuna

Approved for the Graduate School of Engineering and Science:

Ezhan Karaşan

Director of the Graduate School

ABSTRACT

FUNCTIONAL BACTERIAL AMYLOID NANOMATERIALS

Tuğçe ÖNÜR

M.S. in Materials Science and Nanotechnology

Supervisor: Urartu Özgür Şafak Şeker

September 2016

Mis-folded or unfolded proteins tend to aggregate and aggregated structures are called as amyloids. Amyloid formation contributes to some human diseases and resulting in death in some cases. On the other hand, functional amyloids are found in nature and they are highly ordered assembled structures and they function in cellular events. Some bacteria, fungi or yeast species synthesize these kind of functional amyloids. For example, curli proteins of *Escherichia coli* play a role in initial attachments for biofilm formation and contribute to stiffness of the biofilm matrix. CsgA is the major subunit while CsgB is the minor subunits which nucleates CsgA polymerization. They are capable of attachment to the abiotic or biotic surfaces. Both of them share some characteristics with non-functional amyloids. For instance, their structures are dominated by β sheets so they have a rigid amyloid core domain that enables to resist stress factors such as proteases and detergent treatment or pH. Their stable structures and adhesive properties make them useful in materials science. Moreover, high yield could be obtained easily by using molecular biology techniques such as cloning and protein purification so they are highly cost-effective materials.

In this study, CsgA and CsgB fibers were proposed as new type of functional biomaterials to do so fiber formations of CsgA and CsgB were analyzed in detail. *csgA* and *csgB* genes were cloned into expression vectors. Their β sheet rich structures were validated with CD analysis and binding capability to Thioflavin T dye were assayed which is the general property of amyloids. Self-seeding and cross-seeding strategies were applied to analyze fiber formation and quartz crystal microbalance with dissipation (QCM-D) was used. Gold coated sensors were deposited with freshly purified proteins and polymerized. Then, sensor surfaces were monitored with SEM and AFM. With self-seeding strategies long and branched fibers were obtained from CsgA proteins while sphere like structures were formed by CsgB proteins. Also, it was concluded from the cross-seeding experiments, the order of protein addition determines the final assembled structures. Furthermore, fluorescent properties of CsgA and CsgB were analyzed in detail for the first time. Finally, binding affinity of the purified proteins to different materials (gold, silica and hydroxyapatite) were determined by using QCM-D.

Keywords: biofilm proteins, biomaterials, functional amyloids, self-assembled biomaterials.

ÖZET

FONKSİYONEL BAKTERİYEL AMİLOİD NANOMALZEMELER

Tuğçe ÖNÜR

Malzeme Bilimi ve Nanoteknoloji Programı, Yüksek Lisans

Tez Yöneticisi: Urartu Özgür Şafak Şeker

September 2016

Katlanmamış ya da doğru katlanmamış proteinler hücre içinde kümelenme eğilimindedirler ve bu kümelenmiş yapılar amiloid olarak adlandırılır. Amiloidler insanlarda bazı hastalıklara neden olurlar ve ölüme yol açabilirler. Fakat, doğada fonksiyonel amiloidler bazı bakteri, mantar ve maya türleri tarafından üretilmektedirler. Fonksiyonel amiloidler oldukça düzenli kümelenmiş yapılardır ve hücrel aktivitelere rol alırlar. Örneğin, *Escherichia coli* tarafından üretilen curli amiloid proteinleri yüzeylere tutunmayı sağlayarak biyofilm oluşmasına katkı sağlarlar. Ayrıca biyofilm matriksinin dayanıklılığına da katkıda bulunurlar. CsgA asıl curli altbirimidir. CsgB ise ikincil altbirimdir ve CsgA proteinlerinin polimer oluşturmasını sağlar. İki protein de canlı veya cansız yüzeye bağlanabilir. Hastalık yapan amiloidlerle bazı ortak özellikleri vardır. Örnek vermek gerekirse, yapılarındaki fazla miktardaki β yaprakları sayesinde sert amiloid çekirdeği oluşur ve proteaz, deterjan ve pH gibi stres faktörlerine karşı stabil kalmalarını sağlar. Stabil kalabilme yetileri ve yapışkan özellikleri bu proteinleri malzeme bilimi için önemli kılmaktadır. Bunlara ek olarak, klonlama ve protein saflaştırma gibi moleküler biyoloji teknikleri ile büyük miktarda uygun maliyetle üretilebilirler.

Bu çalışmada, CsgA ve CsgB yeni nesil fonksiyonel biyomalzeme olarak önerilmiş ve bu proteinlerin fiber oluşumları detaylıca analiz edilmiştir. *csgA* ve *csgB* genleri ekspresyon vektörüne klonlanmıştır. Amiloidlerin genel özelliği olan, yapılarındaki yoğun β yaprak elementleri dairesel dikroizm spektroskopisi (CD) analizi ile gösterilmiştir ve Thioflavin T adlı florasan boyaya bağlanabildikleri analiz edilmiştir. Kendi çekirdeklenme ve çapraz çekirdeklenme yöntemleri izlenerek fiber oluşumu kuvarz kristal mikroterazi (QCM-D) ile analiz edilmiştir. Altın kaplı sensör yüzeyi yeni saflaştırılan proteinlerle kaplanmış ve polimerleşmeleri için bekletilmiştir. Sensor yüzeyi TEM ve AKM ile görüntülenmiştir. Öz çekirdeklenme yöntemi ile CsgA proteinleri kullanılarak uzun ve dallanmış polimer yapılar elde edilmiştir. CsgB proteinlerinden ise büyük küre benzeri yapılar edilmiştir. Elde edilen sonuçlara göre, proteinlerin ortama eklenme sırası oluşan yapıların şeklini belirlemektedir. Bunlara ek olarak bu çalışmada, CsgA ve CsgB proteinlerinin florasan özelliği ilk defa detaylı olarak analiz edilmiştir. Son olarak, saflaştırılan proteinlerin farklı materyallere (altın, silika ve hidroksiapatit) olan bağlanma afinitesi hesaplanmıştır.

Anahtar kelimeler: biyofilm proteinleri, biyomalzemeler, fonksiyonel amiloidler, kendiliğinden örgütlenebilen biyomalzemeler.

ACKNOWLEDGEMENTS

First and foremost, I would like to express my deepest gratitude to my thesis advisor Asst. Prof. Urartu Özgür Şafak Şeker. Studying with him was a big honor for me. I learned a lot from him about research, experiments, lab equipment and life. He was always generous to share his knowledge and experiences in all fields. I believe he made a major contribution to improve myself during the last two years. He has always encouraged and motivated me. He insisted on showing the light at the end of the road when I felt down. I would like to thank for his guidance, knowledge, patience, encouragement and support.

I would like to thank my lab mates for their friendship; also, the peaceful and fruitful work environment. I want to thank Dr. Esra Yuca for her effort to organize this pleasant lab environment and I appreciate her contributions to this study. Also, special thanks to Tolga Tarkan Ölmez and Ebuzer Kalyoncu for their generous help in imaging techniques. I think they made big contribution to me while learning those imaging techniques and they were always kind to me when I asked for help.

Furthermore, I would like to thank my dear friends from my undergraduate study. I had chance to know better Çağla Eren in Ankara. We spent much time together and she has always supported and motivated me. She has found something to say me even though I was too pessimistic. Also, thanks to Behide Saltepe and Recep Erdem Ahan for their long term friendship. I believe our friendship will last and we will explore new cities and novel food. In addition, I would like to thank Onur Apaydın for his friendship.

Moreover, I am grateful to undergraduate researchers for their help and friendship. I believe they made valuable contribution to my study. I would like to

thank Ilgın Buse Korkusuz, she was always ready to prepare deadly buffers. I want to thank Funda Büyükbaş and I will never forget our growth time sadnesses. Also, I want to thank Hazal Beril Çatalak for their help in various fields. In addition, thanks to Nedim Hacıosmanoğlu he also helped me during the summer internship.

Next special thanks go to the yoga team, Ebru Şahin Kehribar, Elif Ergül and Zelal Yavuz. I will never forget our yoga classes and lunch activities. I also hope our friendship and yoga practices will last in the future.

I want to thank my office mates, Aslı Çelebioğlu, Yelda Ertaş, Begüm Dikeçoğlu, Gülistan Tansık, Zeynep Aytaç and Zehra İrem Gürbüz. They made the warm and friendly study environment.

Moreover, I would like to thank my lifelong friends Büşra-Cansın Arıkoç. It was one of my biggest chance in Ankara that I met my high school friend Büşra. When I need any help, Büşra and Cansın were just a call way. I appreciate them for the big brain storms, supports and encouragements.

Finally, I present my special gratitude to my parents Aysel-Nihal Önür. More than anything, I want to thank to my parents for their unconditional love. I would like to present my special thanks to my sister Ayça Önür. She is the most special person in my life. I believe she can do anything for me no matter how far away from me. I want to thank the new member of our family Burak Gürlek. I think he is one of the main contributor of my academic career and thanks for his advices, encouragements and supports.

I would like to thank TÜBİTAK (Project number 114M163) for the financial support.

Bilkent Ankara, 2016

CONTENTS

CHAPTER 1	1
INTRODUCTION	1
1.1 Proteins as Building Blocks of Cells.....	1
1.2 Self-Assembly of Proteins	2
1.2.1 Special Class of Self-Assembled Proteins: Amyloids	4
1.3 Biofilm Proteins	6
1.4 Functional Amyloids.....	8
1.5 Functional Amyloids of <i>Escherichia coli</i> : curli	11
1.6 Major and Minor Curli Subunits	16
1.7 Why Amyloids are Important for Materials Science?.....	18
1.7.1 Usage of Curli Proteins	19
CHAPTER 2	21
EXPERIMENTAL	21
2.1 Preparation of Growth Medium and Buffers	21
2.2 Cloning of <i>csgA</i> & <i>csgB</i> Gene Fragments.....	23
2.2.1 Plasmid Purification	23
2.2.2 Chromosomal DNA Isolation	23
2.2.3 Polymerase Chain Reaction (PCR)	23
2.2.4 Agarose Gel Electrophoresis.....	25
2.2.5 Gel Extraction	26

2.2.6 Endonuclease Digestion Reactions	26
2.2.7 Ligation of Double Digested DNA Fragments	26
2.3 Transformation.....	27
2.3.1 <i>Escherichia coli</i> DH5 α and BL21 Competent Cell Preparation.....	27
2.3.2 Transformation of Recombinant Plasmids to <i>E. coli</i> Competent Cells	27
2.4 Protein Expression, Purification and Characterization	28
2.4.1 Overexpression of CsgA & CsgB Proteins	28
2.4.2 Purification of CsgA & CsgB Proteins	28
2.4.3 Determination of Protein Concentration	29
2.4.4 SDS-PAGE and Western Blot analysis.....	29
2.5 Thioflavin T (ThT) Assay	30
2.6 Secondary Structure Analysis	30
2.7 Quartz Crystal Microbalance with Dissipation (QCM-D).....	31
2.7.1 Sensor Cleaning	31
2.7.2 Fiber Formation Assay.....	31
2.8 Immunochemistry Assay.....	32
2.9 Fluorescence Analysis of CsgA & CsgB Proteins	33
2.10 Kinetic Analysis of CsgA & CsgB Proteins	33
2.11 Imaging of CsgA & CsgB Proteins.....	34
2.11.1 Scanning Electron Microscopy Imaging.....	34
2.11.2 Atomic Force Microscopy Imaging	34
2.11.3 Fluorescence Microscopy Imaging	34
CHAPTER 3	35

RESULTS AND DISCUSSION	35
3.1 Cloning of <i>csgA</i> and <i>csgB</i> Gene Fragments	35
3.2 Purification of Recombinant Proteins	42
3.3 Amyloid Formation Assay	45
3.3 Secondary Structural Analyzes	46
3.4 Immunochemistry Assay.....	49
3.5 Fiber Formation Assay	50
3.5.1 Self-seeding and Cross-seeding of CsgA.....	52
3.5.2 Self-seeding and Cross-seeding of CsgB	60
3.6 Imaging of Curli Materials.....	68
3.6.1 Scanning Electron Microscopy Imaging.....	68
3.6.2 Atomic Force Microscopy Imaging	76
3.7 Fluorescent Analysis of CsgA & CsgB.....	78
3.8 Kinetic Analysis of CsgA & CsgB.....	83
CHAPTER 4	89
CONCLUSION AND FUTURE PERSPECTIVES	89
BIBLIOGRAPHY	91

LIST OF FIGURES

Figure 1- Transcription of curli proteins are regulated via <i>csgBAC</i> and <i>csgDEFG</i> operons. CsgA is the major curli subunit while CsgB is the minor subunit. CsgC shows chaperon activity and CsgD is the regulator protein. Other curli proteins have roles in the secretion machinery.....	12
Figure 2- Curli secretion machinery. CsgA and CsgB proteins have <i>sec</i> signal sequences and are secreted to the ECM after synthesis. CsgB interacts with outer membrane and acts as template for CsgA oligomerization. CsgG forms channel on the outer membrane while CsgE and CsgF are responsible for transportation.....	17
Figure 3- Quartz crystal microbalance with dissipation device and QCM-D sensor.	32
Figure 4- Schematic representation of amplified <i>csgA</i> gene fragment.	36
Figure 5- Bands inside the square belonged to <i>csgA</i> gene fragments expected as ~500 bp. Negative control was on the first lane.....	36
Figure 6- Agarose gel image of the second PCR to obtain designed <i>csgA</i> gene fragments which were expected as ~600bp. Negative control was on the last lane. .	37
Figure 7- Linearized pet22b vectors expected as ~5000 bp were shown in the square.	37
Figure 8- Schematic representation of pET22b plasmid which contained <i>csgA</i> gene fragment.	38
Figure 9- Sequence alignment of cloned <i>csgA</i> gene fragment. Sequences from Genewiz were highlighted with yellow and original sequence on the bottom line. Aligned bases were marked with stars.....	39
Figure 10- Digested plasmids that contained <i>csgA</i> gene. Samples digested with NcoI were on the second lane and digested with XhoI were on the third lane. On the last	

lane, samples were digested with NcoI and XhoI endonucleases. Backbone ~5000 bp shown in the upper square and *csgA* gene ~500 bp shown in the bottom square. 40

Figure 11- Schematic representation of amplified *csgB* gene fragment. 40

Figure 12- Amplified *csgB* gene fragments ~500bp shown in the square. Negative control was on the last lane 41

Figure 13- Plasmid construct which is designed to express CsgB proteins..... 41

Figure 14- Sequence analysis of *csgB* gene. Sequences from Genewiz were highlighted with yellow and original sequence was on the bottom line. Aligned bases were marked with stars..... 42

Figure 15- CsgA monomers, dimers and trimmers shown in SDS polyacrylamide gel. 44

Figure 16- CsgB oligomers were indicating in red square..... 44

Figure 17- PVDF membrane of CsgA (on the left) and CsgB (on the right). They have different assembly characteristics and this might affect antibody binding so CsgB bands are brighter than CsgA. 45

Figure 18- ThT assays of CsgA, CsgB and equimolar mix sample. Binding capabilities of the purified proteins to Thioflavin T dye were proved by measuring fluorescent signals. Measurements were performed during 16 hours CsgA in A), CsgB in B) and mix of CsgA and CsgB in C). The highest RFU values were recorded with CsgB fibers..... 46

Figure 19- Secondary structural analysis of purified proteins and mix sample. CD spectra of the samples are demonstrated on the left and ratio of secondary structural elements are on the right. Data of aged CsgA is demonstrated in A), CsgB in B) and mix sample in C). Samples had low helix content in each case. Behavior of CsgA

similar to mix sample. β sheet ratio of CsgB fibers were increasing with incubation time and 30 days aged CsgB sample had the highest sheet ratio. 48

Figure 20- Antibody binding assays of purified CsgA and CsgB proteins. Sensor surface was coated with CsgA (on the left) and CsgB (on the right), proteins were probed with fluorescent labelled secondary antibodies and frequency changes were recorded. Protein and primary antibody addition points are shown with arrows. Shifts which were caused from primary and secondary antibodies were too small compared to protein polymer shifts. Hence, their shifts were not seen clearly in this figure. Sensor surfaces were examined with laser scanning confocal microscopy. Image of probed CsgA is demonstrated on the left and CsgB is on the right. 50

Figure 21- Self-seeding and cross-seeding strategies are schematized. In this study, interactions of polymerized CsgA with fresh CsgA and fresh CsgB; also, polymerized CsgB with fresh CsgA and CsgB were analyzed. 51

Figure 22- Overnight frequency and dissipation changes of freshly purified CsgA proteins. Gold coated sensor surface was deposited with CsgA proteins overnight frequency changes were demonstrated in A) and dissipation changes in B). Initial attachments which shown in close up views caused sharp rise and decrease in frequency and dissipation signals, respectively. 53

Figure 23- Freshly purified CsgA monomers were added upon polymerized CsgA fibers. Addition of fresh proteins with increasing concentrations resulted in step by step changes in frequency signals A) and dissipation signals B). Highest protein concentration caused the highest shift in this case. 55

Figure 24- Overnight measurements of frequency shifts in A) and dissipation changes in B) of self-seeding CsgA proteins. Changings which caused from seeding

shows in close-up views. During near 25 hours measurements, dissipation signals did not change notably while frequency shift was increasing..... 56

Figure 25- Fresh CsgB proteins flowed through the system to analyze interactions of fresh CsgB and CsgA fibers. Peaks belonged to addition point but no significant changes were recorded after the washing steps. Frequency shifts are shown in A) and dissipation changes in B). 58

Figure 26- Cross-seeding of CsgA fibers with fresh CsgB proteins. Frequency changes are shown in A) while dissipation changes are shown in B). CsgB addition did not cause dramatic changes. Peaks caused from the monomer addition but unbound CsgB proteins were removed with the washing steps. 59

Figure 27- Frequency and dissipation changes of freshly purified CsgB proteins. Purified proteins were deposited on gold coated sensor surface and incubated for overnight for polymerization. Recorded frequency changes in A) and dissipation changes in B). Sharp changes in both signals were caused from the initial attachments. Slight changes were recorded during overnight measurements in both signals..... 61

Figure 28- Grown CsgB fibers seeded with fresh CsgB. Fresh CsgB proteins were flowed through the system with increasing concentrations but small shifts were recorded in frequency shifts in A) and dissipation shifts in B). 63

Figure 29- Overnight measurements of self-seeding of CsgB proteins. Fresh proteins additions shown in close-up view and slightly changes on both signals were recorded during near 20 hours measurement. Frequency shifts are shown in A) and dissipation changes are shown in B). 64

Figure 30- Polymerized CsgB seeded with fresh CsgA as a cross-seeding strategy. Addition of proteins with increasing concentrations cause regular changes on frequency signals in A) dissipation signals in B)..... 66

Figure 31- 20 hours measurements of cross-seeding CsgB fibers with fresh CsgA. Shifts showed the interactions between fibers and fresh proteins. Frequency shifts are shown in A) while dissipation changings are shown in B)..... 67

Figure 32- SEM image of long and branched CsgA fibers. Freshly purified CsgA proteins added upon polymerized CsgA and incubated for overnight for QCM analysis. SEM image of near 3 days aged fibers on gold coated sensor surface in A) and close up view in B)..... 69

Figure 33- CsgB monomers flowed through the system to analyze their interaction with CsgA polymers. Sensor surface was observed with SEM. Long and branch fibers are seen in A) which is similar with self-seeding of CsgA fibers and seeding at the end point is shown in B)..... 71

Figure 34- SEM images of CsgB fibers. Big sphere structures were obtained by self-seeding of CsgB proteins and shown in A); connection sites are shown in close up view in B)..... 73

Figure 35- SEM images of CsgB fibers which seeded with freshly purified CsgA. Sphere structures were observed again but in this case size of them smaller than spheres that formed by self-seeding of CsgB demonstrated in A). Small fibers elongates from the sphere surface which is shown in B)..... 75

Figure 36- After protein deposition and overnight measurements sensors were examined with AFM. Fibers formed by CsgA polymers and fresh CsgA shown in A),

CsgB polymers and fresh CsgB in B) and cross-seeding of CsgA with fresh CsgB in C).....	77
Figure 37- Fluorescent analysis of 9 days aged samples. Bright field images and blue, green, red fibers that were imaged by using different filters of fluorescent microscope are shown. Color intensity was decreasing blue to red but brightness of the images were adjusted to show clearly. Images of CsgA fibers and emission spectra that was recorded by exciting at 338, 375 and 550 nm are demonstrated in A), CsgB fibers images and emission spectra that was recorded by exciting at 339, 413 and 550 nm are shown in B), fluorescent images and emission spectra of mix sample are demonstrated in C). Mix sample was excited at 340, 414 and 550 nm to measure emission spectra. Lines represent 100 μ M.....	79
Figure 38- 18 hours aged samples were examined under fluorescent microscope. Bright field images were given as the first image and images of CsgA in A), CsgB in B) and mix sample images are placed in C). Lines represent 100 μ M.	80
Figure 39- Bright field and fluorescent images of 23 days aged samples. CsgA fibers are demonstrated in A), CsgB fibers in B) and mix samples in C). Lines represent 100 μ M.....	80
Figure 40- After precipitation, CsgA fibers were dissolved in chloroform. Excited at different wavelengths (330, 338, 375 and 418 nm) in order to measure emission spectra. Emission spectra is shown in A) and dense fiber network was observed with SEM in B).	82
Figure 41- Frequency change vs. concentration graph of polymerized CsgA, CsgB and mix sample on the gold QCM sensors. Proteins were diluted and added to the system with increasing concentrations. Dots represent the protein addition points and	

higher concentration caused the higher changes in all cases. CsgA deposition on the gold sensor resulted in lower frequency change than other samples. CsgB addition caused the highest change. Interaction of CsgA and CsgB changed the binding property and binding sites of CsgB might be covered by CsgA. 84

Figure 42- Frequency change vs. concentration plot of polymerized CsgA, CsgB and mix sample on silica coated QCM sensor. In this case, highest change came from the deposition of mix sample and binding capability of CsgB fibers was higher than CsgA fibers. Proteins were flowed through the system with diluted concentrations and dots represent the addition points. 85

Figure 43- Frequency change vs. concentration graph of CsgA, CsgB and mix of CsgA-CsgB fibers on hydroxyapatite QCM sensors. Smaller changes were obtained by binding the polymers to hydroxyapatite sensors. Binding of CsgB fibers to HAP surface caused the highest changes while lowest shifts were obtained by the mix sample. 86

Figure 44- Binding equilibrium constants of polymerized proteins and polymerized mix samples on gold, silica and hydroxyapatite (HAP) coated sensors. CsgA and CsgB higher tendency of binding to the gold surfaces. Mix sample had higher affinity for binding to HAP surface than others. 87

Figure 45- Binding free energy of aged CsgA, CsgB and mix sample on gold, silica and hydroxyapatite (HAP) surfaces were calculated. All of them had closer binding free energy. It might be cause from same assembly route of the samples. 88

LIST OF TABLES

Table 1- Components of 12% resolving gel.....	22
Table 2- Components of 4% Stacking Gel.....	22
Table 3- PCR Components	23
Table 4- Reaction Conditions	24
Table 5- Primers that were used in this study	25
Table 6- Digestion reaction components.....	26
Table 7- Ligation reaction components.....	27
Table 8- Ligation reaction components.....	27

LIST OF ABBREVIATIONS

ECM	:	Extracellular Matrix
COP	:	Cytoplasmic Coat Proteins
CCMV	:	Cowpea Chlorotic Mottle Virus
ThT	:	Thioflavin T
PrP	:	Prion Protein
rPrP	:	Recombinant Mammalian Prion Protein
CJD	:	Creutzfeldt–Jakob Disease
BSE	:	Bovine Spongiform Encephalopathy
EPS	:	Extracellular Polymeric Substances
DNA	:	Deoxyribonucleic Acid
eDNA	:	Extracellular Deoxyribonucleic Acid
FAP	:	Functional Amyloid in <i>Pseudomonas</i>
BAP	:	Biofilm Associated Protein
PSMs	:	Phenol Soluble Modulins
MRSA	:	Methicillin-Resistant <i>Staphylococcus aureus</i>
MTP	:	<i>Mycobacterium tuberculosis</i> pili
CSG	:	Curli Specific Gene
TAFI	:	Thin Aggregative Fimbriae
MFPs	:	Mussel Foot Proteins
LB	:	Luria-Bertani
TAE	:	Tris EDTA Acetic Acid
TSS	:	Transformation & Storage Solution

DMSO	:	Dimethyl Sulfoxide
PEG	:	Polyethylene Glycol
GdnHCl	:	Guanidine hydrochloride
SDS-PAGE	:	Sodium Dodecyl Sulfate Polyacrylamid Gel Electrophoresis
PBS	:	Phosphate Buffer Saline
TBS	:	Tris Buffer Saline
TBS-T	:	Tris Buffer Saline-Tween 20
PCR	:	Polymerase Chain Reaction
TEV	:	Tobacco Etch Virus
IPTG	:	Isopropyl 3-D-Thiogalacto-Pyranoside
CSLM	:	Confocal Laser Scanning Microscopy
CD	:	Circular Dichroism
QCM-D	:	Quartz Crystal Microbalance with Dissipation
SEM	:	Scanning Electron Microscopy
AFM	:	Atomic Force Microscopy
HAP	:	Hydroxyapatite

CHAPTER 1

INTRODUCTION

1.1 Proteins as Building Blocks of Cells

Proteins are one of the major components of cells and they have crucial roles in cellular activities. Many chemical reactions are catalyzed and channels for transportation on the membrane are formed by proteins also they function as hormones, antibodies, fibers or luminescence.[1] 20 amino acids that have different chemical properties are coded in DNA of the organisms. These amino acids linked to each other via peptide bonds and long amino acid chains form that are called as oligopeptide or polypeptide. Proteins are polypeptide and each of them compose of unique amino acid sequences. Amino acids portions that do not contribute to peptide bonds are side chains. They could be negatively or positively charged and polar or nonpolar so they have crucial effects on the amino acid properties.[2, 3] Weak non-covalent interactions occur between these side chains and these interactions determine the stability of the protein. Hydrogen bonds, Van der Waals and electrostatic attractions are the weak interactions that affect the protein folding and also hydrophobicity is the other factor that contributes the protein conformation. Depends on energy minimization, nonpolar residues on the peptide chain tend to cluster in the interior of the molecule to reduce interactions with water. Also, hydrogen bonds are formed between side chain residues and water molecules. Hence, hydrophobicity is the major factor that determine confirmation of the proteins which has important effects on protein functionality. Proteins could be 50 and 2000 amino acids long and found in varied shapes. Large proteins are composed of domains that fold independently of each other. Hydrogen bonds between the N–H and C=O groups

in polypeptide backbones result in α helix and β sheet motifs. Regular and repeating conformation occur in both cases. β sheets are found parallel or anti-parallel orientation and each types of β sheets are highly rigid structure. Rigid cylinder is formed if peptide chain turns around on itself and it is called as α helix. Primary structures of the proteins are known as amino acid sequences and α helix/ β sheet are constituted secondary structure of the proteins. The final three dimensional confirmation is refereed as the tertiary structure. Moreover, some proteins are composed of more than one polypeptide chain and known as quaternary structure.[2-8]

1.2 Self-Assembly of Proteins

As previously mentioned, weak bonds which require low energy are formed and dissolved in the cells during metabolic activities and weak interactions occur between protein subunits to stabilize their structure. Flat sheets or closed structures such as tube, spheres could be formed and they are much more stable because formation of those structures require more bonds. They have important roles in cellular activities. For example, cytoplasmic coat proteins (COP) are responsible for capture cargo proteins and they assemble on the membrane surface if budding occurs. They polymerize into spherical cages to capture the cargo molecules and their polymerization causes deformation of the membrane. Cargo molecules inside of the bud are transferred to their target inside the cells.[9] Different types of COP complexes are found in eukaryotic organisms which bud cargo molecules from Golgi apparatus, endoplasmic reticulum or plasma membrane.[10]

Ferritin protein is another example of cage proteins and responsible for iron storage in many species. Hollow cage structure is formed with the assembly of

ferritin subunits. Iron molecules are stored in 8 nm inner cavity of ferritin and autocatalytic reaction occurs naturally in the cavity. Oxidation of Fe^{2+} ions is an enzymatic activity of ferritin proteins. These proteins are highly stable and resistant to temperature, pH, etc. Dissociation occurs at temperatures higher than 70 °C and extreme extreme pH (2-10). [11, 12] In another study, it was proved that hydrolysis of Co (II) was achieved and products were entrapped in the horse spleen ferritin. [12] With these properties ferritin promises a wide range usage with varies purposes in materials science, bioengineering, drug delivery.

Furthermore, capsid proteins self-assemble to protect viral genetic materials. Protein repeating units assemble around the genetic materials and they are classified according to final assembled structure. There are three types of capsid proteins: helical, icosahedral and complex. Any of them coat DNA or RNA of the viruses to protect from host immune system. In some cases, self-assembled capsid structure is surrounded by host cell membrane. Proteins, lipids which are found on the host membrane and capsid proteins are responsible for the host cell attachments, entry and release into the cells, genetic materials transportation between cells, packaging of the viral particles. Also, they provide stability against chemical or physical stresses.[13] Identical protein subunits of capsid proteins self-assemble, *in vitro*. Inner and exterior surfaces have different electrochemical properties. Inner cavity forms a suitable environment for mineralization and neutral charge of the outer surface is important for localization. Cavity size changes in pH dependent manner so releasing of the entrapped molecule could be controlled by environmental stimuli.[14, 15]

In addition, self-assembled cage structures promise wide range of applications in biomedicine. For instance, encapsulation ability is important for drug

delivery and catalysis applications. Cowpea chlorotic mottle virus (CCMV) is a model system for switchable molecular entrapment studies.[16] CCMV virions have positively charge interior cavity while cage surfaces are not highly charged. Hence, they offer unique chemical environment. Assembly and disassembly of CCMV virions were triggered with pH changes in a study and it was stated that virions with different interior size properties were versatile strategy for molecular encapsulation.[17]

1.2.1 Special Class of Self-Assembled Proteins: Amyloids

In some cases, soluble proteins could aggregate and form insoluble and stable structures which are called as amyloid fibers. Amyloid term was firstly described by Schleiden and by Virchow in the middle of 19th century. During autopsy, iodine stained deposits were found in the liver and firstly they were thought as natural carbohydrates but their high nitrogen content was explored later. Moreover, further studies showed that those structure were capable of binding to Congo red dye. Also, their fibrillar structures were observed with electron microscopy techniques and some techniques were developed to isolate amyloids to identify their specific structure. X-ray diffraction analysis showed that they had cross- β structure.[18, 19] Amyloid cores are highly stable structure and protect the structure against stress factors. Some of them are non-functional and contribute to some human diseases such as Parkinson's disease, diabetes type 2 and Alzheimer's disease and they are the reason of the mortality for some patients. Their pathogenicity causes from deposition in the extracellular matrix and protein structure studies prove that β -sheet elements are found as predominantly in amyloids. In addition, amyloids give fluorescent shift when bind to Thioflavin T (ThT) fluorescent dye.[20] Also, cross- β -sheet structure

is the main characteristic of the non-functional pathogenic amyloids. According to literature, more than two dozen of plasma proteins that could form amyloids have been recognized. Although they did not share amino acid sequences identity, they have common β -sheet conformation. Hence, it was suggested that their stable and insoluble characteristics come from the β -sheet elements.[21] It was proved that amyloids cause some human diseases but it is unclear that amyloid formation is the major reason or the secondary event. Aggregation and plaque formation cause the neurofibrillary tangles and compromise synaptic connections. Hence, they are the reasons of cell loss and dementia.[22, 23]

On the other hand, prion proteins which show amyloidogenic property have been identified by Prusiner in 1982. They cause human diseases but those kind of diseases could be spread from patients to another patient unlike amyloidogenic diseases.[24] Some human and animal diseases such as Creutzfeldt–Jakob disease (CJD) in humans and bovine spongiform encephalopathy (BSE) in cattle are caused from aggregation of prion (PrP) proteins that are found on the outer surface of the plasma membrane. Properly folded proteins are converted to amyloids that have same pathological form. Because of the positive feedback loop, disease is spread easily cell to cell. Yet, it is hard to convert normal PrP to abnormal PrP form without abnormal PrP in the environment.

In addition, same polypeptide chain could formed different types of amyloid fibrils and each of them were capable of converting the normal proteins to abnormal form, according to studies in yeast cells.[25, 26]

Illumination of amyloid formation mechanism is crucial for the development of therapeutic approaches. Studies showed that partially unfolded intermediates were

produced during the conversion of soluble peptide to insoluble form.[27, 28] Intermediates were not thermodynamically stable so they turned immediately amyloid fibers which were energetically favorable. Biophysical techniques such as light scattering and fluorimetry were used to identify the transition kinetics. Nucleation dependent polymerization model was suggested in order to identify fibril formation.[29] In that model, a heterogeneous nucleus, which was called as seed, was formed above the critical concentration (threshold) and monomers bound to the free ends irreversibly in order to elongate amyloid fibril. Fibril growth process could be classified as lag and log phase. If seeds were added to the media, lag phase will be shorter than normal process.[30, 31]

X-ray diffraction studies were conducted to identify structure of silk proteins of the lacewing, *Chrysopa*, firstly. Hydrogen bonds were formed in the parallel direction to the fiber axis and β -strands were elongated perpendicular to the fiber axis. This confirmation was called as cross- β structure.[32] β -sheet elements formed the amyloid core generally and it was thought to provide stability because of the side chain interactions.[33-36] Also, β -sheets could be parallel or anti-parallel direction to the each other that depended on the precursor of the polypeptide chain.[37]

1.3 Biofilm Proteins

Firstly, microorganisms have been defined as planktonic cells that grown in rich culture media. The ability to attach abiotic surfaces of microorganisms have been identified later by van Leeuwenhoek and those surface-associated microorganisms have different growth rate and gene transcription level so distinct phenotypes are observed. This surface associated micro colonies are covered by polysaccharide layer and this structure is called as biofilm. Biofilms have

complicated and distinct three dimensional architecture. Micro-colonies are divided by water channels and biofilms are resistant to stress factors. Four processes occur during biofilm formation: initial attachment, biofilm development, biofilm maturation and dispersal. Microorganisms attach to surfaces by the aid of various cellular components such as pili, fimbria and adhesive proteins.[38] Then, microbial communities are covered with extracellular polymeric substances (EPS). EPS provides resistance against mechanical or chemical stress factors also stabilizes bacterial cells on the surfaces. Hence, it was thought that it has remarkable effects on most microbial infections.[39, 40] Biofilm development changes gene expression and reduces growth rate. Specific genes are up regulated while some of them are turned off. Communities in the biofilm matrix could communicate with each other via secretion of chemicals and this process is known as quorum sensing. It is important for the fate of biofilm structure by determining the attachment or detachment from surfaces and it also affects gene expression profiles. In addition, various types of biomolecules are found in biofilm matrix such as polysaccharides, proteins and extracellular DNA (eDNA), etc. Each of them contributes to the formation of hydrated and polar structural scaffold.[41] For instance, structural stability is obtained with polysaccharides and coherent cells are aligned by eDNA.[42] Different types of proteins, which are up regulated during the development process, are found in the biofilm matrix. They contribute structural stability and have role in metabolic pathways. For example, amyloid proteins are produced during biofilm development but they have specific functions for the cells unlike pathogenic amyloids. They have thought as amyloids because they share structural properties with disease causing amyloids. For instance, both types are non-branching, have cross- β structure and they

could resist against chemical or physical forces. In addition, they give red shift when bind to Congo red dye and fluorescent shift in the presence of ThT dye that are the main characteristics of amyloids. On the other hand, they are synthesized by a special machinery which is tightly regulated. They are beneficial for microorganisms and have specific roles in cellular behaviors. Because of these reasons they have defined as functional amyloids not cellular mishap.[43-46]

Bacterial amyloid fibers associate with each other and also bind to the small molecules such as quorum-sensing metabolites. Hence, they have crucial role in retaining the nutrients and other molecules under aquatic flow.[47] Amyloids give the high tensile strength to the biofilm structure.[48] They can resist against mechanical strengths while offer soft environment for bacterial life. Studies clarify that amyloids increase the hydrophobicity of biofilm structure and stiffness, significantly. Hence, it could be concluded that amyloids make the most crucial contribution to the robustness of biofilms.[49]

1.4 Functional Amyloids

As mentioned above amyloids are non-functional and cause many diseases. In contrast, functional amyloids were found in nature according to recent studies. They share cross- β structure but they are not misfolded or unfolded proteins. They are produced by a special machinery which is tightly regulated. Some enteric bacteria species, fungi species and also yeast synthesize them and they have role in cellular activities. For example, Pmel17 is a mammalian protein that shows fibrous structure and shares same amyloid fibril properties. It is located at the surface of melanosomes and it was suggested that Pmel17 played a role in melanin synthesis.[50] In addition, hydrophobins are amyloid like proteins that function in

fungal development. During sporulation, they form a coat to repel water.[51] Moreover, recombinant mammalian prion protein (rPrP) was toxic for cultured cells and cell apoptosis could be induced by fibrils of rPrP. On the other hand, monomeric form of rPrP, which was α -helices abundant structure instead of β -strands, promoted neurite development and neuron survival. According to the study, β structure dominated fibrillar form were highly toxic; also, caused cell death.[52]

Furthermore, *Pseudomonas* strains have ability to form biofilm and *fap* (Functional Amyloid in *Pseudomonas*) operon was discovered in *Pseudomonas*.[53] When it was overexpressed in *Escherecia coli*, biofilm formation increased. Six proteins (FapA-F) are synthesized and FapC is the main amyloid component.[54] Moreover, *fap* operon are found in beta- and delta- *Proteobacteria* not only in *Pseudomonas*.[55]

Staphylococcus aureus is an example of the opportunistic pathogen species and produces biofilm associated protein (Bap) that shows self-assembly properties in order to build biofilm matrix depending upon the environmental stimuli. In acidic environment and low calcium concentration, Bap proteins form amyloid like structures. Yet, cation binding to the molten globule like state that is the intermediate state prevents self-assembly and amyloid fiber formation. If calcium concentration increases in the media, Bap coordinates with cation ions so fibrillation process is hindered. It was concluded that Bap proteins function as sensors and they are scaffold proteins that promote biofilm formation according to environmental stimuli.[56] In addition, they are found at the cell surface and compose of a repetitive structure. Also, they have high molecular weight and compose of domains.[57] They are responsible for initial attachment to the different surfaces and interactions with

bacterial or host cells. They are capable of adhere to the mammalian epithelial cells so they prevent internal localization by immune cells. Because of the adhesive property, they have remarkable effects on the persistence of the infections.[58, 59]

Another study suggests that small peptides which are named as phenol soluble modulins (PSMs) promote biofilm integrity in *S. aureus* species. PSMs lacking mutants do not form robust biofilm structure. Mechanical stress and also enzymes disrupt biofilm structure of the mutant strains. While soluble forms of PSMs are disperse in the biofilm matrix, aggregated fibrils, which have amyloid characteristics, function in metabolic activities in the biofilm.[60] Their antimicrobial activity against other bacteria was also proved and they are responsible for recruiting and lysing neutrophils hence they prevent host immune response. In addition, community-associated Methicillin-resistant *Staphylococcus aureus* (MRSA) strains synthesize virulence factors that contain PSMs.[61, 62]

Also, *Mycobacterium tuberculosis* produces functional amyloid proteins. It produces special types of pili that are known as *M. tuberculosis* pili (MTP) and they are formed by protein subunits that have low molecular weights. Adhesive property of MTP was suggested in a study and binding to the laminin that is an extracellular matrix protein was showed. Hence, it is important for host colonization. Morphological, functional and biochemical characteristics of MTP are similar with curli amyloids.[63, 64]

Furthermore, *Bacillus subtilis* is capable of endospore production. Endospores are coated by complex proteins so they could resist against stress factors such as protease treatment, pH changes, etc. Exopolysaccharides and TasA proteins are the main components of the matrix and TasA is associated with spores and

functions as antimicrobial. Later studies proved that TasA proteins were the major protein components and formed amyloid fibers that were crucial for the biofilm integrity.[65, 66] Spores of *tasA* lacking mutant strains have asymmetric material distribution and altered outer coat unlike wild-type strains. Another study suggested that TasA and GerE acted synergistically for endospore formation. Also, maturation of TasA depends on another protein which is called as SipW. It has bifunctional activity: signal peptidase and regulatory roles. Signal peptidase activity is not required for the biofilm development but it is still required for that process. Hence, its regulatory role was suggested in a recent study.[67] If mother cell engulf the pre-spore cell, precursor TasA is translocated to the spore membranes in order to nucleate the organization of the under endospore coat.[68] TasA proteins self-assemble and form stable fiber that are similar with functional amyloids. TapA is the assistant protein of TasA. *Bacillus subtilis* biofilm formation relies on the assembly of a fibrous scaffold which is formed by TasA protein. TasA polymerizes into highly stable fibers. 8 amino acids residues at the N term of TapA are essential for TasA fibrillation. In the absence of those residues, biofilm formation delays, *in vivo*. [69]

1.5 Functional Amyloids of *Escherichia coli*: curli

The most studied functional amyloid is curli that is produced by *Escherichia coli* and discovered in the 1980s. *Salmonella* species also produce curli fimbria. Both type of curli have similar roles such as cell to cell contact, host cell adhesion and invasion.

In *E. coli*, transcription of curli subunits, other regulatory and transporter proteins are regulated by curli specific gene operons: *csgBAC* and *csgDEFG* which are represented in Figure 1.[70]

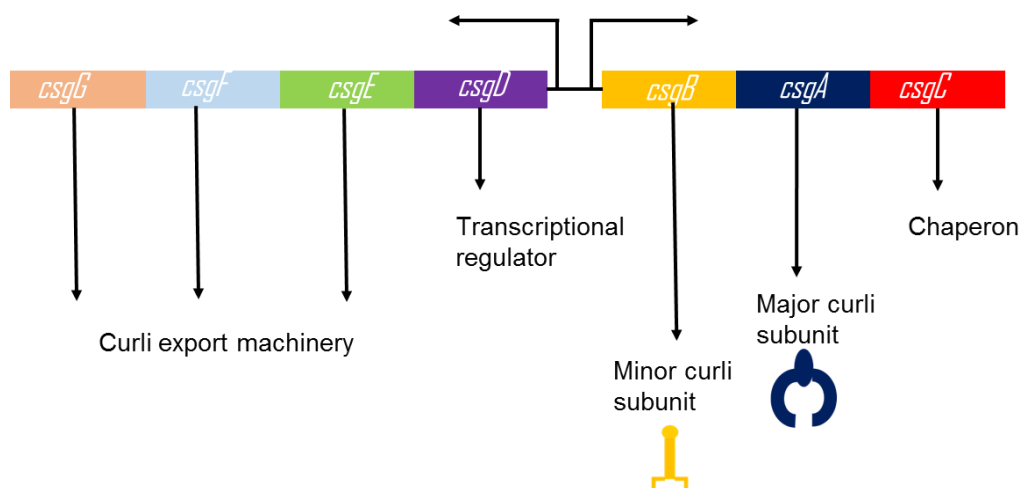


Figure 1- Transcription of curli proteins are regulated via *csgBAC* and *csgDEFG* operons. CsgA is the major curli subunit while CsgB is the minor subunit. CsgC shows chaperon activity and CsgD is the regulator protein. Other curli proteins have roles in the secretion machinery.

On the other hand, *agfBA* and *agfDEFG* operons regulate curli production in *Salmonella* spp. Mutations on those genes have similar effects with *csg* operons. Tafi (thin aggregative fimbriae) is the special name of curli fimbriae that is synthesized by *Salmonella typhimurium*. [71]. CsgB is the minor subunit while CsgA is the major curli subunits. Chaperone activity of CsgC protein was recently identified. During translocation to the extracellular environment, CsgC prevents aggregation of curli subunits in the periplasmic space. [72] Major and minor subunits have 30% sequence identity. Also, both of them compose of five imperfect repeating units. [73] CsgA polymerization requires CsgB minor subunit. CsgB and CsgA could be synthesized by different cells. If *csgA* lacking mutants and *csgB* lacking mutants are found in the same media, polymerization occurs because of the interbacterial complementation. Yet, this process do not occur in *Salmonella enterica*. [74] Accessory proteins are also required for assembly and they are encoded by *csgDEFG* operon. While CsgD

regulates the other operon positively, synthesis of CsgD proteins is not regulated by itself.[70, 75] Because of helix-turn-helix motif at C terminal, DNA binding capability of CsgD was suggested but there was no experimental evidence to prove its potential. Also, it was proposed that its activation is triggered by phosphorylation event but mechanisms that control expression and activation are not clear.[75] CsgG forms a channel on the outer membrane so it is required for secretion of curli subunits.[76, 77] CsgG protein is analog of other outer membrane channel-forming proteins.[78, 79] According to studies, fiber formation did not occur in *csgG* lacking strains. Also, those strains were not capable of functional major or minor curli subunit production.[80] CsgE is found in the periplasmic space and little amount of fiber formation was observed in mutant strains. They were less stable than wild-type subunits and they did not compensate polymerization by using wild-type subunits from wild-type strains. Although those mutants synthesized a few CsgA fibers, they were not similar with wild-type fibers, morphologically.[76] Another important point is the interaction of CsgE and CsgG at the outer membrane. It was thought that CsgE or CsgG act cooperatively because CsgE or CsgG deficient strains had similar phenotypes. Yet, exact role of CsgE on curli assembly is still unknown. However, CsgF is a periplasmic protein which interacts with CsgG, phenotype of *csgF* lacking strains is different from *csgE* lacking mutants. On the other hand, *csgF* lacking mutants had similar phenotype with *csgB* deficient mutants since soluble and unpolymerized CsgA produced by mutant strains.[76-79]

As mentioned before, curli subunits are functional amyloids and they are synthesized by a special machinery that is controlled tightly. In addition to CsgD control on *csgBAC* operon, environmental factors affect curli expression. Below

30°C curli expression is promoted; also, many *E. coli* strains could synthesize curli at 37°C.[81, 82] Contents of growth media also affect curli expression. For example, in the absence of salt, curli proteins are transcribed maximally. Limitations of phosphate, iron and nitrogen trigger curli biosynthesis.[83] Oxygen content of the environment also affects, maximal CsgD expression occurs at low oxygen environment.[84]

Furthermore, curli expression level changes during bacterial growth. Studies showed that maximum transcription of curli genes occurred during stationary phase and that process depended on RpoS that was the stationary-phase sigma factor.[85, 86] Moreover, Crl protein was proposed as thermal sensor and it increased curli protein synthesis at low temperature. Crl is more stable at low temperature so it was thought that its stability could have positive effects on curli transcription.[81, 87] In addition, RpoS and Crl act cooperatively to regulate *csgBAC* operon. Also, RpoS activates MlrA expression that regulates CsgD biosynthesis, positively.[88, 89]

Additionally, there are dual regulatory systems which regulate transcription of curli protein and they affect dramatically curli gene expression more than other factors. One of them is OmpR/EnvZ system and it regulates curli expression according to osmolarity of the environment. EnvZ is sensor kinase protein that senses changes to activate OmpR regulator protein. Furthermore, expression of CsgD that is another curli operon regulator protein is regulated positively by OmpR.[83, 90] The other two component regulator system is the CpxA/R system which is activated by overexpression of *csgA* when *csgG* gene is not overexpressed. CpxA is a sensor kinase like EnvZ and CpxR is the regulator like OmpR but it regulates negatively. In addition, membrane and misfolded proteins in the periplasm activate that system and

cause the upregulation of periplasmic chaperones and proteases. It was suggested that curli subunits were found transiently in the periplasmic space due to the CpxA/R system.[91-93] Moreover, outer membrane stress results in the activation of Rcs pathway which regulates *csgD* transcription negatively. Rcs pathway has important roles in biofilm formation so it could be concluded that regulation of biofilm formation is linked to the regulation of curli operons. It was suggested that curli had roles in initial stages of biofilm development. They might be responsible for the initial adhesion. It was proposed that curli expression was turned off by CspX and Rcs pathways.[94-96] Curli gene expression was triggered in non-adherent strains of *Escherichia coli* to form biofilm, according to a study. Biofilm formation ability was identified as CsgA dependent process in that strain.[97] Morphology of the biofilm which was developed by curli lacking mutants was analyzed in another study. They formed flat biofilm which was not similar with wild-type biofilm.[98]

Although they are beneficial for microorganisms, they could contribute human diseases. For instance, curli proteins contribute to the host cell attachment and invasion, induce host immune response by interacting with host proteins.[82, 86, 99] Also, interactions with host proteins enable to spread in host organisms.[82] CsgA proteins that are major subunits of curli were detected in sera of sepsis patients.[82] In addition, it was reported that polymerization of the disease-associated amyloid protein A was induced by injection of curli proteins to the mice. Curli might act as a seed for disease-associated amyloid protein A polymerization.[100] Furthermore, curli proteins are capable of binding to the plant cells but this ability changes strains to strains because other cellular components also have roles in attachment according

to mutant studies. Moreover, adherence of alfalfa sprouts decreased in *csgB* lacking strains of *S. enterica* but not in *csgA* deficient mutants.[101, 102]

1.6 Major and Minor Curli Subunits

Major and minor curli subunits (CsgA and CsgB) have similar characteristics. For instance, they have *sec* signal sequence at N terminals and following 22 amino acids in CsgA and 23 amino acids in CsgB important for secretion. Five imperfect repeating units that are responsible for β sheet formation follow these sites. Also, they have %49 sequence similarity and 30% sequence identity. Amyloid core which is resistant to many stress factors are formed by these repeating units.[73, 103]

According to studies, CsgA and CsgB proteins are synthesized as monomers which are soluble forms and then they are translocated to the extracellular media because *sec* signal sequences at N terminals direct them to the periplasmic space and they are cleaved here. CsgB anchors the outer membrane via fifth repeating unit and acts as a template for CsgA polymerization. Other CsgA proteins bind to each other for elongation and secretion machinery is represented in Figure 2. *csgB* lacking mutants are capable of soluble CsgA secretion. Without CsgB subunits CsgA do not form oligomers, polymerization could be achieved by interbacterial complementation, *in vivo*. [73, 76] On the other hand, self-seeding occurs for CsgA and CsgB, *in vitro*. Also, CsgA polymerization is induced by addition of preformed CsgA fibers to the environment. The first and fifth repeating units of CsgA serve as interaction sites.[104] Moreover, Ser-X₅-Gln-X₄-Asn-X₅-Gln residues are conserved in the five repeating units of CsgA so they may contribute the amyloid formation. Studies proved that specific side chain interactions are important for self-seeding and CsgB nucleation. Polar side chains participate CsgB nucleation while self-seeding of CsgA

does not depend on polar side chains. Also, aromatic residues that found in CsgA do not affect positively amyloid formation.[105] Predicted structure of CsgA was identified as β strand-loop- β strand and it could be right or left handed that were energetically equal. Also, β strands elongated as parallel. Interactions between β sheet layers resulted in rectangular core domains which were highly hydrophobic. This predicted structure was in agreement with previous studies.[106]

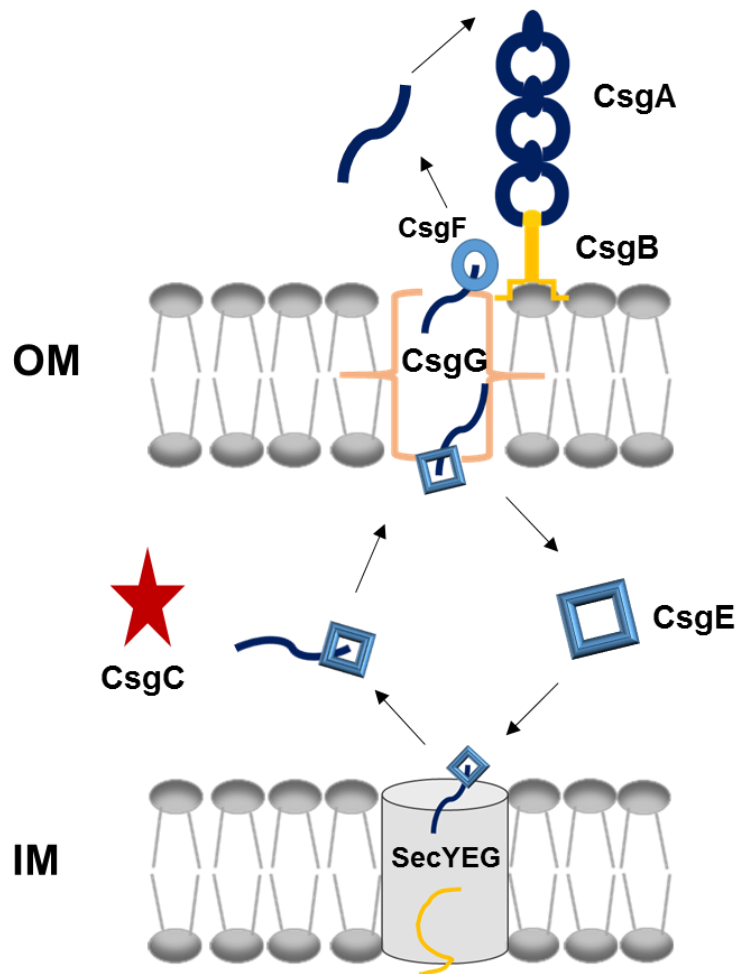


Figure 2- Curli secretion machinery. CsgA and CsgB proteins have *sec* signal sequences and are secreted to the ECM after synthesis. CsgB interacts with outer membrane and acts as template for CsgA oligomerization. CsgG forms channel on the outer membrane while CsgE and CsgF are responsible for transportation.

1.7 Why Amyloids are Important for Materials Science?

Amyloids are dominated by β -sheet structures which are highly stable and energetically favorable form. According to microscopic studies, they are few micrometers with 7–10 nm diameters. Another important property is their stiffness which is comparable to silk. Based on the physical measurements, it was proved that they were as strong as steel. Much as described above, they could resist stress factors such as detergent or protease treatment, temperature, etc. Molecular biomaterials such as wires, scaffolds, liquid crystals could be fabricated by using amyloids with bottom-up strategy. They assemble into highly ordered structures and they are produced easily with low cost. Also, they could be tuned easily with protein engineering techniques. All of these properties make them useful source for materials science. For example, nanoscale electrical circuits could be designed according to a study. Protein fibers with 10 nm wide, which were highly stable, produced from prion proteins of *Saccharomyces cerevisiae* that were known as Sup35p. Length of the fiber were controlled easily and could be reached to hundreds micrometers. Silver and gold wires by deposition of ions on colloidal surface were achieved and near 100 nm wide conductive wires were obtained.[50] Also, water filled nanotubes may be produced from amyloid assembly which may be useful for nanowire production.[107] Amyloid proteins could be formed liquid-crystal phases like many polymers. It was suggested that liquid-crystal phases were observed with hen lysozyme at low pH. New type of soft-solid like materials that is biodegradable and also biocompatible could be obtained with hen lysozyme.[108, 109] Natural amyloids have adherent properties and they function in attachment to the biotic or abiotic surfaces. In a study, hydrophobins were used to change chemical properties

of surfaces to improve biocompatibility. It was possible with their amphipathic nature. Hence, they may serve scaffolds for tissue engineering.[110] Furthermore, amphiphilic peptides were produced artificially which could undergo ordered assembled structure in liquid medium. Hence, those novel artificial peptides may support cell growth and they have big potential to use in tissue engineering.[111] Also, amyloid peptides were designed to increase carbon dioxide capture capacity and gene transfer efficiency.[112] In addition, protein film was created to form hierarchically assembled amyloids fibers.[113]

To sum up, protein based materials could be easily manipulated and recent studies proved that they could be controlled and stable structures could be obtained. Molecular biology techniques and protein engineering have been developing day by day to improve recombinant protein production strategies, decrease cost and increase the yield. As discussed above, amyloids have big potential to use in various fields such as tissue regeneration, sophisticated three-dimensional scaffolds formation, cage for controlled drug release, coating materials, conductive wires, biosensors or bioswitches.[114-116]

1.7.1 Usage of Curli Proteins

Curli subunits are highly adhesive proteins which function in surface attachment. They were suggested as underwater adhesives and CsgA proteins fused with mussel foot proteins (Mfps) of *Mytilus galloprovincialis* in a study. The highest underwater adhesion energy was determined from the fused proteins.[117] Furthermore, they are good candidate for enzyme immobilization. CsgA were used to immobilize α -amylase enzyme via covalent bonds. Stability was tested at different pH and with organic solvents.[118] In another study, genetic circuits were designed

to produce CsgA which depended on environmental signals. CsgA fibrils were interfaced with quantum dots and gold nanoparticles. With this strategy gold nanowires or nanorods could be produced.[119] Peptides were fused with CsgA and new recombinant proteins synthesized and secreted by *E. coli* cells. CsgA proteins were assembled onto the outer membrane without losing peptide functionality. This system was called as Biofilm-Integrated Nanofiber Display (BIND).[120]

CHAPTER 2

EXPERIMENTAL

2.1 Preparation of Growth Medium and Buffers

To prepare 1 L of Luria-Bertani (LB) broth media, 10 g tryptone, 5 g sodium chloride and 5 g yeast extract were dissolved in deionized water and final volume was adjusted to 1 L. Also, for 1 L agar media, 15 g agar was added to LB media.

50X Tris-Acetic acid-EDTA (TAE) media was prepared and diluted to use in agarose gel electrophoresis. 242 g Tris was dissolved in deionized water and 100 mL of EDTA from 0,5 M EDTA solution was added. Finally, 57,1 mL of 100% acetic acid was added. Deionized water was added to reach 1 L.

To prepare Transformation & Storage Solution (TSS), 5 g polyethylene glycol (PEG) mixed with 1,5 mL of 1 M MgCl₂ and 2,5 mL of dimethyl sulfoxide (DMSO). LB was added to reach 50 mL. Then, solution was filtered with 0,22 µm filter.

10X SDS (Sodium Dodecyl Sulfate) running buffer was prepared with 30 g Tris, 10 g SDS and 144 g glycine. All components were dissolved in deionized water and final volume was adjusted to 1 L. It was diluted to 1X before use in SDS-PAGE (Sodium Dodecyl Sulfate-Polyacrylamide Gel Electrophoresis).

2X Laemmli sample buffer was prepared by mixing 65,8 mM Tris-HCl, 2,1% SDS, 26,3% (w/v) glycerol and 0,01% bromophenol blue.

TGX Stain-Free FastCast acrylamide solutions were used to prepare 10% SDS gel according to manufacturer instructions.

Furthermore, SDS-PAGE was performed with 12% resolving gel and 4% stacking gel. Components of them given the following tables.

Table 1- Components of 12% resolving gel

Deionized water	3,2mL
Acrylamide/Bis-acrylamide (30%/0.8% w/v)	4 mL
1,5M Tris(pH=8.8)	2,6 mL
10% (w/v)SDS	0,1 mL
10% (w/v) ammonium persulfate (AP)	100 μ L
TEMED	10 μ L

Table 2- Components of 4% Stacking Gel

Deionized water	2,975 mL
Acrylamide/Bis-acrylamide (30%/0.8% w/v)	1,25 mL
0,5M Tris(pH=8.8)	0,05 mL
10% (w/v)SDS	0,67 mL
10% (w/v) ammonium persulfate (AP)	50 μ L
TEMED	5 μ L

10X phosphate buffer saline (PBS) was prepared with 80 g sodium chloride, 1 g potassium chloride, 14,4 g sodium dihydrogen phosphate and 2,4 g potassium dihydrogen phosphate. All of them dissolved in deionized water and final volume was adjusted to 1 L. Before use, stock solution was diluted.

Recombinant proteins were purified in denaturing conditions. To prepare wash buffer, 6 M GdnHCl was dissolved in phosphate buffer saline (PBS) and 10 mM imidazole was added while 150 mM imidazole added for elution buffer. Wash buffer used as lysis buffer to dissolve cells. Also, 8 M GdnHCl in PBS was used as extraction buffer.

Tris buffered saline (TBS) was used for western blot analysis. 20 mM Tris and 150 mM sodium chloride was dissolved in deionized water. 5% (w/v) non-fat milk powder was added and it was used to block membrane. Antibodies were also diluted in that solutions. Tris buffered saline with Tween 20 solution was used to wash western blot membrane by adding 0,1% Tween 20 to TBS.

2.2 Cloning of *csgA* & *csgB* Gene Fragments

2.2.1 Plasmid Purification

Plasmid isolation was performed by using Qiagen miniprep kit according to manufacturer's instructions. Plasmid DNA was eluted with preheated water (65°C). Plasmid concentrations were determined with Nanodrop. They were stored at -20°C.

2.2.2 Chromosomal DNA Isolation

Qiagen genomic DNA isolation kit was used to purify *E. coli* genome according to manufacturer's instructions.

2.2.3 Polymerase Chain Reaction (PCR)

csgA gene fragments were amplified from *E. coli* genome and GS soft linker sequences that compose of three repeats of GGS amino acids (G for glycine and S for serine), Tobacco Etch Virus (TEV) protease restriction site and same soft linker sequence were added to the 3' prime of *csgA* genes. Two different PCR reactions were performed. First PCR components and conditions are given in Table 3 and 4, respectively. For two-step PCR, first annealing temperature was calculated as 70°C and second was 89 °C.

Table 3- PCR Components

	Reaction components (μL)	Control experiment (μL)
5X Phusion buffer	5	5
10mM dNTP mix	0,5	0,5
10 uM Forward primer	1,25	1,25
10 uM Reverse primer	1,25	1,25
DNA (1 ng/μL)	1	-
Phusion Polymerase	0,25	0,25
Deionized water	16	17
Total volume	25	25

Table 4- Reaction Conditions

	Temperature (°C)	Time	Cycle
Initial denaturation	98	30 sec	
Denaturation	98	10 sec	5 cycle
Annealing	70	20 sec	
Extension	72	20 sec	
Denaturation	98	10 sec	30 cycle
Annealing	89	20 sec	
Extension	72	20 sec	
Final Extension	72	7 min	

Second reaction was set up according to Table 3. PCR products of the first reaction were used as template in the second reaction. Same PCR conditions by just changing annealing temperatures were set. First annealing temperature was calculated as 60°C and the second was 82°C.

Furthermore, *csgB* gene was amplified from *E. coli* genome and reactions were set up according to Table 3 and PCR conditions are given in Table 4. Annealing temperature were calculated as 59°C and 72°C. Primers are listed in Table 5.

Table 5- Primers that were used in this study

	Primers	Oligonucleotide sequences
The first reaction of <i>csgA</i>	Forward	GTCCTCGCTGCCCAGCCGGCGATGGCCATGGAT GAAACTTTTAAAAGTAGCAGCAATTGCAGCAAT CGT
	Reverse	AAAATACAGGTTTTTCGCCGCTACCGCCTCCGCTA CCGCCACCGCTACCGCCGGTACCGTACTGATGAG CGGTCGCGTTGTT
The second reaction of <i>csgA</i>	Forward	GCTGCCGACCGCTGCTGCTGGTCTGCTGCTCCTC GCTGCCAG
	Reverse	GTGCTCGAGGCCGCTACCGCCTCCGCTACCGCCA CCGCTACCGCCGCCCTGAAAATACAGGTTTTTCGC CGCT
The reaction of <i>csgB</i>	Forward	GTCCTCGCTGCCCAGCCGGCGATGGCCATGGAT GAAAACAAATTGTTATTTATGATGTT
	Reverse	CTCCGCTACCGCCACCGCTACCGCCGGTACCACG TTGTGTCACGCGA

2.2.4 Agarose Gel Electrophoresis

1% (w/v) agarose gel was used to observe DNA fragments. 1 g of agarose was dissolved in 1X TAE and boiled. After cooling, SYBR® Safe was added and it was poured into the gel cast. PCR products were loaded to the agarose gel and 1X TAE buffer was used as a running buffer. Horizontal electrophoresis apparatus was used to carry out experiments. Purple loading dye (NEB) was added to the samples before loading to gel and 100 Volts were applied for 40 minutes to carry out gel electrophoresis. 2-log DNA ladder marker was used to determine molecular weights of the PCR products.

2.2.5 Gel Extraction

QIAquick Gel Extraction Kit was used to extract DNA from agarose gel by applying manufacturer's protocol. Final DNA concentration was calculated with Nanodrop.

2.2.6 Endonuclease Digestion Reactions

PCR products of *csgA* gene were digested with NcoI and XhoI (NEB) endonucleases and pET22b(+) expression vector was also digested with same endonucleases. Reaction components were given in Table 6. Mixes were incubated at 37 °C for an hour and loaded onto agarose gel. DNA was extracted from the gel and concentration was calculated with Nanodrop.

Also, PCR products of *csgB* gene were digested with NcoI and KpnI (NEB) endonucleases and the new recombinant pET22b(+) plasmids that had *csgA* gene fragments were digested with same enzymes to extract *csgA* gene.

Table 6- Digestion reaction components

Component	Amount
DNA	200 ng
Enzyme 1	0,2 µL
Enzyme 2	0,2 µL
10x cut smart buffer	2 µL
Deionized water	Up to 20 µL

2.2.7 Ligation of Double Digested DNA Fragments

Ligation reaction was set up according to the Table 7. Insert backbone amount was calculated as 3:1 insert vector ratio. Reaction mixtures were incubated at room temperature for an hour.

Table 7- Ligation reaction components

Components	Amount
Vector pET22b(+) (13 ng/μL)	16 μL
Insert <i>csgA</i> (32 ng/μL)	4 μL
10x ligase buffer	2,5 μL
T4 ligase	1 μL
Deionized water	1,5 μL
Total volume	25 μL

Furthermore, 1:1 insert vector ratio was used to clone *csgB* gene. Components are given in Table 8.

Table 8- Ligation reaction components

Components	Amount
Vector (15 ng/μL)	1 μL
Insert <i>csgB</i> (15 ng/μL)	0,8 μL
10x ligase buffer	0,5 μL
T4 ligase	0,25 μL
Deionized water	2,9 μL
Total volume	5 μL

2.3 Transformation

2.3.1 *Escherichia coli* DH5α and BL21 Competent Cell Preparation

Overnight grown *E. coli* cells were diluted as 1/100 and grown on shaker at 37 °C until OD₆₀₀ was reached ~0,6. Then, culture was incubated on ice for 10 minutes and centrifuged for 10 minutes at 3000 rpm at 4°C. Cell pellets were dissolved in 10% of culture volume of TSS buffer and aliquoted into 100 μL portions to store at -80°C.

2.3.2 Transformation of Recombinant Plasmids to *E. coli* Competent Cells

Competent cells that were stored at -80°C were out and incubated on ice near 20-30 minutes to thaw. Ligation reaction mixtures were added to the cells and

incubated on ice for 15 minutes. Then, cells were incubated at 42°C for 45 seconds and immediately placed on ice for 5 minutes. 1 mL of LB medium was added to the cells and cells were grown on shaking incubator for near 1-1,5 hours. Cells were harvested with centrifugation at 3000 g for 5 minutes and 900 mL of supernatant was removed. Cell pellets were dissolved with the rest of the supernatant and inoculated onto the carbenicillin contained agar plates. Recombinant plasmids were sequenced by Genewiz.

2.4 Protein Expression, Purification and Characterization

2.4.1 Overexpression of CsgA & CsgB Proteins

The recombinant plasmids were transformed to *E. coli* BL21 cells for overexpression. *E. coli* BL21 cells that contain *csgA* or *csgB* plasmids were incubated in 3 mL of LB medium with carbenicilin (100µg/mL) as a selective antibiotic. Culture were grown in shaking incubator at 37 °C, 180-200 rpm for 6-8 hours. After 6-8 hours, cultures were diluted at the 1/5 ratio in fresh LB medium with carbenicilin (100µg/mL) and grown for overnight. Overnight grown cultures were also diluted at the same ratio and OD₆₀₀ value of the culture was followed. When it reached near 0,9, IPTG was added as inducer (0,5 mM final concentration). The culture was grown for an hour and cells were harvested at 10000 g for 15 minutes to store -80°C.

2.4.2 Purification of CsgA & CsgB Proteins

Proteins were purified under denaturing conditions and GdnHCl was used as a denaturing agent. Cell pellets were dissolved in the lysis buffer and treated with lysozyme and incubated for an hour at 4°C. Then, sonicated for 5 minutes at 50 watt. Cell lysate was centrifuged for 20 minutes at 10000 g 4°C. Supernatant was

transferred to the sterile tube and cobalt resin was added at the ratio of 50:1. Supernatant-resin mixture was incubated in a rotator at 4°C for an hour. After immobilization of Histidine tagged proteins, samples were centrifuged at 1000 g for 1 minute to precipitate resin and supernatant was removed. Resin was washed with wash buffer for three times. After an additional centrifugation to remove the rest of the wash buffer, proteins were eluted with elution buffer.

Moreover, purification protocol was modified from another study.[121] Cell pellets were dissolved in extraction buffer (PBS that contain 8 M GdnHCl) and incubated in a rotator for overnight at 4°C. Cell lysate was also centrifuged for 20 minutes at 10000 g, 4°C. Same washing and elution steps were applied to elute recombinant proteins.

Whole characterization experiments were performed with recombinant proteins in phosphate buffer saline (PBS) media. Hence, 10 kDa Amicon ultra centrifugal filters (Millipore) were used to exchange media of the purified proteins. Also, protein oligomers and monomers were separated by using 30 kDa Amicon ultra centrifugal filters (Millipore).

2.4.3 Determination of Protein Concentration

Pierce® BCA protein assay (Thermo Scientific) was performed to calculate protein concentration according to manufacturer's protocol.

2.4.4 SDS-PAGE and Western Blot analysis

Formic acid was dropped onto the proteins in PBS media and samples were lyophilized to evaporate formic acid.[73] Protein samples were dissolved in 2x Laemmli SDS sample buffer and loaded onto the 10% TGX stain free gels (Bio-Rad) or SDS polyacrylamide gel. To visualize bands, SDS gel was stained with Coomassie

Blue. For Western Blot analysis, proteins were transferred to the PVDF membrane by using Trans-Blot system (Bio-Rad). 5% nonfat milk powder in TBS-T solution was used to block membrane and blocking was performed at RT for an hour. Membrane was incubated in 1:5000 diluted anti-his mouse primary antibody (Thermo) in TBS-T solution for overnight at 4°C or room temperature for an hour. Then, membrane was washed with TBS-T for three times during 30 minutes. Primary antibodies were probed with 1:5000 anti-mouse horseradish peroxidase conjugated secondary antibody (Abcam) in TBS-T. Membrane was also washed with TBS-T during 30 minutes. ECL substrate (Bio-Rad) was applied according to the manufacturer's protocol and Chemidoc MP (Bio-Rad) was used to visualize the membrane.

2.5 Thioflavin T (ThT) Assay

Polymerization kinetics of the purified proteins were determined with ThT assay. ThT was dissolved in deionized water. Samples in PBS environment were loaded on 96-well plate and ThT dye was added at a final concentration of 20 μ M. In order to measure fluorescence intensities, excitation and emission wavelengths were set at 438 and 495 nm (475 nm cutoff), respectively. During 15 hours, fluorescence intensities were recorded with 10 minutes intervals and 5 seconds shaking before each reading by using Spectramax M5 plate reader. Relative fluorescence intensities were normalized as previously described in the literature.[117]

2.6 Secondary Structure Analysis

Jasco J-815 Spectrophotometer was used and CD analysis was performed in far ultra-violet spectra (190-250 nm). Samples were transferred to the quartz cell

with 1-mm path length. Web based tool (<http://bestsel.elte.hu/>) that developed by Siligardi et al. 2015 was used for a linear curve fitting.[122]

2.7 Quartz Crystal Microbalance with Dissipation (QCM-D)

2.7.1 Sensor Cleaning

Gold coated sensor surfaces were washed with mild piranha solution which was prepared by mixing deionized water: ammonium (25%): hydrogen peroxide (30%) (5: 1: 1 ratio). Gold coated sensors were placed into the mild piranha solution and heated up to 70°C for 5 minutes. Then, sensors were placed in deionized water for 15 minutes. By blowing with nitrogen gas, sensor surfaces were dried and treated with UV/ozone.

Silica coated sensors were treated for 10 minutes with UV/ozone and placed into 2% SDS solution for 30 minutes at room temperature. Then, sensors were washed with deionized water. They were dried with nitrogen gas and treated with UV/ozone for 10 minutes.

Hydroxyapatite (HA) coated sensors were also treated with UV/ozone for 10 minutes and placed into 95% ethanol solution for 30 minutes at room temperature. After washing with deionized water, they were dried with nitrogen gas and treated with UV/ozone for 10 minutes.

2.7.2 Fiber Formation Assay

Quartz crystal microbalance Q-Sense E1 was used to monitor absorption and assembly of the CsgA and CsgB proteins in real time.

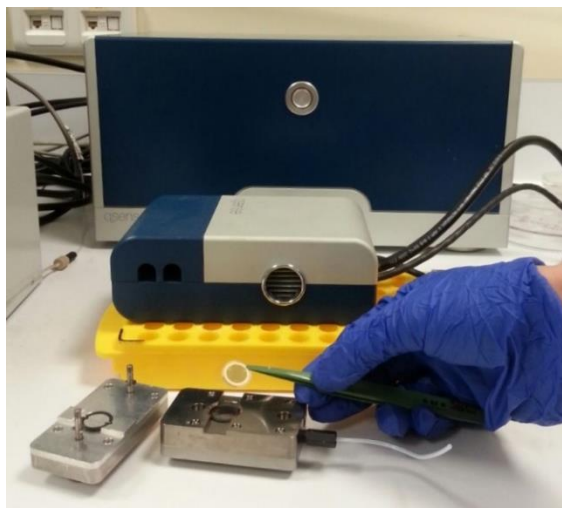


Figure 3- Quartz crystal microbalance with dissipation device and QCM-D sensor.

Temperature and the flow rate were set as 25°C and 0.10 $\mu\text{L}/\text{min}$, respectively. PBS was used to wash sensor surface till both signals frequency and dissipation reached the equilibrium. Then, purified proteins in PBS buffer was flowed into the QCM-D. System and surface were also washed with PBS. When both signals reach the equilibrium, flow was stopped and changings on the signals were recorded for overnight. On the next day, freshly purified proteins were separated as monomers and oligomers by using Amicon filter units (Millipore) and monomers were diluted to 4 or 5 concentrations. Protein monomers with diluted concentrations were run through the system low to high concentrations and also system was washed with PBS between protein flows. After the final washing step, signals reached the equilibrium and changings were recorded for overnight. At the end of the run, system was washed with deionized water.

2.8 Immunochemistry Assay

Freshly purified proteins were deposited on the gold coated sensor surface and proteins were probed with antibodies. Frequency and dissipation signals were recorded in real time by using QCM-D. After deposition of 2 μM freshly purified

CsgA, 1:5000 diluted anti-his mouse primary antibodies (Thermo) in PBS were run through the system and system was washed with PBS until signals reached the equilibrium. 1:5000 diluted fluorescent labelled secondary antibodies (DyLight 550 Thermo) in PBS were added to the system and then system was washed with PBS to remove unbound molecules till both signals reached the equilibrium. Sensor surfaces were examined with confocal laser scanning microscopy (CLSM, Zeiss LSM 510). 5 μ M freshly purified CsgB proteins were probed with same primary and secondary antibody solutions and sensor surface was observed with confocal laser scanning microscopy.

2.9 Fluorescence Analysis of CsgA & CsgB Proteins

Cary 100 Bio spectrophotometer was used to analyze fluorescence excitation and emission spectra of aged CsgA and CsgB samples in PBS buffer. Also, CsgA and CsgB samples were mixed in equimolar concentration as a third sample. In addition, aged CsgA proteins were centrifuged for 30 minutes and precipitated amyloid fibers were dissolved in chloroform. Fluorescence excitation and emission spectra was also measured.

2.10 Kinetic Analysis of CsgA & CsgB Proteins

After buffer exchange process, purified CsgA and CsgB proteins in PBS media were incubated at room temperature for a few days to induce polymerization. Also, mix samples were prepared by mixing pure CsgA and CsgB in equimolar concentrations and incubated. To identify protein-materials interactions, gold, silica and hydroxyapatite coated QCM sensors were used. For each cases, samples were diluted and flowed through the system with increasing concentrations. Temperature and the flow rate were set as 25 °C and 0.10 μ L/min, respectively. Between proteins

flows washing steps with PBS were applied to remove weakly or unbound proteins until dissipation and frequency signals reached the equilibrium. Both signals were recorded during protein addition and washing steps. At the end, system was washed with deionized water.

2.11 Imaging of CsgA & CsgB Proteins

2.11.1 Scanning Electron Microscopy Imaging

Proteins in PBS buffer were dropped on silica substrates and spotted coated with 5 nm of Au/Pd composite using precision coating system (Gatan Inc, USA). Samples were examined under high vacuum conditions with 5-15 KeV electron beam energy.

2.11.2 Atomic Force Microscopy Imaging

MFP3D Asylum microscope was used in this study. Protein coated gold surfaces were analyzed in tapping mode by the aid of Si probes with a resonance frequency of 300 kHz and a nominal spring constant of 40 N/m (Ted Pella Inc, USA).

2.11.3 Fluorescence Microscopy Imaging

Axio Scope A1 (Zeiss, Germany) was used to analyze fluorescence properties of the samples. Excitation wavelengths were set up as 546 nm for red, 455 nm for green and 365 nm for blue fluorescence and emission wavelengths were 575-640 nm, 500-550 nm and 420-470 nm, respectively. Exposure times were all equal.

CHAPTER 3

RESULTS AND DISCUSSION

3.1 Cloning of *csgA* and *csgB* Gene Fragments

CsgA and CsgB proteins were synthesized under *lacI* control and those recombinant proteins were purified by the aid of histidine tags. For this aim, *csgA* and *csgB* gene fragments were inserted into pET22b(+) expression vector. GS linker sequences (compose of three repeats of GGGs amino acids) were added to prevent protein-tag interactions. Also, TEV protease restriction site was added between *csgA* fragment and histidine residues in order to cleave histidine tags for further analysis. Gene fragments were amplified from *E. coli* genome. GS linker sequence and TEV site were added with the first PCR. The second PCR was performed with one forward primer and two reverse primers. Also, the first PCR products were used as template to set up the second reaction. Other GS linker and backbone overlap residues were added with the second PCR. Final PCR product was shown schematically in Figure 4. PCR products were loaded to agarose gel and gel images are shown Figure 5-6. PCR products were cloned into pET22b vector with cut ligate method. Hence, PCR products and vector were digested with NcoI and XhoI endonucleases. Linearized vector was run onto agarose gel electrophoresis and image is demonstrated in Figure 7. Digested gene fragments were ligated with T4 DNA ligase. Plasmid construct is shown in Figure 8. Sequences were validated by Genewiz and sequence alignment is demonstrated in Figure 9.

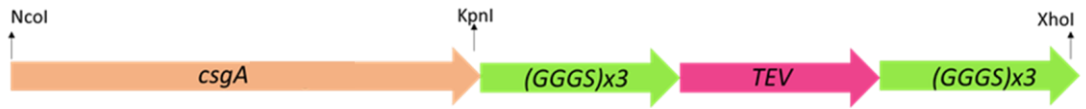


Figure 4- Schematic representation of amplified *csgA* gene fragment.

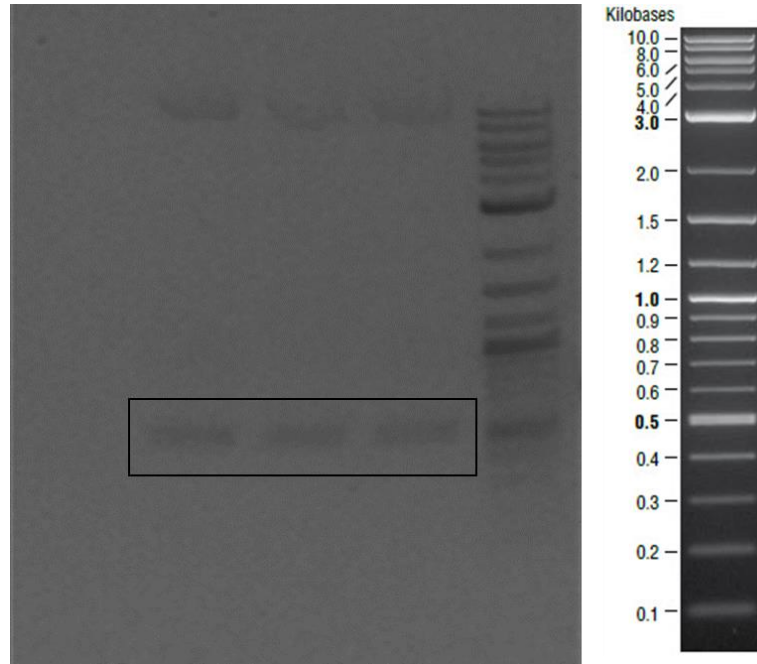


Figure 5- Bands inside the square belonged to *csgA* gene fragments expected as ~500 bp. Negative control was on the first lane.

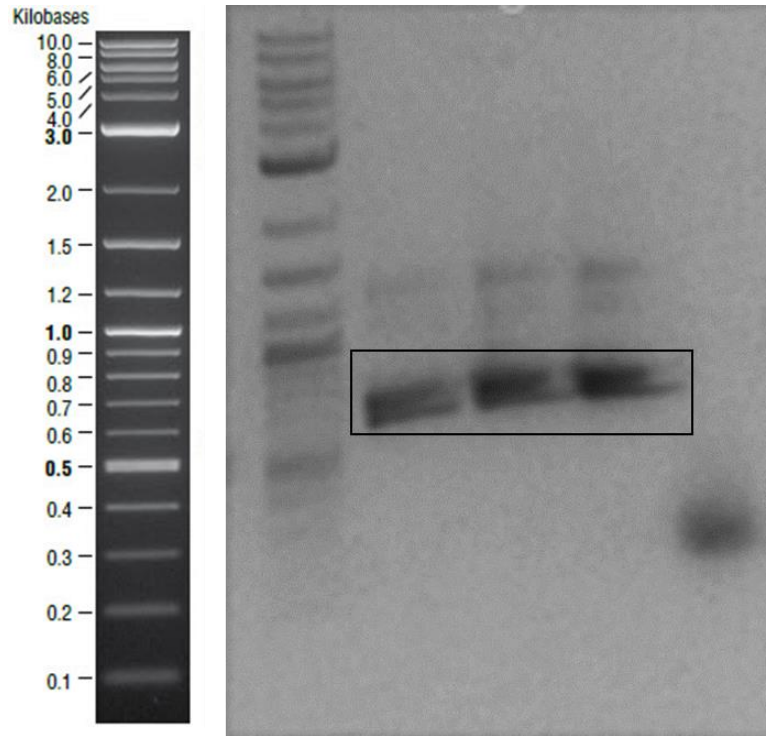


Figure 6- Agarose gel image of the second PCR to obtain designed *csgA* gene fragments which were expected as ~600bp. Negative control was on the last lane.

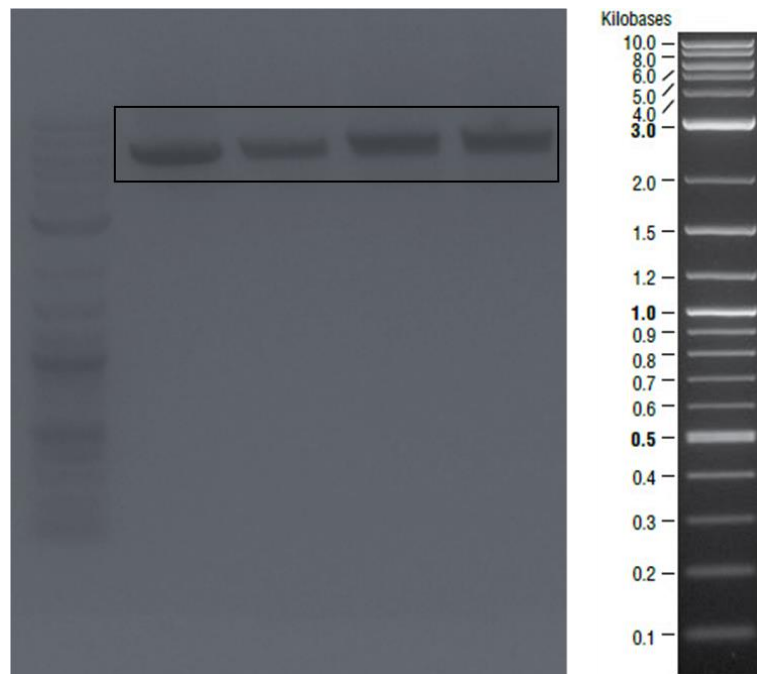


Figure 7- Linearized *pet22b* vectors expected as ~5000 bp were shown in the square.

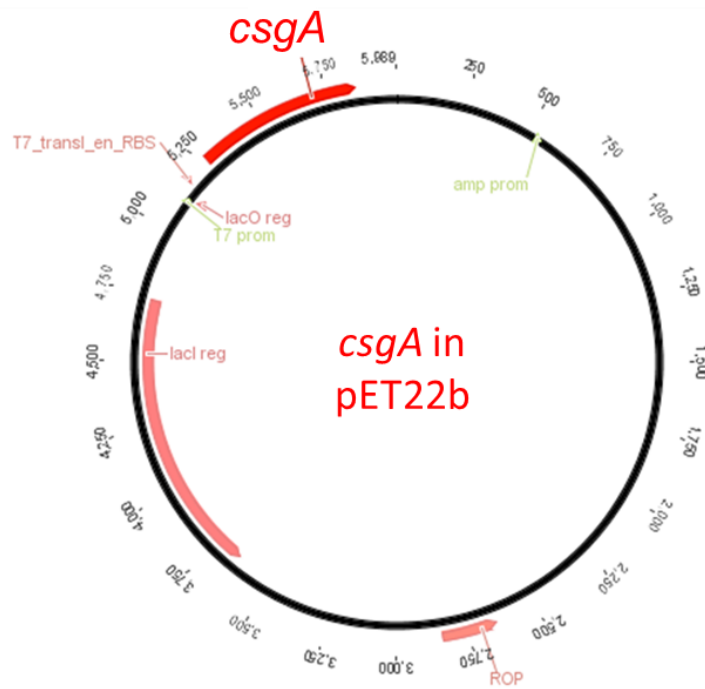


Figure 8- Schematic representation of pET22b plasmid which contained *csgA* gene fragment.

```

-----NNNNNNNNNNNAGCA-ITGCAGCAATCGTATTCTCCGGTAGCGCTCTGGCA
ATGAARCTTTTAAAAGTAGCAGCAATTGCAGCAATCGTATTCTCCGGTAGCGCTCTGGCA
*****
GGTGTGTTCCTCAGTACGGCGGCGGCGGTAACCACGGTGGTGGCGGTAATAATAGCGGC
GGTGTGTTCCTCAGTACGGCGGCGGCGGTAACCACGGTGGTGGCGGTAATAATAGCGGC
*****
CCAAATTCAGCTGAACATTTACCAGTACGGTGGCGGTAACCTCTGCACCTGCTCTGCAR
CCAAATTCAGCTGAACATTTACCAGTACGGTGGCGGTAACCTCTGCACCTGCTCTGCAR
*****
ACTGATGCCCGTAACCTCTGACTTGACTATTACCCAGCAITGGCGGCGGTAATGGTGCAGAT
ACTGATGCCCGTAACCTCTGACTTGACTATTACCCAGCAITGGCGGCGGTAATGGTGCAGAT
*****
GTTGGTCAGGGCTCAGATGACAGCTCAATCGATCTGACCCAACGTTGGCTTCGGTAACAGC
GTTGGTCAGGGCTCAGATGACAGCTCAATCGATCTGACCCAACGTTGGCTTCGGTAACAGC
*****
GCTACTCTTGATCAGTGGAAACGGCAAAAATTCGAAATGACGGTTAAACAGTTCGGTGGT
GCTACTCTTGATCAGTGGAAACGGCAAAAATTCGAAATGACGGTTAAACAGTTCGGTGGT
*****
GGCAACGGTGCAGCAGTTGACCAGACTGCAICTAACTCCTCCGTCAACGTGACTCAGGTT
GGCAACGGTGCAGCAGTTGACCAGACTGCAICTAACTCCTCCGTCAACGTGACTCAGGTT
*****
GGCTTTGGTAACAACGCGACCGCTCATCAGTACGGTACCGGCGGTAGCGGTGGCGGTAGC
GGCTTTGGTAACAACGCGACCGCTCATCAGTAC-----
*****

```

Figure 9- Sequence alignment of cloned *csgA* gene fragment. Sequences from Genewiz were highlighted with yellow and original sequence on the bottom line. Aligned bases were marked with stars.

Then, new recombinant plasmid was digested with NcoI and KpnI enzymes to extract *csgA* gene fragment and loaded to the agarose gel. Backbone was extracted from the gel (Figure 10). *csgB* gene fragment was amplified from *E.coli* genome and PCR products of CsgB are shown schematically in Figure 11. Also, agarose gel image is demonstrated in Figure 12. Then, extracted PCR products were digested with NcoI and KpnI to insert *csgB* gene fragment into pET22b vector. Designed plasmid construct is represented in Figure 13. Plasmid constructs were sequenced by Genewiz and alignment is shown Figure 14.

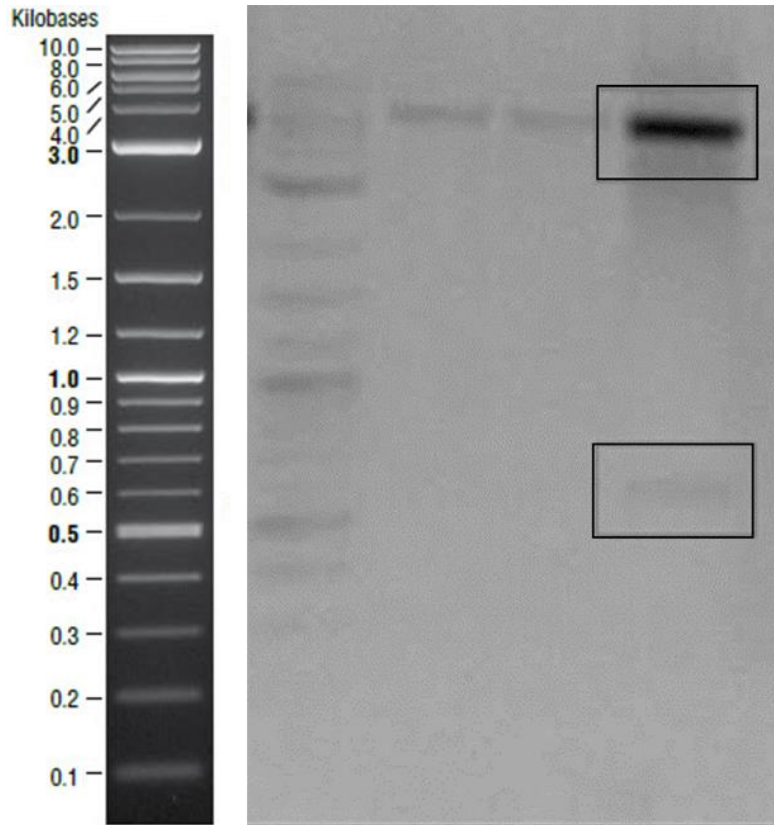


Figure 10- Digested plasmids that contained *csgA* gene. Samples digested with *Nco*I were on the second lane and digested with *Xho*I were on the third lane. On the last lane, samples were digested with *Nco*I and *Xho*I endonucleases. Backbone ~5000 bp shown in the upper square and *csgA* gene ~500 bp shown in the bottom square.



Figure 11- Schematic representation of amplified *csgB* gene fragment.

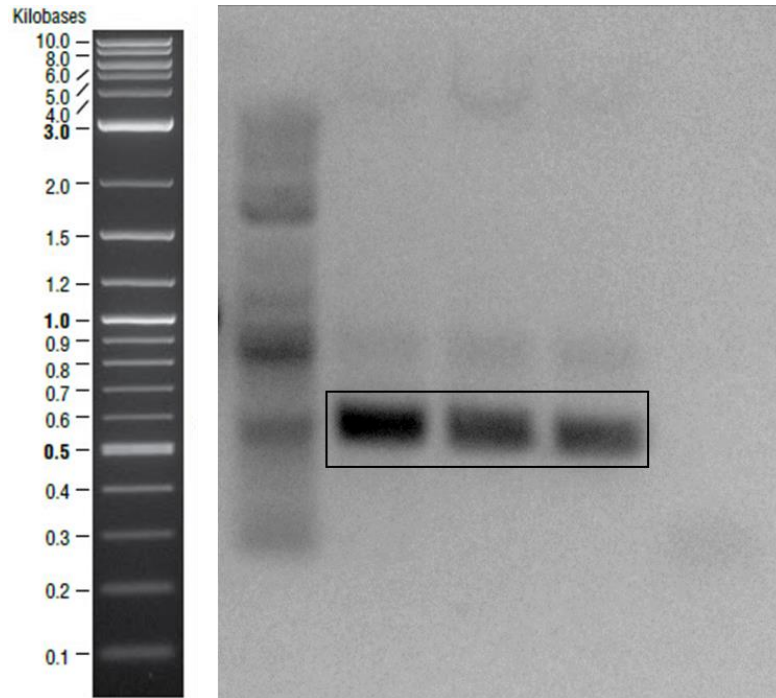


Figure 12- Amplified *csgB* gene fragments ~500bp shown in the square. Negative control was on the last lane

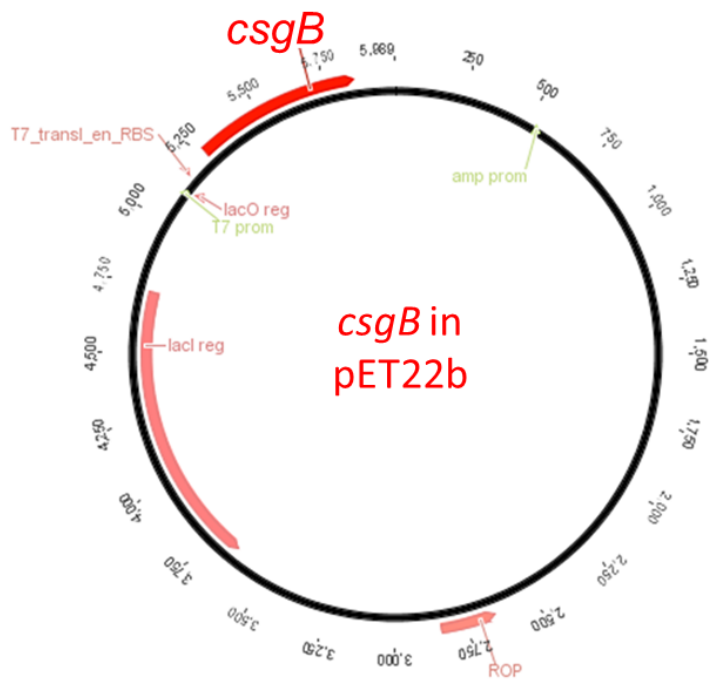


Figure 13- Plasmid construct which is designed to express CsgB proteins.

```

NNNNNNNNNNNNNNNNNNNNNNNNNNNNNNANGATGTNA-CAATACTGGGTGCGCCTGGGATT
-----ATGAAAAACAAATTGTTATTTATGATGTTAACAACTACTGGGTGCGCCTGGGATT
* * ***** * *****
GCAGCCGCAGCAGGTTATGATTTAGCTAATTCAGAATATAACTTCGCGGTAATGAATTG
GCAGCCGCAGCAGGTTATGATTTAGCTAATTCAGAATATAACTTCGCGGTAATGAATTG
*****
AGTAAGTCTTCATTTAATCAGGCAGCCATAATTGGTCAAGCTGGGACTAATAATAGTGCT
AGTAAGTCTTCATTTAATCAGGCAGCCATAATTGGTCAAGCTGGGACTAATAATAGTGCT
*****
CAGTACGGCAGGGAGGCTCAAACTTTTGGCGGTGTGTCGCAAGAAGGTAGTAGCAAC
CAGTACGGCAGGGAGGCTCAAACTTTTGGCGGTGTGTCGCAAGAAGGTAGTAGCAAC
*****
CGGGCAAGATTGACCAGACAGGAGATTATAACCTTGCATATAITGATCAGGCGGGCAGT
CGGGCAAGATTGACCAGACAGGAGATTATAACCTTGCATATAITGATCAGGCGGGCAGT
*****
GCCAACGATGCCAGTATTTTCGCAAGGTGCTTATGGTAATACTGCGATGATTATCCAGAAA
GCCAACGATGCCAGTATTTTCGCAAGGTGCTTATGGTAATACTGCGATGATTATCCAGAAA
*****
GGTCTGGTAAATAAGCAATATTACACAGTATGGTACTCAAAAAACGGCAATTGTAGTG
GGTCTGGTAAATAAGCAATATTACACAGTATGGTACTCAAAAAACGGCAATTGTAGTG
*****
CAGAGACAGTCGCAAAATGGCTATTCGCGTGACACAACGTGGTACCGCGGTAGCGGTGGC
CAGAGACAGTCGCAAAATGGCTATTCGCGTGACACAACGTGGTACCGCGGTAGCGGTGGC
*****

```

Figure 14- Sequence analysis of *csgB* gene. Sequences from Genewiz were highlighted with yellow and original sequence was on the bottom line. Aligned bases were marked with stars.

3.2 Purification of Recombinant Proteins

Recombinant proteins were produced with affinity tags at C term. Guanidine hydrochloride (GdnHCl) was used as denaturing agent because of high tendency of the proteins of oligomerization. It has been reported that after purification of CsgA and CsgB immediately polymerized and amyloid fibers should be disrupted to linearize those proteins. Boiling and SDS were not enough to break amyloid core. Although boiling is enough to break soluble proteins, in that case fading bands on the

SDS polyacrylamide gel were observed on the SDS polyacrylamide gel.[53] In addition, GdnHCl should be removed before SDS PAGE because of its ionic nature. Hence, eluted proteins were washed with PBS in order to remove GdnHCl and imidazole contents. In this study, whole characterization assays were performed in PBS media. After elution and buffer exchange steps, amyloid core disrupted with formic acid to load gel. Low pH of formic acid also changes pH of the gel hence formic acid should be vaporized. For this aim, a few drops of formic acid were added to the eluted proteins in PBS media and lyophilized to vaporize formic acid. Lyophilized samples were dissolved in Laemmli sample buffer and loaded to the gel. Expected molecular weight of CsgA and CsgB were calculated as 18670 and 19620 Da, respectively. ExPASy tool was used in molecular weight calculation.[123] TGX satin free gel used to visualize CsgA samples and protein oligomers were shown in Figure 15. CsgB oligomers observed in SDS polyacrylamide gel in Figure 16. Recombinant proteins were validated with Western Blot and membrane image was shown in Figure 17.

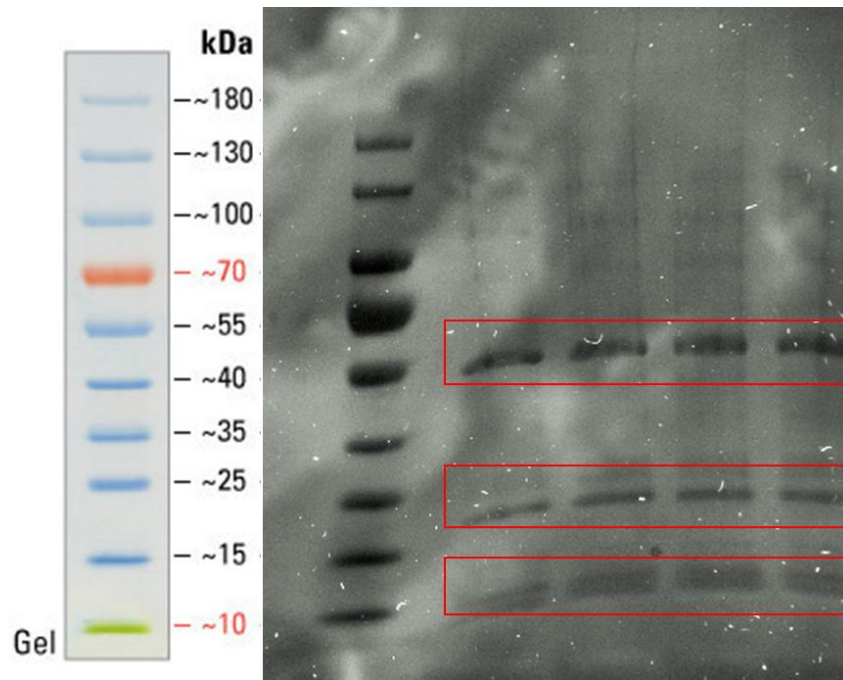


Figure 15- CsgA monomers, dimers and trimers shown in SDS polyacrylamide gel.

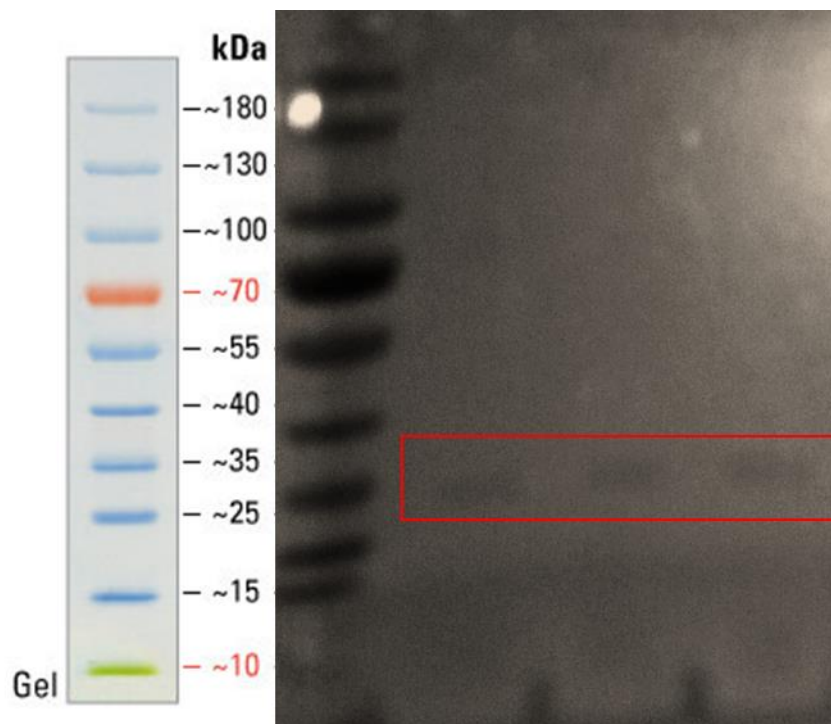


Figure 16- CsgB oligomers were indicating in red square.

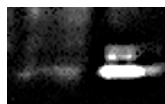


Figure 17- PVDF membrane of CsgA (on the left) and CsgB (on the right). They have different assembly characteristics and this might affect antibody binding so CsgB bands are brighter than CsgA.

3.3 Amyloid Formation Assay

One of the shared properties of amyloids is binding ability to Thioflavin T which is a fluorescent dye. After buffer exchange, equimolar mix samples of CsgA and CsgB were prepared. Sample concentrations were determined with BCA Assay. 7 μ M pure CsgA, 7 μ M pure CsgB and equimolar mix samples were treated with ThT (20 μ M final ThT concentration). Fluorescence signals were measured during 16 hours with ten minutes intervals and 5 second shaking before each measurement. Fluorescent signals were normalized which is previously described.[117] Graphs belong to each sample is shown in Figure 18. Fluorescent signals were recorded in each case. Yet, CsgB samples gave much signals than others. This might be caused from faster polymerization of CsgB which was reported previously.[124] Mix sample had similar behavior with CsgA. It has been known that CsgA and CsgB interact with each other and this might slow down CsgB oligomerization so lower signals might be recorded in that case.

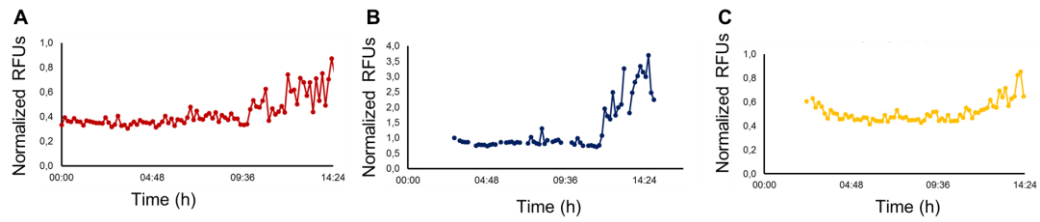


Figure 18- ThT assays of CsgA, CsgB and equimolar mix sample. Binding capabilities of the purified proteins to Thioflavin T dye were proved by measuring fluorescent signals. Measurements were performed during 16 hours CsgA in A), CsgB in B) and mix of CsgA and CsgB in C). The highest RFU values were recorded with CsgB fibers.

3.3 Secondary Structural Analyzes

Amyloids have β sheet rich structures which constitute rigid amyloid core formation.[76] Far UV CD spectra of samples were measured in PBS media. Equimolar mixed sample was also prepared after buffer exchange. Samples were incubated at room temperature to induce fiber formation after buffer exchange process. CD spectra of aged samples are shown in Figure 19. By using web based tool which was introduced previously was used to analyze secondary structure elements.[122] Proportion of secondary structure elements were calculated. Data of differently aged samples (3 hours, 15 days and 30 days) are demonstrated in Figure 18. In all cases, samples had low helix content. β sheet content was changing with incubation time in CsgA samples. The most important increment was recorded in CsgB samples. 30 days aged CsgB samples had the highest β sheet ratio and high β sheet ratio was achieved with longer incubation time. Also, β sheet elements have role in stable and rigid core formation of amyloids. It could be concluded that more rigid structure may be obtained by using CsgB proteins. In addition, it was proved

that CsgB polymerize faster than CsgA hence to convert more β sheet elements as high as CsgB might be required more incubation period. Behavior of the mix samples were similar with pure CsgA samples like ThT assay. It was also in agreement that CsgA interacts with CsgB proteins and CsgA may prevent CsgB oligomerization by binding it to interaction sites. Rearrangements of secondary structural elements were demonstrated with this data.

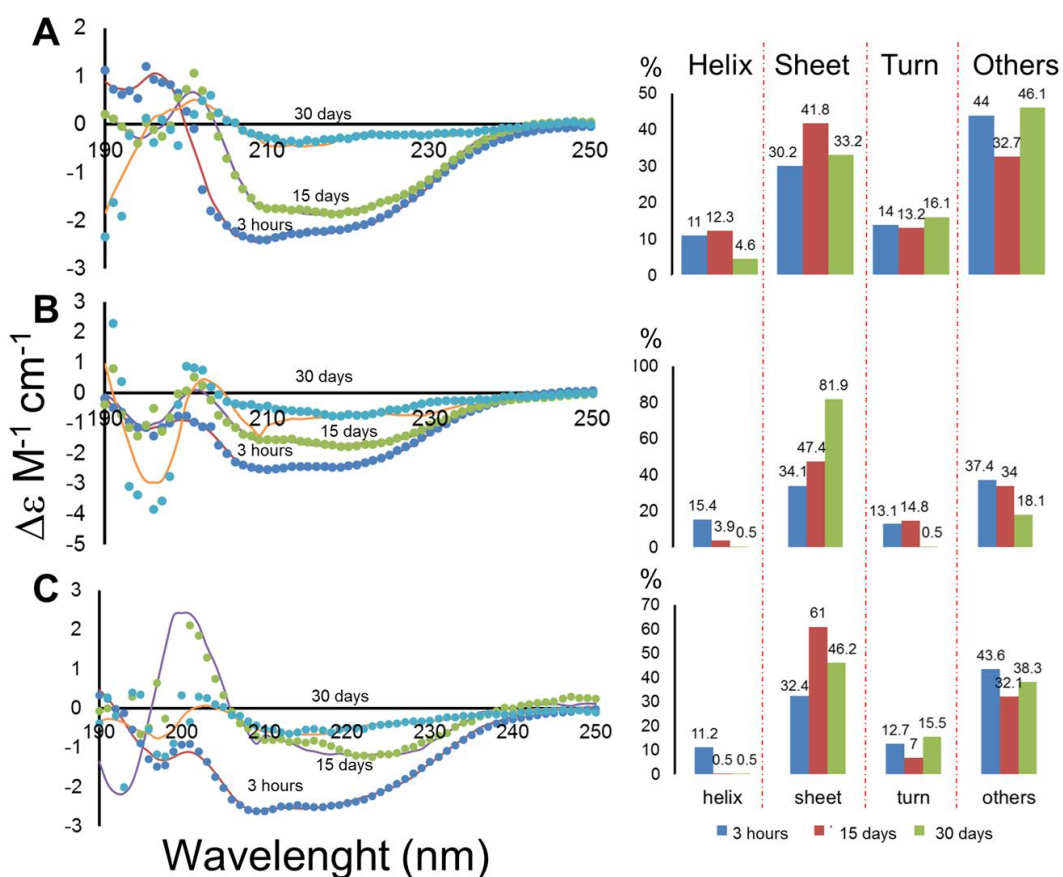


Figure 19- Secondary structural analysis of purified proteins and mix sample. CD spectra of the samples are demonstrated on the left and ratio of secondary structural elements are on the right. Data of aged CsgA is demonstrated in A), CsgB in B) and mix sample in C). Samples had low helix content in each case. Behavior of CsgA similar to mix sample. β sheet ratio of CsgB fibers were increasing with incubation time and 30 days aged CsgB sample had the highest sheet ratio.

3.4 Immunochemistry Assay

Quartz crystal microbalance with dissipation is highly sensitive technique to identify protein-protein or protein-cell, protein-material interactions.[125-127] Structural changes/rearrangements could be analyzed quantitatively. Frequency and dissipation changes are recorded. Frequency changes reflect mass deposition on the sensor surface while dissipation changes are related to water holding capacity of the sample. For instance, increment in the dissipation signals reflect gel-like sample while water loss result in a decrease.[128-130] Hence, it was concluded that dissipation signal showed the rigidity of samples. Water loss could be occur during the changing or rearrangement of the structural elements and easily detected by monitoring dissipation signals. Also, binding ability of sample to the materials is assumed from frequency changes.

In addition to Western Blot analysis, purified proteins were validated with immunochemistry assay. Purified proteins in PBS media deposited on the gold coated sensor surface and washed with PBS in order to remove unbound proteins. PBS flowed through the instrument until two signals reach the equilibrium. When signal changes reached the equilibrium, anti-his primary antibodies were flowed. System was also washed with PBS to remove unbound molecules. Then, fluorescent labelled secondary antibodies were added to probe primary antibodies. Washing step was also applied. Those assays were performed for 2 μ M freshly purified CsgA and 5 μ M freshly purified CsgB proteins. Sensor surfaces were monitored with laser scanning confocal microscopy (LSCM) which is demonstrated in Figure 20. In addition, antibodies were diluted in PBS to get rid of side effects on both signals.

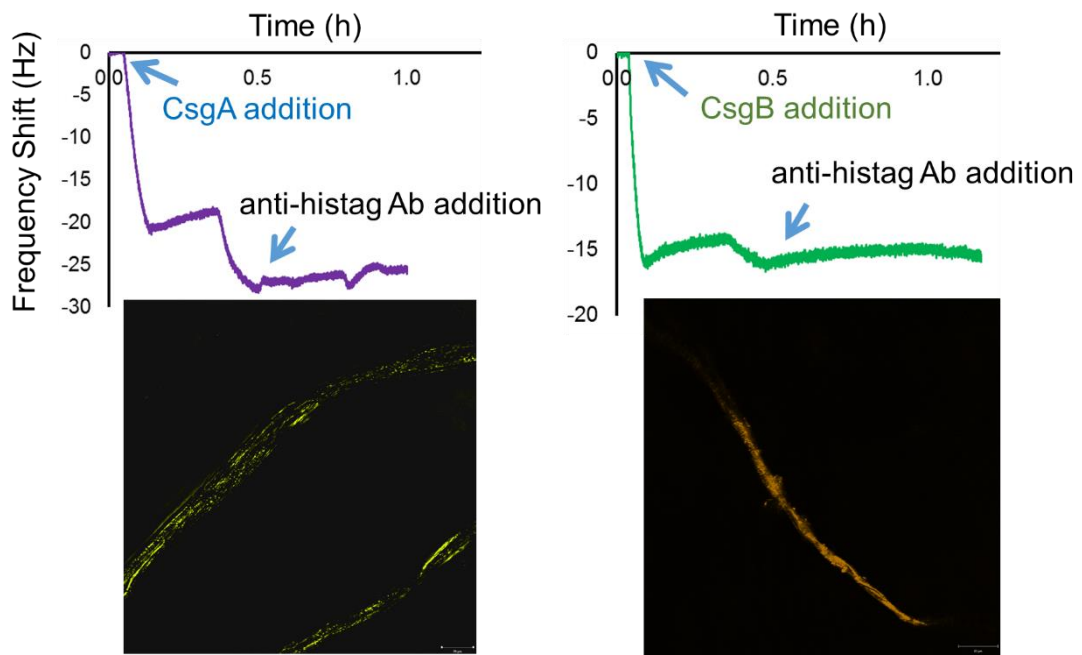


Figure 20- Antibody binding assays of purified CsgA and CsgB proteins. Sensor surface was coated with CsgA (on the left) and CsgB (on the right), proteins were probed with fluorescent labelled secondary antibodies and frequency changes were recorded. Protein and primary antibody addition points are shown with arrows. Shifts which were caused from primary and secondary antibodies were too small compared to protein polymer shifts. Hence, their shifts were not seen clearly in this figure. Sensor surfaces were examined with laser scanning confocal microscopy. Image of probed CsgA is demonstrated on the left and CsgB is on the right.

3.5 Fiber Formation Assay

To analyze in vitro polymerization kinetics of the purified proteins gold coated sensors were used in QCM experiments. Self-seeding and cross-seeding strategies were applied which is represented schematically in Figure 21. Self-seeding strategies which fibers seeded with same fresh proteins and also cross-seeding strategies that fibers seeded with other purified proteins were applied. In these cases,

fresh CsgA were added upon CsgB fibers and vice versa. Hence, four different cases were identified in this study.

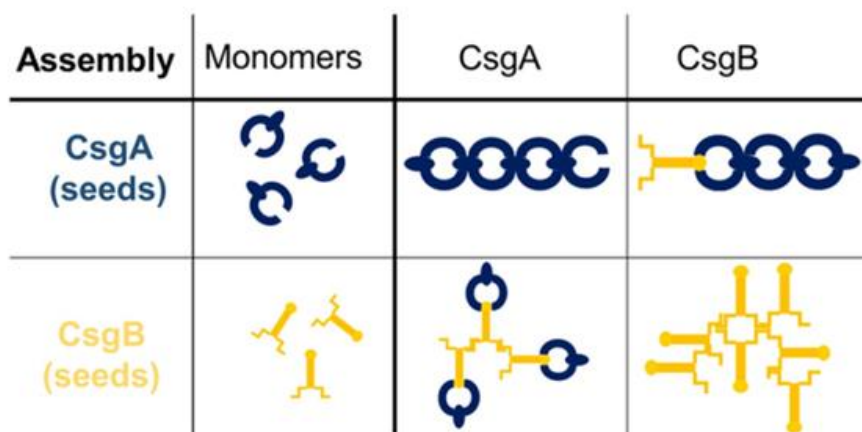


Figure 21- Self-seeding and cross-seeding strategies are schematized. In this study, interactions of polymerized CsgA with fresh CsgA and fresh CsgB; also, polymerized CsgB with fresh CsgA and CsgB were analyzed.

Recombinant proteins were overexpressed and purified in denaturing conditions. Denaturing agents removed and media of the purified proteins exchanged with PBS. After buffer exchange processes, eluted proteins separated as monomers and oligomers by using 30 kDa Amicon filter units in order to analyze fiber formation, *in vitro*.

Firstly, gold coated QCM sensors were coated with fresh CsgA or fresh CsgB. For polymerization incubated for overnight; also, changes in frequency and dissipation signals were recorded.

On the next day, to analyze fiber formation, fresh proteins were added upon the fibers with increasing concentrations. Low to high concentrations of fresh proteins were added and higher shifts were expected with increasing concentrations.

3.5.1 Self-seeding and Cross-seeding of CsgA

On the first day, gold coated QCM sensor was deposited with 10 μM CsgA (oligomers and monomers) and system was washed with PBS to remove unbound proteins. For polymerization, proteins were incubated on the sensor surface. Also, frequency and dissipation changes were recorded for overnight which are demonstrated in Figure 22. Initial attachment to the surfaces resulted in shifts in both signals. After ten hours frequency signal of CsgA sample was decreasing while dissipation signal was increasing. Those changings could be caused from rearrangements of the structural elements.

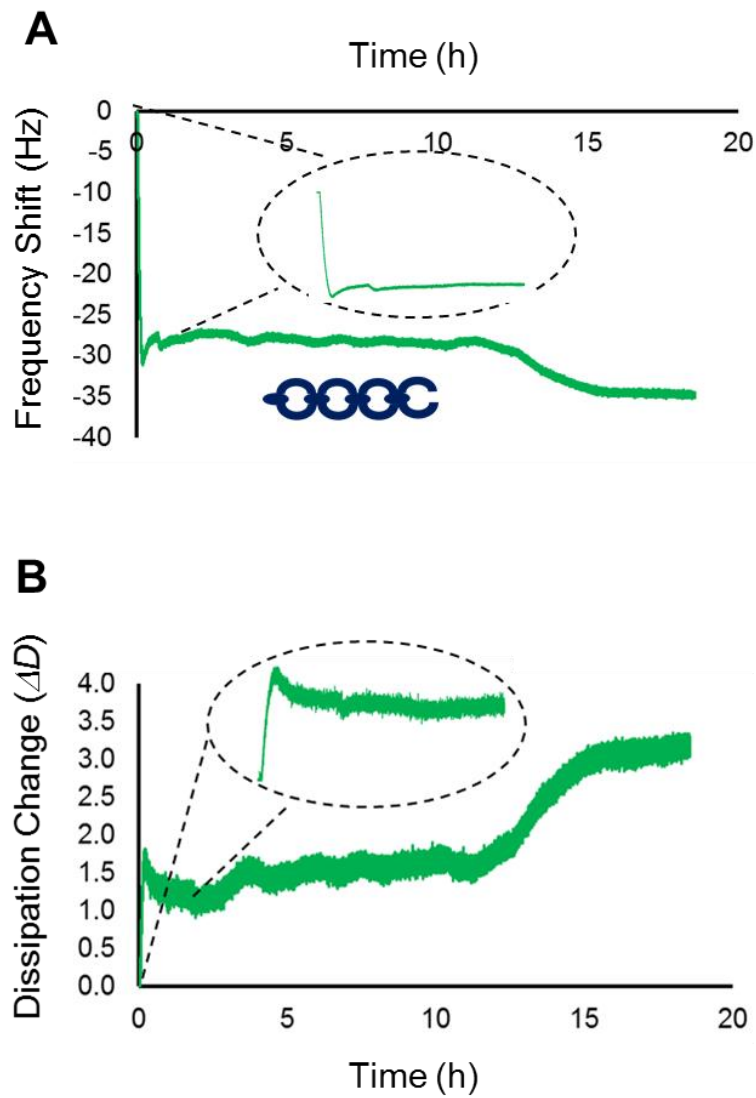


Figure 22- Overnight frequency and dissipation changes of freshly purified CsgA proteins. Gold coated sensor surface was deposited with CsgA proteins overnight frequency changes were demonstrated in A) and dissipation changes in B). Initial attachments which shown in close up views caused sharp rise and decrease in frequency and dissipation signals, respectively.

On the second day, freshly purified CsgA proteins were separated with centrifugal filter units. Molecular weight between 30 kDa and 10 kDa refer as protein

monomers hereafter. Protein monomers with diluted concentrations were flowed through the system low to high concentrations. 4 μM , 5 μM , 6 μM and 7.5 μM of fresh CsgA proteins were added upon overnight grown CsgA fibers. To identify fiber growth frequency and dissipation changes were also recorded during fresh proteins addition that is demonstrated in Figure 23. Step by step changes were recorded in both signals as shown in the graph and they show self-seeding capability of CsgA proteins. CsgA fibers could be elongated by adding fresh CsgA proteins with this strategy.

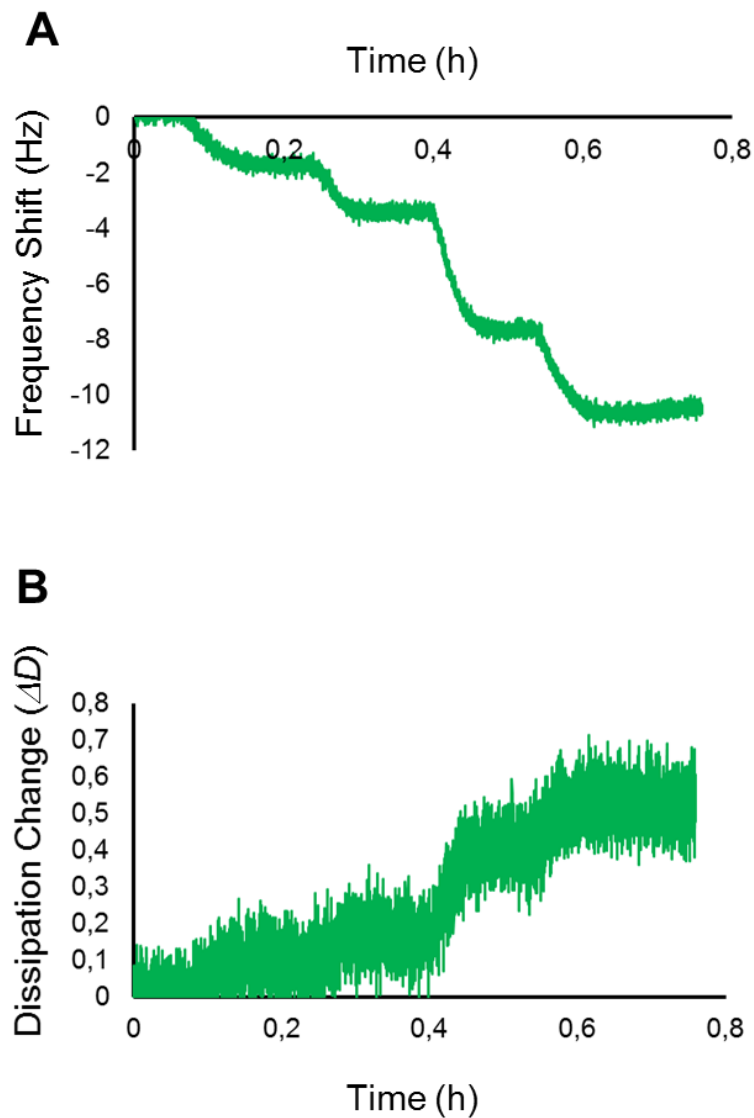


Figure 23- Freshly purified CsgA monomers were added upon polymerized CsgA fibers. Addition of fresh proteins with increasing concentrations resulted in step by step changes in frequency signals A) and dissipations signals B). Highest protein concentration caused the highest shift in this case.

Moreover, to obtain polymerized assembled structure freshly seeded fibers were incubated to measure frequency and dissipation changes for near 25 hours. Changes in both signals are demonstrated in Figure 24. Material growth could be continued by adding more amount of CsgA monomers. According to the graphs, no

significant changes were recorded in dissipation signals while frequency signal was increasing. Also, low dissipation signals gave the information about the material rigidity. Rigid structure was obtained from near 3 days growth CsgA fibers.

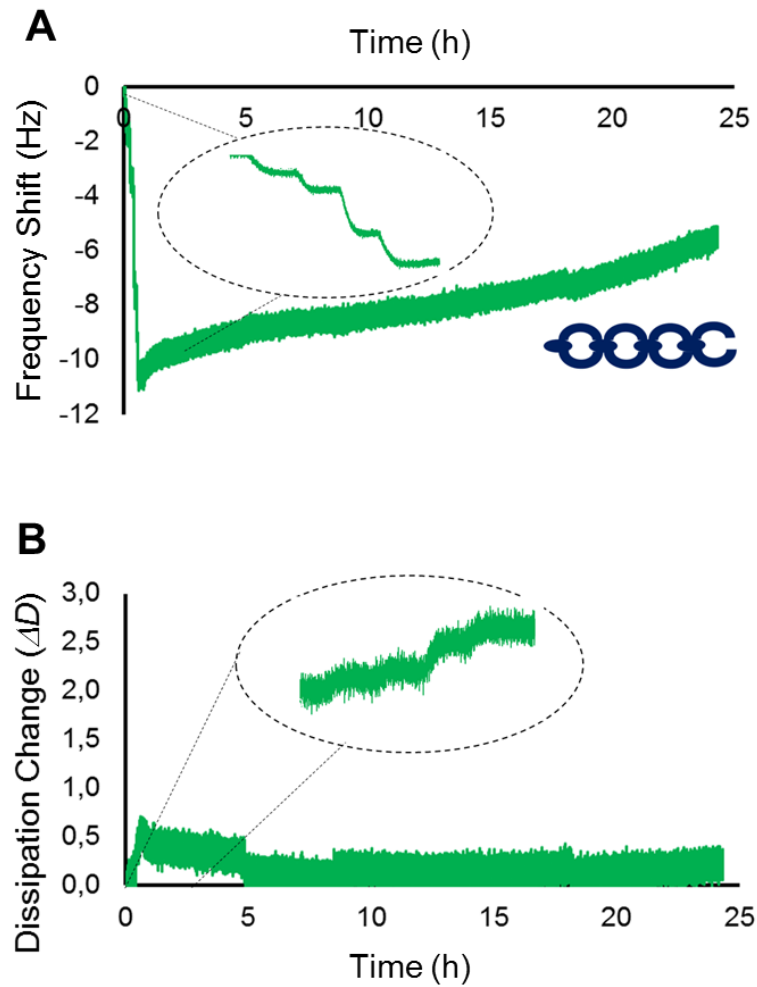


Figure 24- Overnight measurements of frequency shifts in A) and dissipation changes in B) of self-seeding CsgA proteins. Changes which caused from seeding shows in close-up views. During near 25 hours measurements, dissipation signals did not change notably while frequency shift was increasing.

Furthermore, in the second case cross-seeding of CsgA was analyzed. For this aim, overnight grown fibers which is demonstrated in Figure 22 seeded with freshly purified CsgB monomers after separation from oligomers by using spin filter units. Monomers were also added to the system with low to high concentrations (0.084 μM , 0.105 μM , 0.126 μM and 0.1575 μM fresh CsgB, respectively) but in this case, changes were not recorded during addition process which demonstrated in Figure 25. Monomer additions resulted in peaks in both signals and unbound or weakly bound proteins were removed with the following washing steps. After washing step, the signals reached the starting points which showed the loosely binding of fresh CsgB to polymerized CsgA. May be interaction sites for CsgB blocked during CsgA self-polymerization. In addition, after secretion to the ECM CsgA proteins interact with outer membrane bound CsgB to form hierarchically ordered fibers, naturally.[131]

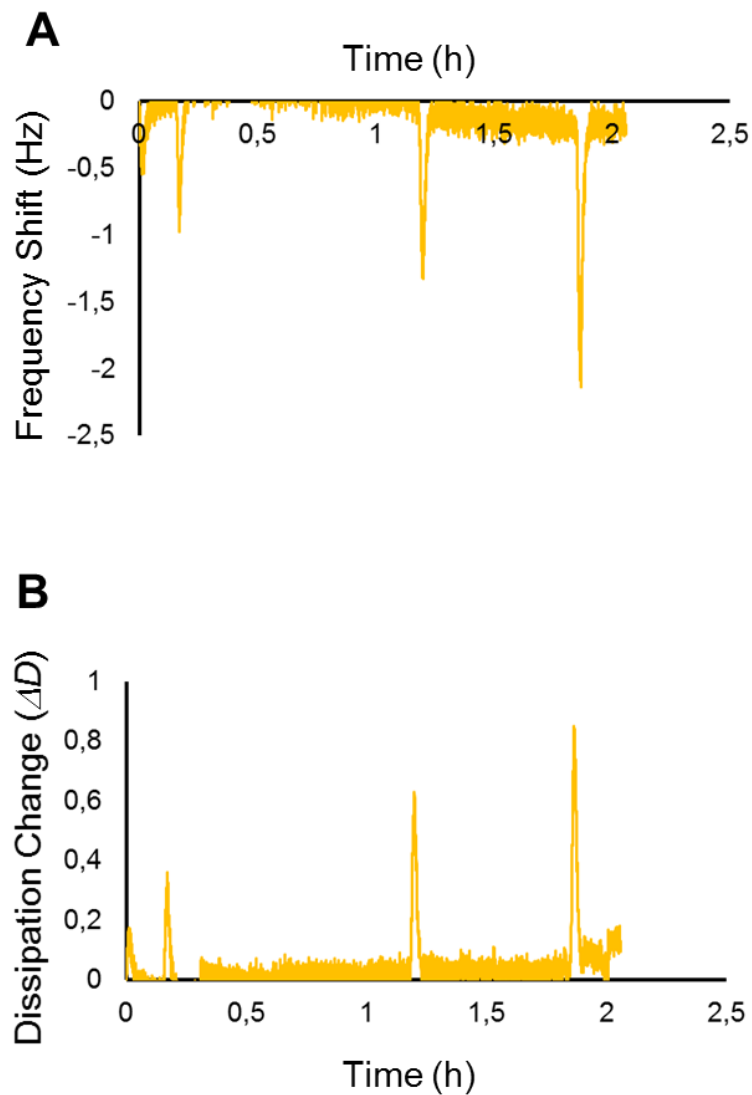


Figure 25- Fresh CsgB proteins flowed through the system to analyze interactions of fresh CsgB and CsgA fibers. Peaks belonged to addition point but no significant changes were recorded after the washing steps. Frequency shifts are shown in A) and dissipation changes in B).

Frequency shift and dissipation change were also recorded for near 20 hours which is demonstrated in Figure 26. Notable changes did not recorded in both signals as shown clearly in the graphs. Moreover, dissipation did not change significantly in

both self-seeding and cross-seeding of CsgA fibers and it showed the formation of dense protein layers.

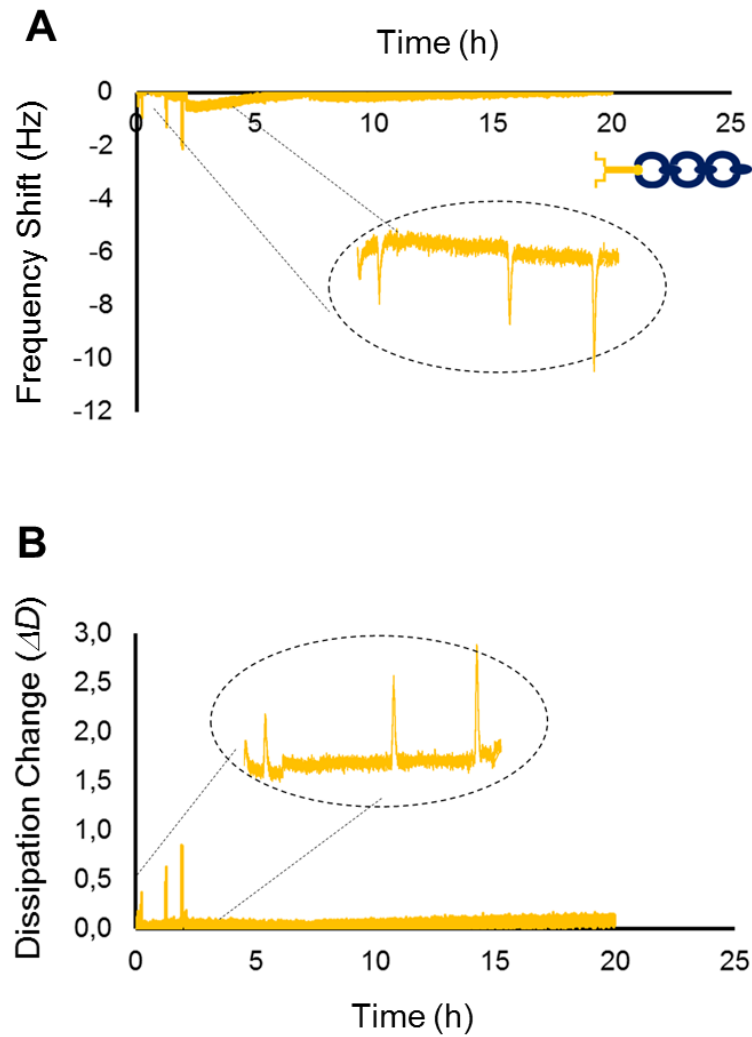


Figure 26- Cross-seeding of CsgA fibers with fresh CsgB proteins. Frequency changes are shown in A) while dissipation changes are shown in B). CsgB addition did not cause dramatic changes. Peaks caused from the monomer addition but unbound CsgB proteins were removed with the washing steps.

3.5.2 Self-seeding and Cross-seeding of CsgB

In the third case, self-seeding of CsgB was identified. Firstly, freshly purified 6,3 μM CsgB proteins were deposited on the gold coated sensor surface, like CsgA case. To obtain polymers fresh proteins were incubated at room temperature and changes on the both signals were recorded that is shown in Figure 27. Protein deposition caused shifts in both signals. No significant changes were recorded during overnight incubation for CsgB proteins.

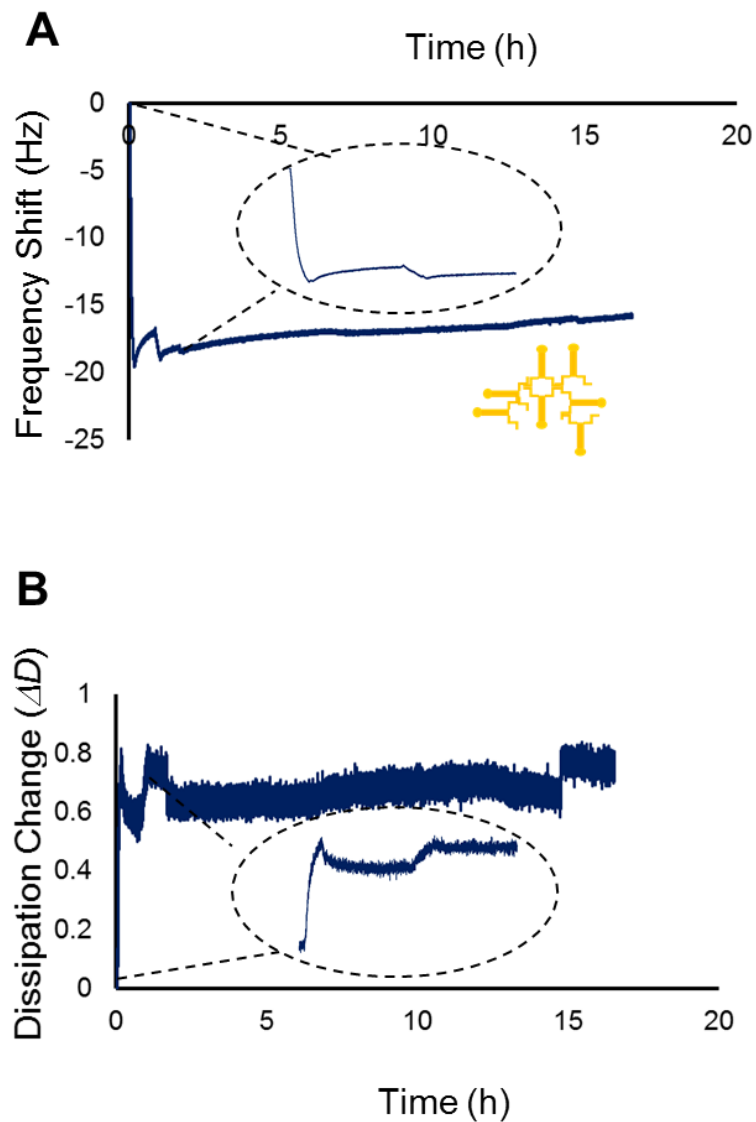


Figure 27- Frequency and dissipation changes of freshly purified CsgB proteins. Purified proteins were deposited on gold coated sensor surface and incubated for overnight for polymerization. Recorded frequency changes in A) and dissipation changes in B). Sharp changes in both signals were caused from the initial attachments. Slight changes were recorded during overnight measurements in both signals.

On the second day, 1.35 μM , 1.8 μM , 2.25 μM , 2.7 μM and 3.6 μM of fresh CsgB, respectively, added upon CsgB fibers. Changes on both signals were recorded during fresh protein addition are demonstrated in Figure 28 and during near 20 hours incubation are shown in Figure 29. Small peaks were recorded which caused from the protein addition. System washed with PBS until both signals reach the equilibrium and in this case experiment lasted near 6 hours because of the long washing steps. Also, faster shifts were observed in self-seeding of CsgB and it indicates that CsgB interactions stronger than self-CsgA interactions.

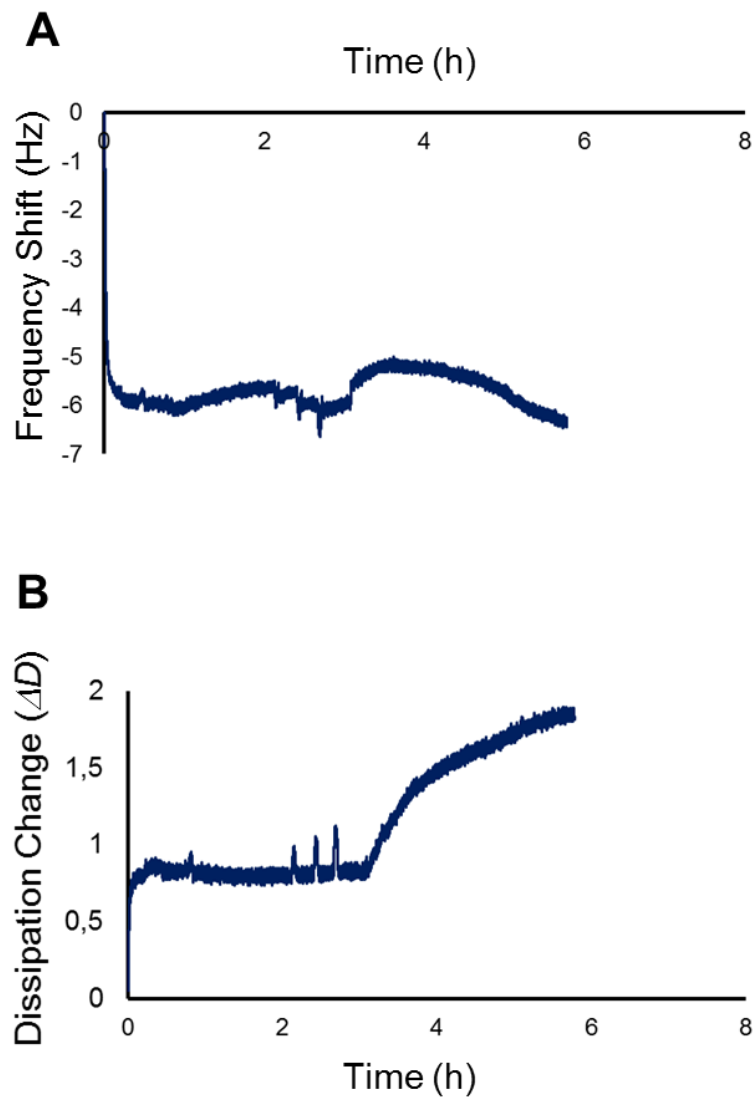


Figure 28- Grown CsgB fibers seeded with fresh CsgB. Fresh CsgB proteins were flowed through the system with increasing concentrations but small shifts were recorded in frequency shifts in A) and dissipation shifts in B).

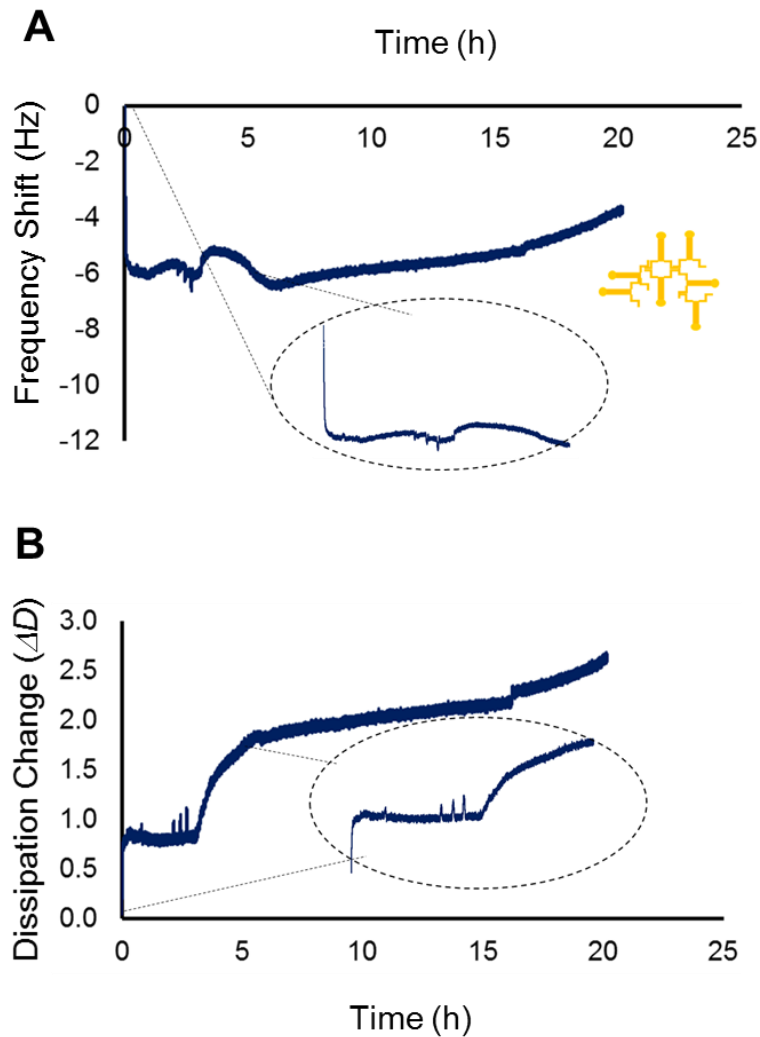


Figure 29- Overnight measurements of self-seeding of CsgB proteins. Fresh proteins additions shown in close-up view and slightly changes on both signals were recorded during near 20 hours measurement. Frequency shifts are shown in A) and dissipation changes are shown in B).

In the last case, CsgB fibers seeded with fresh CsgA proteins with diluted concentrations. $0.09 \mu\text{M}$, $0.12 \mu\text{M}$, $0.15 \mu\text{M}$, $0.18 \mu\text{M}$ and $0.24 \mu\text{M}$, of fresh CsgA were added upon CsgB polymers, respectively. Step by step changings were observed which is similar with self-seeding of CsgA case. Step by step changings are demonstrated in Figure 30 clearly. Higher shifts obtained with higher protein

concentrations. Moreover, the signals were recorded during 20 hours which are shown in Figure 31. Fresh protein addition processes are also shown in both graphs. During overnight measurements, both signals were increasing which showed structural rearrangements.

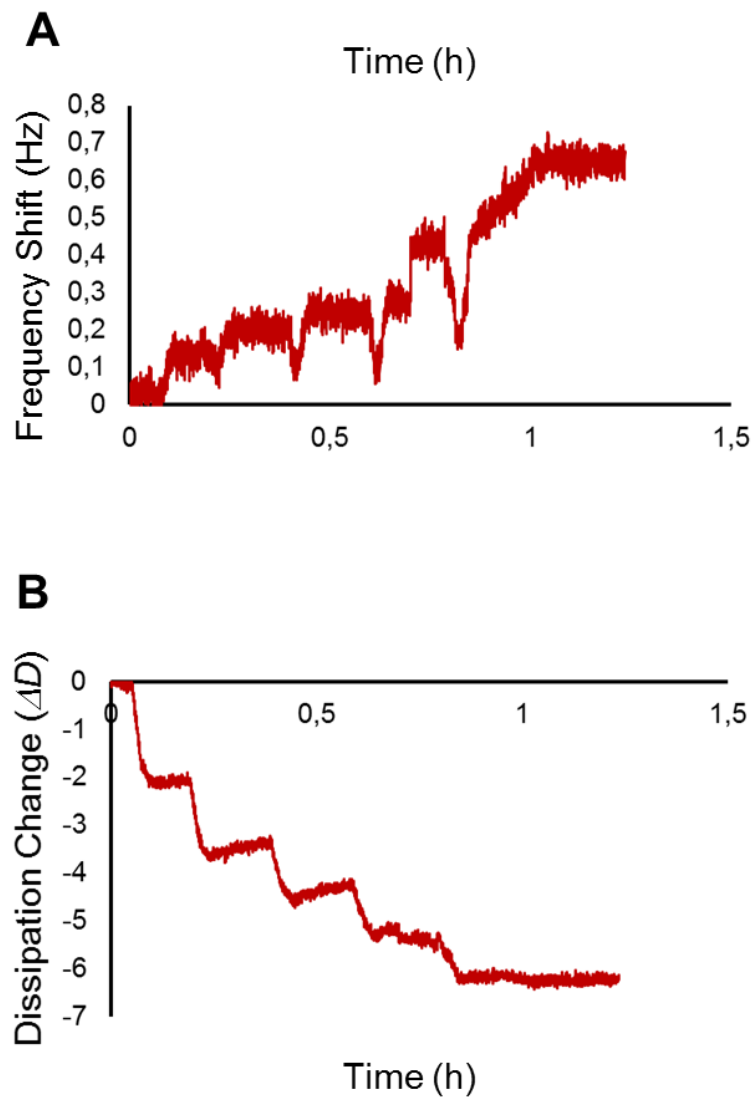


Figure 30- Polymerized CsgB seeded with fresh CsgA as a cross-seeding strategy. Addition of proteins with increasing concentrations cause regular changes on frequency signals in A) dissipation signals in B).

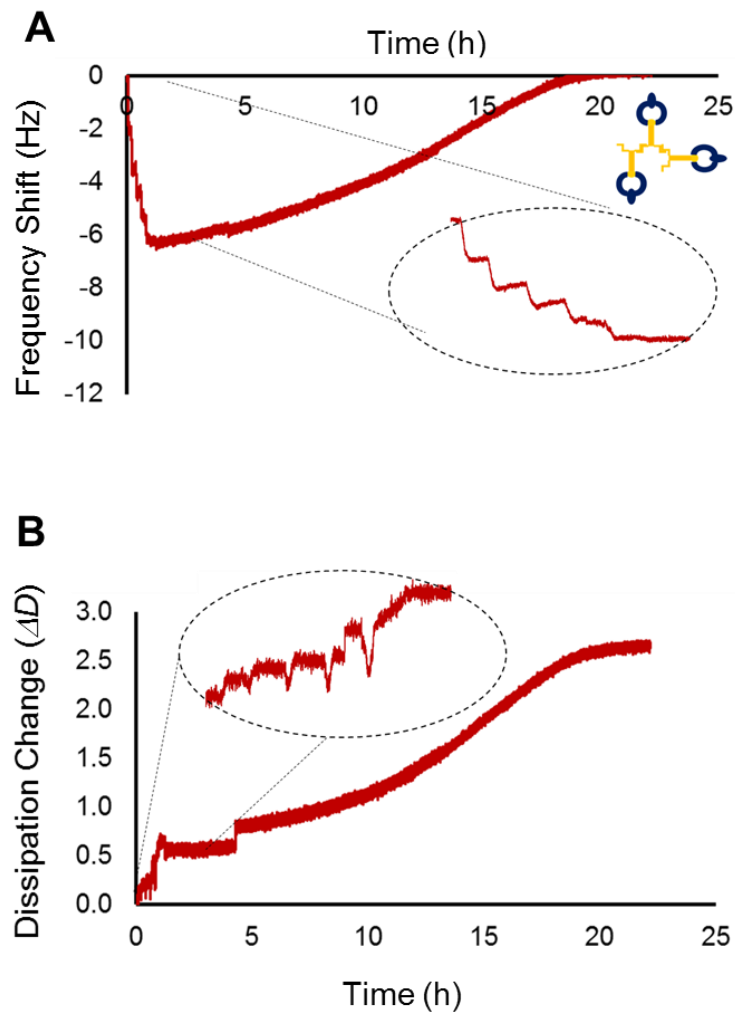


Figure 31- 20 hours measurements of cross-seeding CsgB fibers with fresh CsgA. Shifts showed the interactions between fibers and fresh proteins. Frequency shifts are shown in A) while dissipation changings are shown in B).

To sum up, step by step changings which show strong interactions were observed in self-seeding of CsgA and cross-seeding of CsgB polymers. Fiber elongation could be achieved by adding more amount of fresh CsgA upon CsgA fibers for materials growth. On the other hand, small shifts observed in self-seeding of CsgB and cross seeding of CsgA polymers with CsgB monomers. While seeding CsgB fibers with fresh CsgB, faster shifts were recorded which are a good indicator

that showed self CsgB interactions were stronger than self CsgA interactions. Small shifts which recorded from polymerized CsgA and fresh CsgB interactions showed the loose binding capability. It may be caused from blocking of interaction sites during the polymerization. Moreover, low dissipation signals showed the formation of dense protein layers. According to data of dissipation signals, rigid structures were obtained with polymerized CsgA feeding with CsgA monomer. Softer structures were obtained by seeding of overnight growth CsgB. Also, it was concluded that protein addition order determine the final fiber structure.

3.6 Imaging of Curli Materials

3.6.1 Scanning Electron Microscopy Imaging

Protein deposited sensor surfaces were examined with scanning electron microscopy (SEM) in order to analyze final morphology of assembled structures. It was shown clearly final assembled structure changed with order of the protein addition. Polymerized CsgA fed with fresh CsgA was shown in Figure 32. Long and branched fibers were formed with assembly of CsgA proteins. Small particles around the elongated fibers were observed so fiber could serves seeding site to increase the thickness. Also, with the addition of fresh CsgA more dense and elongated fiber networks could be formed. According to CD data of CsgA proteins, they were less structured and so they were more flexible and suitable for interaction with other proteins.

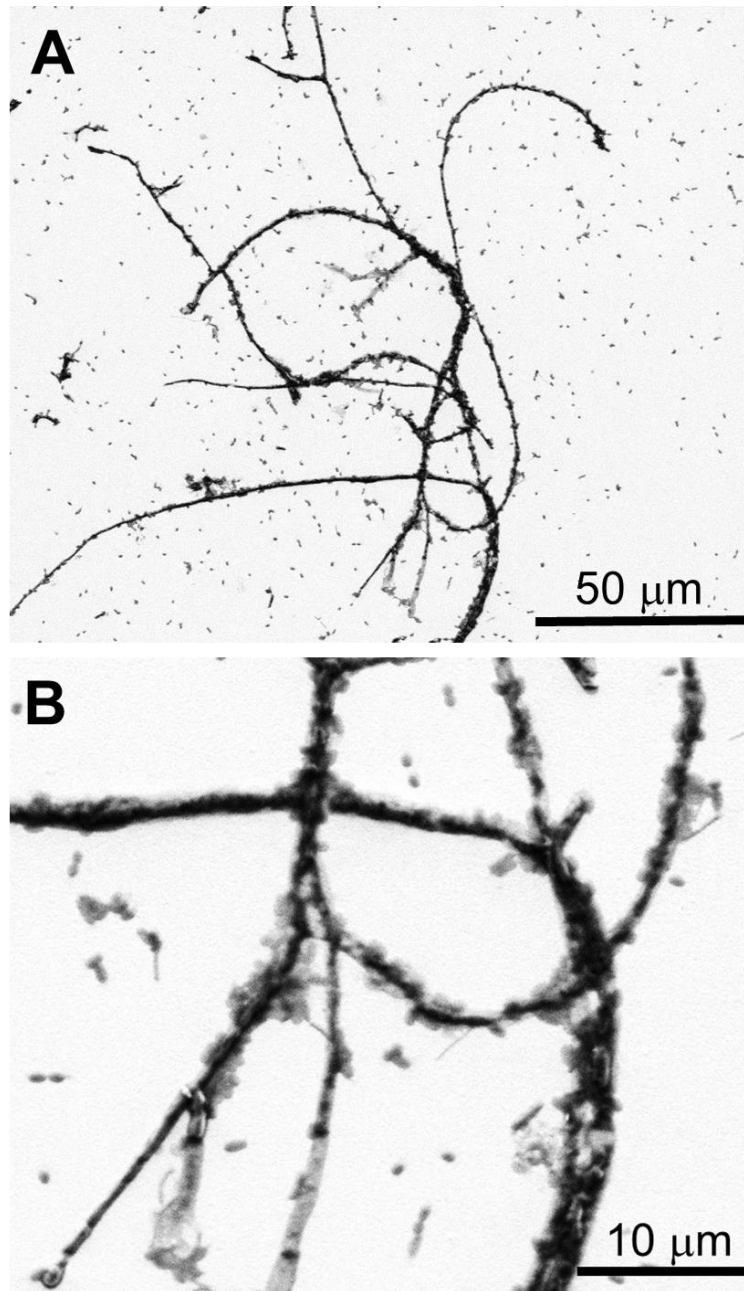


Figure 32- SEM image of long and branched CsgA fibers. Freshly purified CsgA proteins added upon polymerized CsgA and incubated for overnight for QCM analysis. SEM image of near 3 days aged fibers on gold coated sensor surface in A) and close up view in B).

In the second situation, polymerized CsgA fed with CsgB polymers and as discussed above no significant changes in frequency and dissipation signals were recorded. Morphology of the protein fibers were similar with self-seeding CsgA fibers (Figure 33 A). CsgB is reported as nucleator protein this result in agreement with it.[132] Furthermore, seeding site at the end of the fiber shown clearly when zoom in the fiber tip (Figure 33 B).

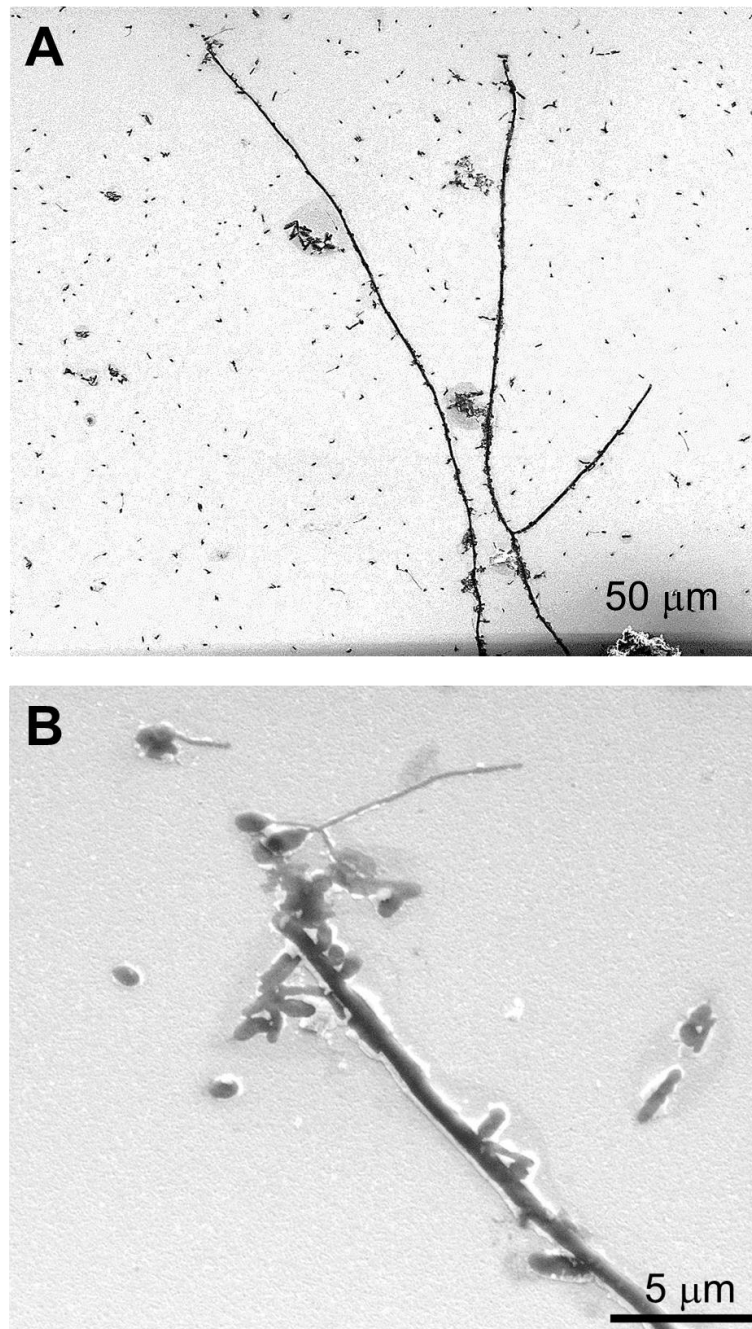


Figure 33- CsgB monomers flowed through the system to analyze their interaction with CsgA polymers. Sensor surface was observed with SEM. Long and branch fibers are seen in A) which is similar with self-seeding of CsgA fibers and seeding at the end point is shown in B).

SEM image of self-seeding CsgB is demonstrated in Figure 34. In this case, big spheres were obtained. The roughness on sphere surfaces were shown clearly in SEM image. Connection point was also shown. Previously known as, CsgB form short fibers on the cell surface and in this case assembly of those small fibers enable to grow big fiber spheres. In addition, CsgB proteins have more β sheet structure than CsgA according to CD analysis. Hydrophobicity of β sheet elements acts on the closed structure formation like sphere.

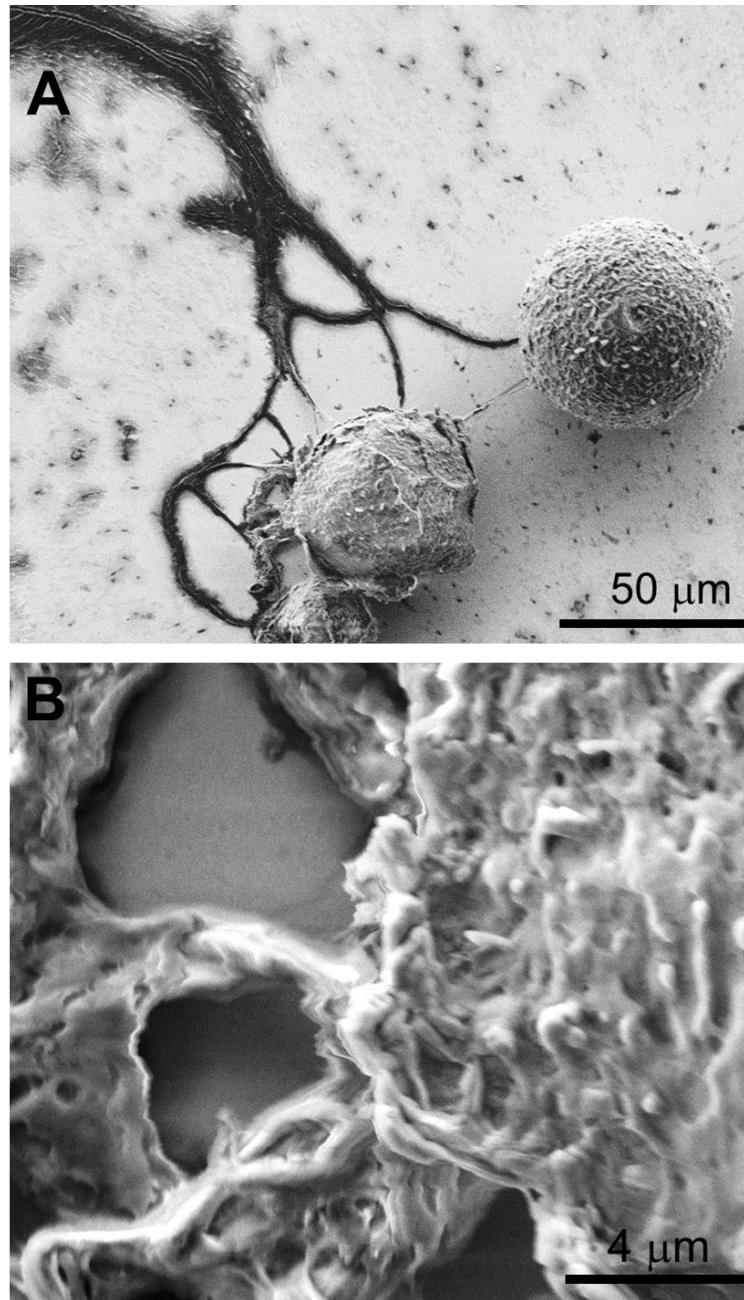


Figure 34- SEM images of CsgB fibers. Big sphere structures were obtained by self-seeding of CsgB proteins and shown in A); connection sites are shown in close up view in B).

Cross-seeding of CsgB fibers with CsgA monomers on the sensor surface are indicated in Figure 35. Spheres were observed but in this case they had smaller size. They were close to each other and connected. Interaction with CsgA monomers could result in a decrease in sphere size. Small fibers elongated from spheres are shown in Figure 35B. Those fibers might serve interaction sites for CsgA and so growth of sphere might be blocked and neighbor spheres began to grow. Hence it was concluded that sphere growth and the size could be controlled even though protein concentrations were low. As described above, elongation of fibers were also controlled in self-seeding CsgA case.

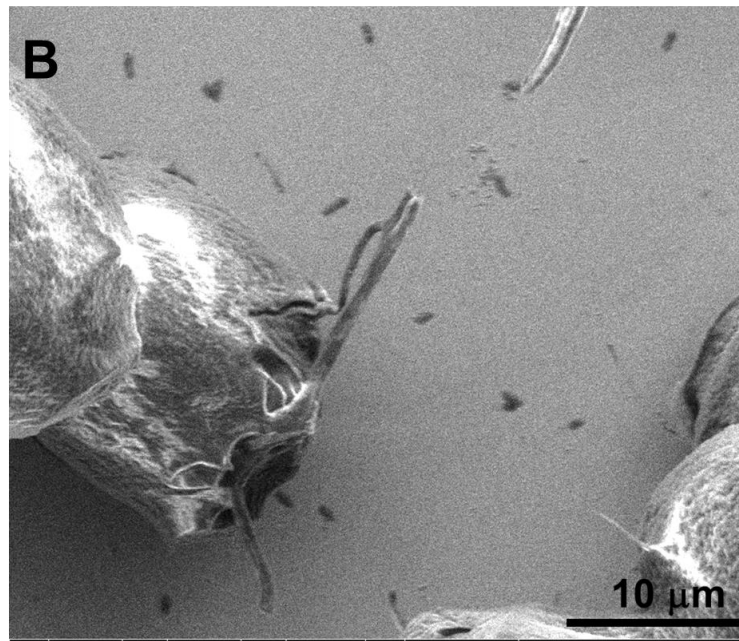
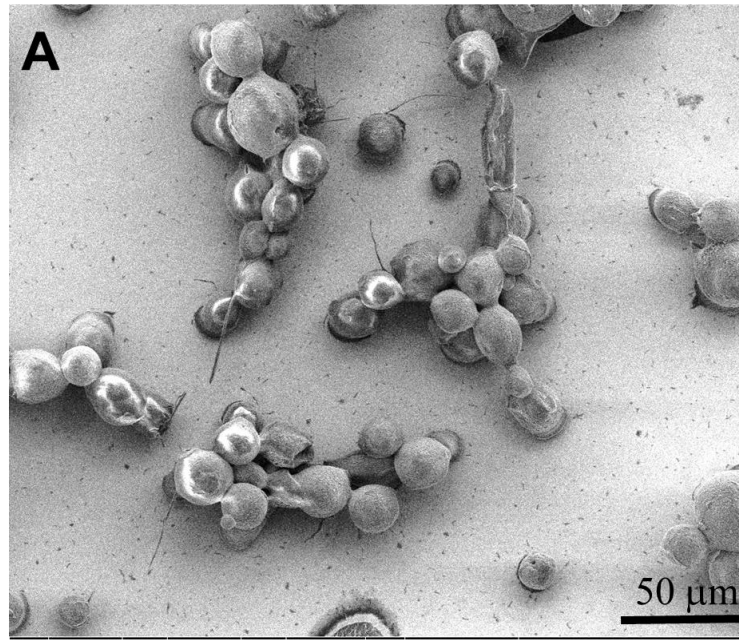


Figure 35- SEM images of CsgB fibers which seeded with freshly purified CsgA. Sphere structures were observed again but in this case size of them smaller than spheres that formed by self-seeding of CsgB demonstrated in A). Small fibers elongates from the sphere surface which is shown in B).

3.6.2 Atomic Force Microscopy Imaging

After QCM analysis, deposited QCM sensors were examined with AFM which is demonstrated in Figure 36. Dense fiber networks are shown in Figure 36A which formed by self-seeding of CsgA. ~200 nm thick fibers were formed by assembly of CsgA while ~50 nm thick particles were obtained from self-seeding of CsgB polymers. Mix fibers which are similar to self-seeded CsgA fibers are shown in Figure 36C.

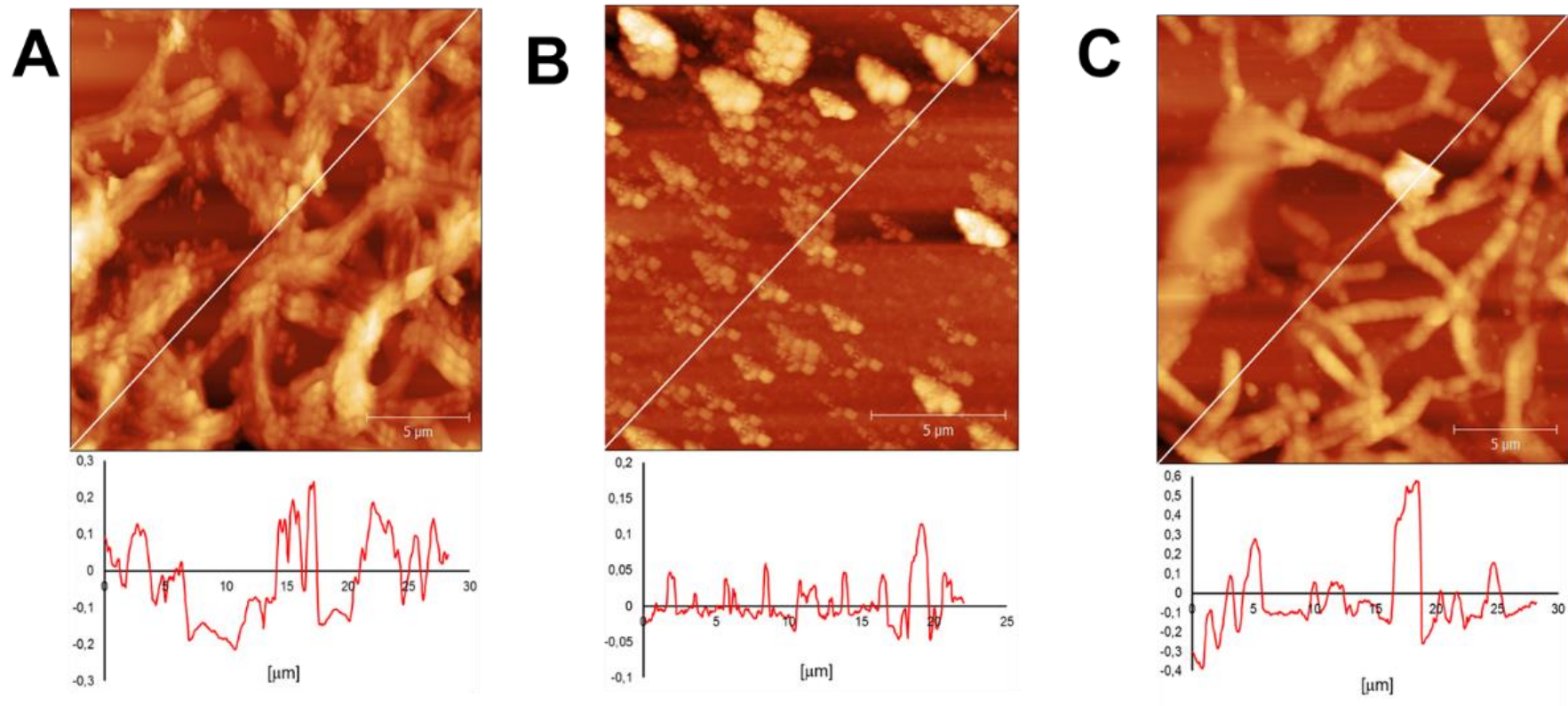


Figure 36- After protein deposition and overnight measurements sensors were examined with AFM. Fibers formed by CsgA polymers and fresh CsgA shown in A), CsgB polymers and fresh CsgB in B) and cross-seeding of CsgA with fresh CsgB in C).

3.7 Fluorescent Analysis of CsgA & CsgB

Intrinsic fluorescent property of amyloids has been known before but detailed experimental analysis was not recorded.[117] In this study, it was showed quantitatively and qualitatively. After purification and buffer exchange, samples were incubated at room temperature. By using fluorescent spectrophotometer, emission spectra of samples were measured. Bright field and fluorescent microscope images were taken; also, blue, green and red images were taken by the aid of different filters. Images and fluorescent spectra of 9 days aged samples are demonstrated in Figure 37. Samples were excited at different wavelength and emission spectra were measured. Measurements were also performed for the mix sample. To identify excitation wavelength UV-Vis measurements were performed. 9 days aged CsgA fibers were excited at 338, 375 and 550 nm while CsgB fibers were excited at 339, 413 and 550 nm. Mix sample was excited at 340, 414 nm and 550 nm. Excitation at 340 nm gave the highest signal. According to fluorescent microscope images intensity was decreasing blue to red. In addition, differently aged samples 18 hours and 23 days were examined under fluorescent microscope and fluorescent images are shown in Figure 38-39.

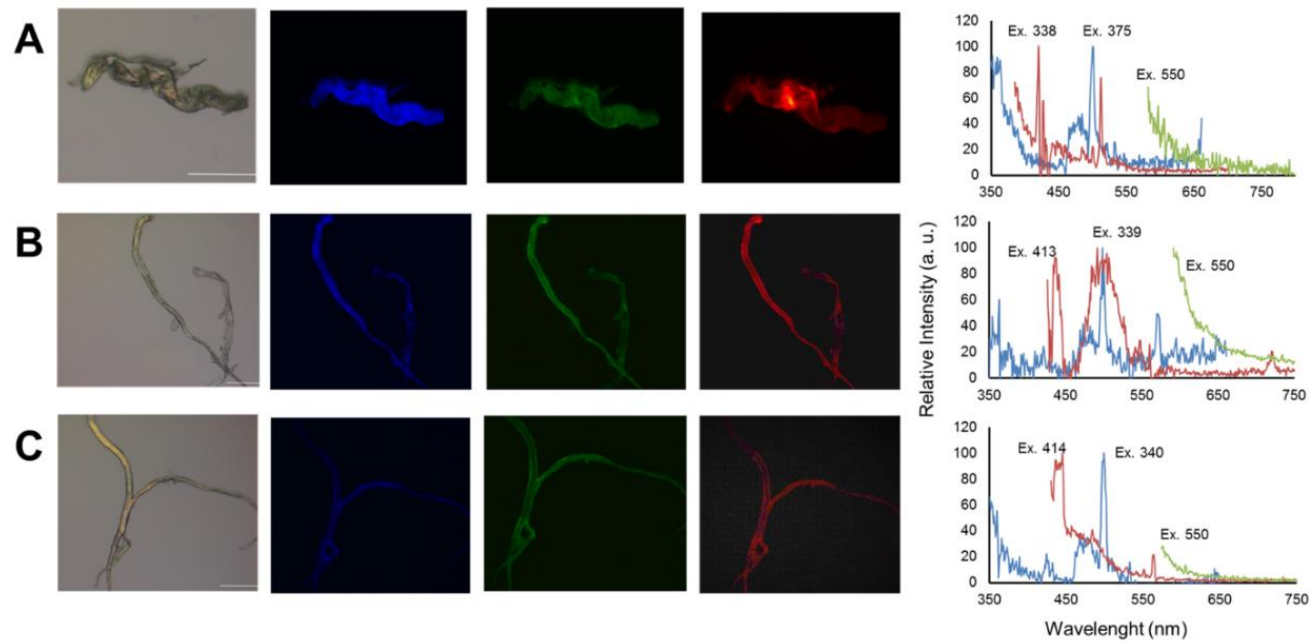


Figure 37- Fluorescent analysis of 9 days aged samples. Bright field images and blue, green, red fibers that were imaged by using different filters of fluorescent microscope are shown. Color intensity was decreasing blue to red but brightness of the images were adjusted to show clearly. Images of CsgA fibers and emission spectra that was recorded by exciting at 338, 375 and 550 nm are demonstrated in A), CsgB fibers images and emission spectra that was recorded by exciting at 339, 413 and 550 nm are shown in B), fluorescent images and emission spectra of mix sample are demonstrated in C). Mix sample was excited at 340, 414 and 550 nm to measure emission spectra. Lines represent

100

μM .

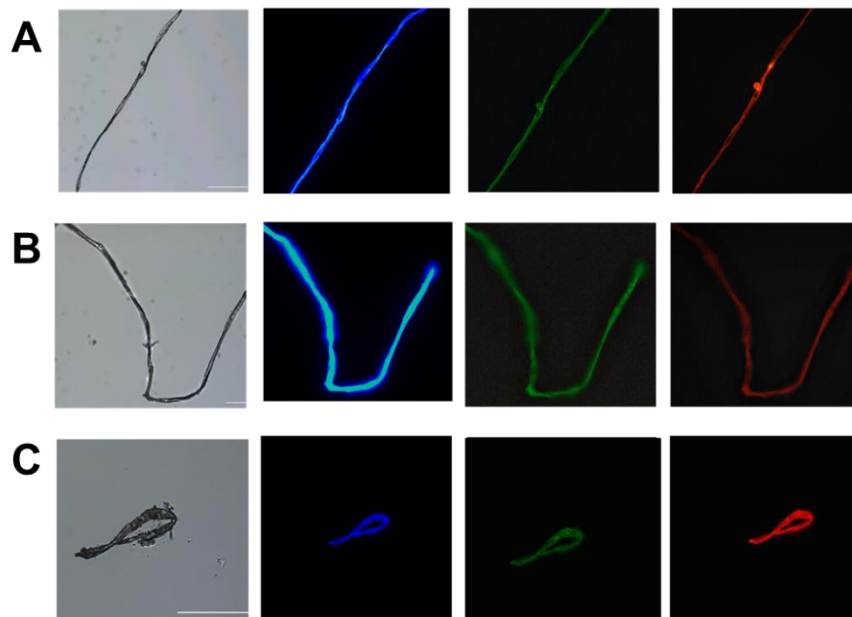


Figure 38- 18 hours aged samples were examined under fluorescent microscope. Bright field images were given as the first image and images of CsgA in A), CsgB in B) and mix sample images are placed in C). Lines represent 100 μ M.

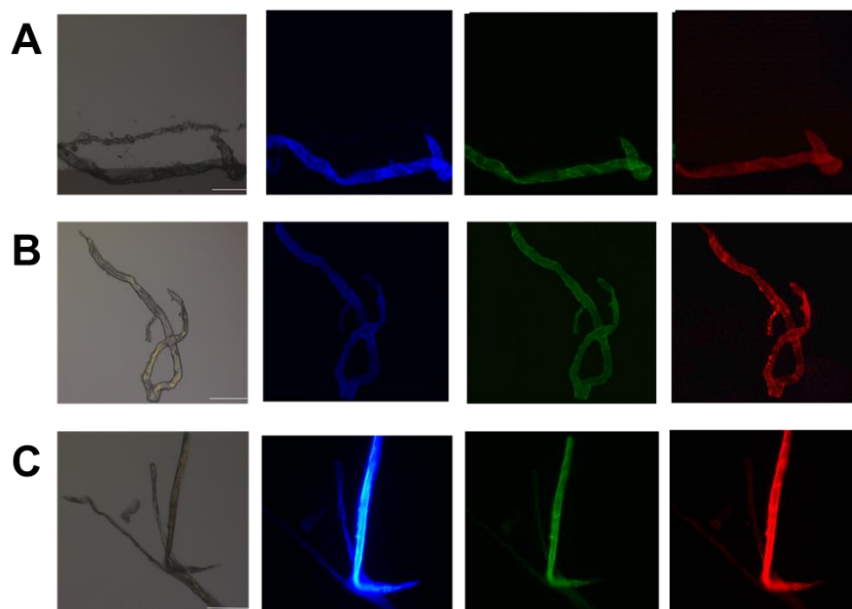


Figure 39- Bright field and fluorescent images of 23 days aged samples. CsgA fibers are demonstrated in A), CsgB fibers in B) and mix samples in C). Lines represent 100 μ M.

Moreover, to proof fluorescent shift came from proteins not result in protein-PBS interactions aged CsgA fibers were precipitated by centrifuging at max speed. Then, dissolved in chloroform. Broad emission spectra were recorded (Figure 40 A). Also, dissolved samples in chloroform were examined with electron microscope and dense fibrillar structures were observed (Figure 40 B). Hence it could be concluded that they are optically active and assemble formation change the optical properties.

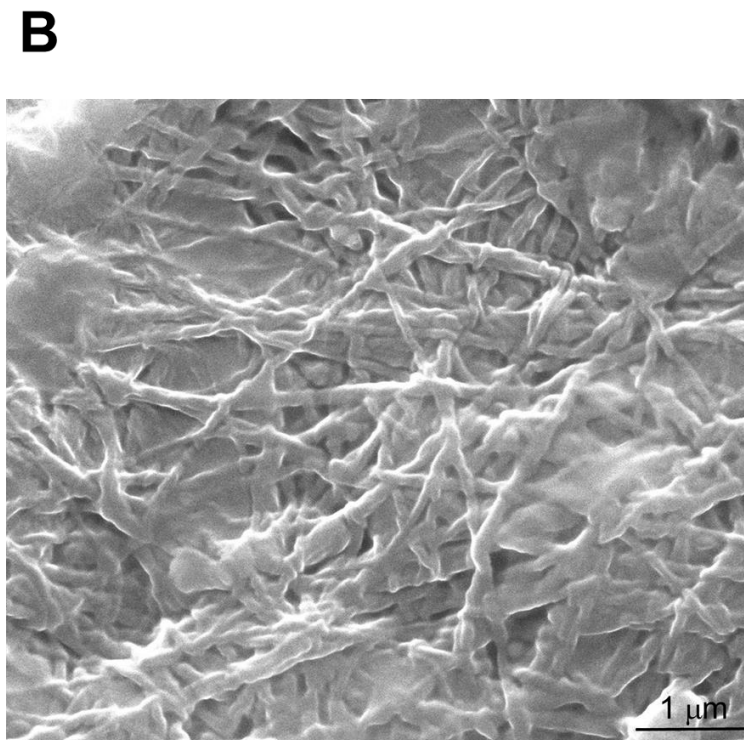
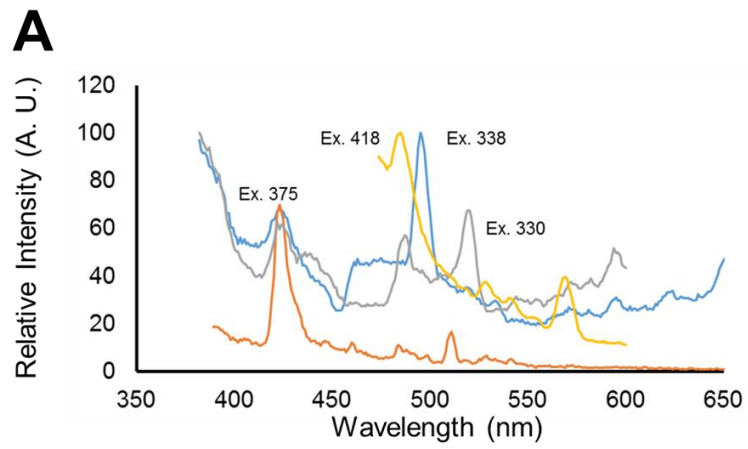


Figure 40- After precipitation, CsgA fibers were dissolved in chloroform. Excited at different wavelengths (330, 338, 375 and 418 nm) in order to measure emission spectra. Emission spectra is shown in A) and dense fiber network was observed with SEM in B).

3.8 Kinetic Analysis of CsgA & CsgB

Curli are surface adhesive proteins that enable to attach to surfaces for the biofilm development, as described above in detail.[133] This adherence property make them useful for materials science and biomedical applications, etc. Hence, in this study their binding affinity to the some materials were determined. In this case, gold, silica and hydroxyapatite coated QCM crystals were used. Because they are widely used in biomedical applications such as tissue engineering, drug delivery, etc.[134-140]

Purified proteins in PBS environment were incubated at room temperature to induce fiber formation. After purification CsgA and CsgB proteins were also mixed in equimolar concentration and incubated for kinetic analysis. Interactions of these three samples with the three different materials (gold, silica and hydroxyapatite) were analyzed and three replicates of each case were performed. Experimental design was similar with the fiber formation assay but in this case samples were not incubated on QCM sensors for overnight because polymerized proteins were deposited on the sensor surface. Protein fibers were diluted and flowed through the system with increasing concentration like fiber formation assays. Each protein addition steps followed by PBS washing steps and PBS flushes were continued until signals reach the equilibrium to obtain absolute shift of adherent proteins. Frequency and dissipation changes were measured during protein addition processes and washing steps. Step by step changes were recorded. Binding equilibrium constant and binding free energy of proteins were calculated from those shifts.

Firstly, polymerized samples were deposited on the gold QCM crystals and frequency change vs. concentration graph is shown in Figure 41. Protein addition

with increasing concentration cause regular increment in frequency change. In this case, deposition of CsgB proteins caused the highest frequency change while CsgA caused the lowest change even though they had similar concentration. In natural system, CsgA and CsgB interact with each other and *in vitro* they could still bind to each other which was demonstrated with fiber formation assay. This dual interactions decreased the binding capability of CsgB fibers. CsgA might block suitable sites of CsgB for gold surface interactions.

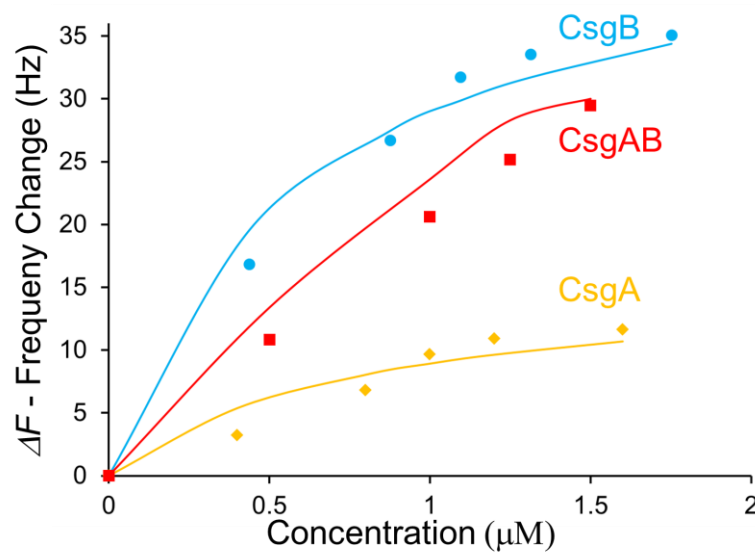


Figure 41- Frequency change vs. concentration graph of polymerized CsgA, CsgB and mix sample on the gold QCM sensors. Proteins were diluted and added to the system with increasing concentrations. Dots represent the protein addition points and higher concentration caused the higher changes in all cases. CsgA deposition on the gold sensor resulted in lower frequency change than other samples. CsgB addition caused the highest change. Interaction of CsgA and CsgB changed the binding property and binding sites of CsgB might be covered by CsgA.

In the second case, protein polymers were deposited on the silica coated QCM sensors. Experimental design was same with the previous case. PBS washing steps were applied after protein additions. Frequency change versus concentration plot is demonstrated in Figure 42. In this case, samples had closer changes in frequency but changes that caused from the mix sample were little bit higher than others. CsgA had the lowest changes like the previous case. If the two graphs were compared with each other, it could be concluded that CsgA had the higher affinity to silica than gold while CsgB had lower affinity to silica than gold.

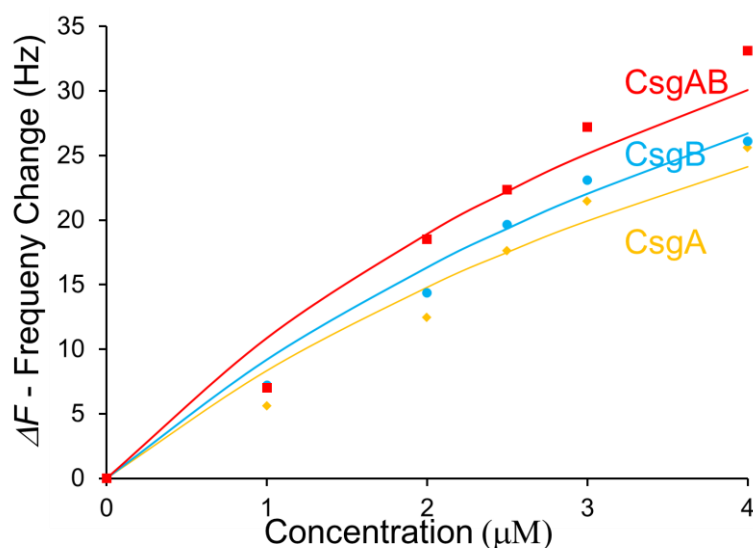


Figure 42- Frequency change vs. concentration plot of polymerized CsgA, CsgB and mix sample on silica coated QCM sensor. In this case, highest change came from the deposition of mix sample and binding capability of CsgB fibers was higher than CsgA fibers. Proteins were flowed through the system with diluted concentrations and dots represent the addition points.

In the last case, hydroxyapatite coated QCM crystals were used to analyze binding capability of the purified proteins and plot is indicated in Figure 43.

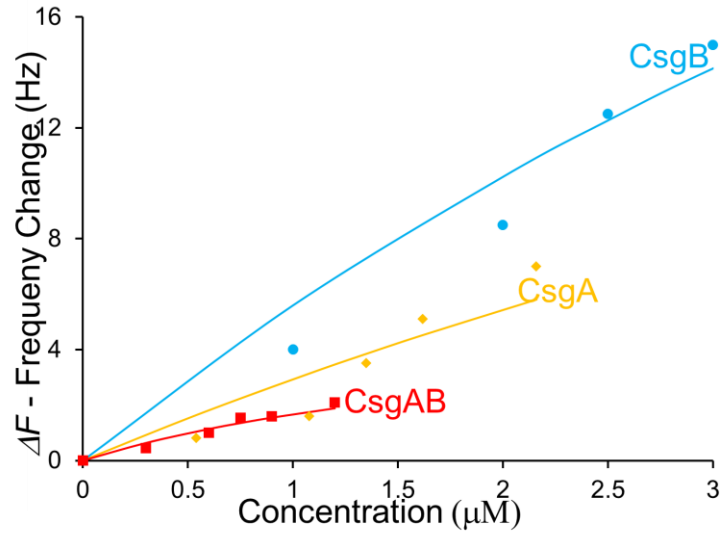


Figure 43- Frequency change vs. concentration graph of CsgA, CsgB and mix of CsgA-CsgB fibers on hydroxyapatite QCM sensors. Smaller changes were obtained by binding the polymers to hydroxyapatite sensors. Binding of CsgB fibers to HAP surface caused the highest changes while lowest shifts were obtained by the mix sample.

Frequency changes were recorded to determine tendency of the protein fibers to the some special materials. Concentrations, frequency changes and maximum frequency values were placed in to the following equations to determine binding ability of the proteins to the substrate. Furthermore, binding ability to the 3 different materials were summarized with bar graphs in Figure 44. According to the graphs, CsgA and CsgB fibers had the highest binding capability to gold surfaces and binding ability of all samples to the HAP and silica surfaces were similar. Yet, mix sample had little higher affinity to HAP coated materials than others.

$$\Delta f \times \left(\frac{1}{K_{eq}} + C \right) = f_{max} \times C$$

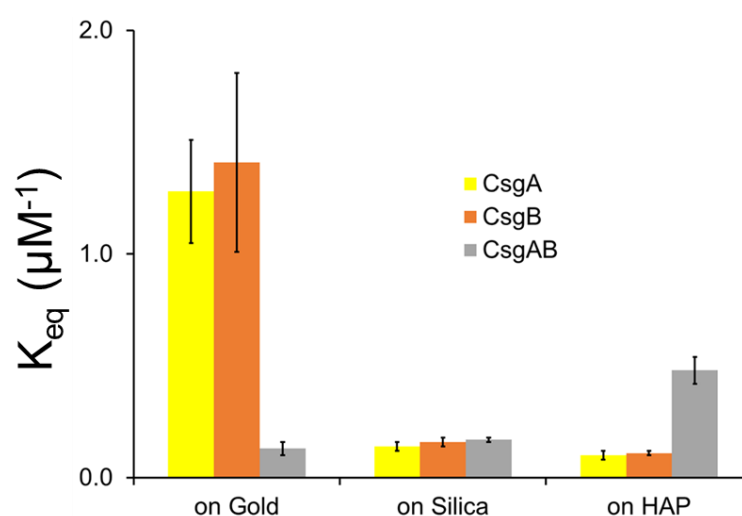


Figure 44- Binding equilibrium constants of polymerized proteins and polymerized mix samples on gold, silica and hydroxyapatite (HAP) coated sensors. CsgA and CsgB higher tendency of binding to the gold surfaces. Mix sample had higher affinity for binding to HAP surface than others.

Then, binding free energies were calculated with the following formula and calculated values are represented in Figure 45. All samples had closer free energy because they share similar route to the attachment on surfaces during assembly.

$$\Delta G = -RT \ln (K_{eq})$$

The results implied that all of the biofilm protein fibers have the highest affinity towards gold surface. This is not surprising as the protein fibers, similar to many other amyloid structures are very hydrophobic and un-functionalized gold surface is also hydrophobic. On the other hand both silica and HAP surfaces are hydrophilic and they have a hydration layer around them. Eventually all of the proteins showed a degree of binding. On gold surface, there is a very interesting observation was made. According to this CsgA and CsgB fibers have a high affinity

to gold surface whereas the mixture of CsgA and CsgB monomers made fibers have a lower affinity. It is known that CsgB and CsgA are interacting strongly during the fiber formations. CsgA and CsgB monomers made fibers may have a higher number of available sites for surface attachment; however these available sites might be blocked during the formation of the composite nanofibers. This finding is also supported with the case for HAP. In that case the composite nanofiber has a higher affinity to the HAP surface which is obviously a hydrophilic surface. This result reveals that composite nanofibers displays higher numbers of hydrophilic groups for surface binding whereas displayed hydrophobic sites are limited.

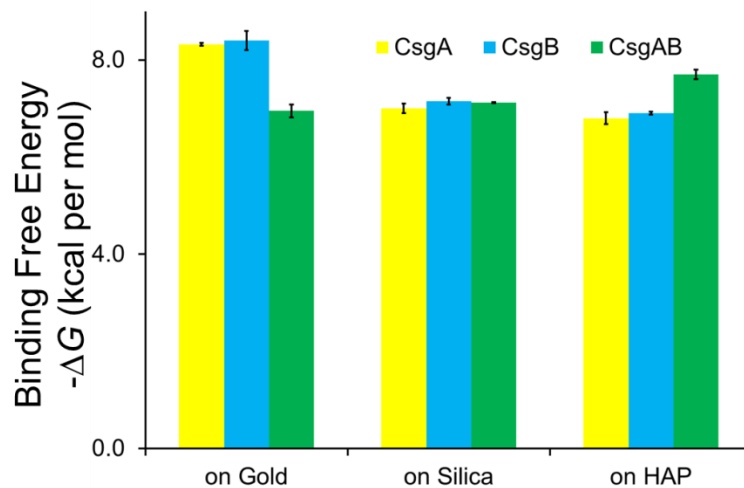


Figure 45- Binding free energy of aged CsgA, CsgB and mix sample on gold, silica and hydroxyapatite (HAP) surfaces were calculated. All of them had closer binding free energy. It might be cause from same assembly route of the samples.

Binding free energies were also calculated for each case. These results showed that the binding energies are in the same magnitude for all of the nanofibers on all of the surfaces. This is an indication for all cases that the route of the assembly on various solid surfaces of various biofilm protein nanofibers can be similar.

CHAPTER 4

CONCLUSION AND FUTURE PERSPECTIVES

In this study, major and minor curli subunits were proposed as functional biomaterials. Fibers with various shape and size properties were produced from freshly purified CsgA and CsgB proteins. Also, their structures were dominated by β sheet. With these properties they are good candidates for materials science applications.

Firstly, CsgA and CsgB proteins were overexpressed and purified by the aid of affinity tag. ThT assay was performed to demonstrate their amyloidogenic characteristic. Also, secondary structural elements were analyzed with CD and ratio of secondary structure elements were determined. Hence, β sheet dominated characteristic which is another general property of amyloids were proved.

In addition, fiber formation of freshly purified proteins were analyzed with QCM-D. With self-seeding and cross-seeding strategies fibers were produced on the gold coated QCM-D sensor. Fibers on the sensor surface were observed with SEM and AFM. According to microscope images, the order of protein addition affected the final shape of the assembled structure. Sphere like structures were grown by CsgB proteins and size of the spheres were increasing with fresh CsgB addition. Also, in self-seeding CsgA case long and branched fibers were produced and fiber elongation could be achieved with addition of fresh CsgA. If fresh CsgA added upon polymerized CsgB, small and adjoint spheres were produced. In contrast, CsgA lose the ability to binding of CsgB nucleator protein if it was polymerized, *in vitro*.

Furthermore, intrinsic fluorescent properties of the purified proteins were analyzed in detail. By using fluorescent microscope, blue, green and red images were

taken from aged CsgA, CsgB and also mix sample. In addition, fluorescent properties of the aged fibrils were demonstrated with fluorescent spectroscopy, quantitatively. Aged protein samples were excited at different wavelength in order to measure emission spectra.

Finally, binding affinity of the aged samples to gold, silica and hydroxyapatite materials were analyzed with QCM-D. CsgA and CsgB had the highest binding capability to gold surfaces. Also, all samples had similar affinity to silica and hydroxyapatite surfaces but mix of CsgA and CsgB had slightly higher affinity to hydroxyapatite materials.

To sum up, CsgA and CsgB proteins have potential to use in materials science with varied purposes. Highly ordered and stable polymeric structures were formed by CsgA and CsgB proteins. Also, they could be used for intracellular imaging or bio-LED applications due to their intrinsic fluorescence property. They are good candidate for nanomaterial synthesis or nanowire application because of their self-assembly capability. Protein engineering techniques enable to modify them easily and fused with other enzymes or proteins in order to use in biomedicine applications. All of them contribute to make them new generation functional biomaterials and they could be used in different field such as materials science, bioengineering application, tissue engineering, nanotechnology, etc.

BIBLIOGRAPHY

- [1] M. Luckey, *Membrane structural biology: with biochemical and biophysical foundations*: Cambridge University Press, 2014.
- [2] P. Nissen, J. Hansen, N. Ban, P. B. Moore, and T. A. Steitz, "The structural basis of ribosome activity in peptide bond synthesis," *Science*, vol. 289, pp. 920-930, 2000.
- [3] B. Zhang and T. R. Cech, "Peptide bond formation by in vitro selected ribozymes," *Nature*, vol. 390, pp. 96-100, 1997.
- [4] C. Blake, M. Geisow, S. Oatley, B. Rerat, and C. Rerat, "Structure of prealbumin: secondary, tertiary and quaternary interactions determined by Fourier refinement at 1.8 Å," *Journal of molecular biology*, vol. 121, pp. 339-356, 1978.
- [5] J. C. Cambier, W. Bedzyk, K. Campbell, N. Chien, J. Friedrich, A. Harwood, *et al.*, "The B-Cell Antigen Receptor: Structure and Function of Primary, Secondary, Tertiary and Quaternary Components," *Immunological reviews*, vol. 132, pp. 85-106, 1993.
- [6] W. Kabsch and C. Sander, "Dictionary of protein secondary structure: pattern recognition of hydrogen-bonded and geometrical features," *Biopolymers*, vol. 22, pp. 2577-2637, 1983.
- [7] I. K. McDonald and J. M. Thornton, "Satisfying hydrogen bonding potential in proteins," *Journal of molecular biology*, vol. 238, pp. 777-793, 1994.
- [8] S. N. Vinogradov and R. H. Linnell, *Hydrogen bonding*: Van Nostrand Reinhold New York, 1971.

- [9] J. A. Whitney, M. Gomez, D. Sheff, T. E. Kreis, and I. Mellman, "Cytoplasmic coat proteins involved in endosome function," *Cell*, vol. 83, pp. 703-713, 1995.
- [10] J. S. Bonifacino and B. S. Glick, "The mechanisms of vesicle budding and fusion," *cell*, vol. 116, pp. 153-166, 2004.
- [11] O. Céspedes and S. Ueno, "Effects of radio frequency magnetic fields on iron release from cage proteins," *Bioelectromagnetics*, vol. 30, pp. 336-342, 2009.
- [12] T. Douglas and V. T. Stark, "Nanophase cobalt oxyhydroxide mineral synthesized within the protein cage of ferritin," *Inorganic Chemistry*, vol. 39, pp. 1828-1830, 2000.
- [13] W. Lucas, "Viral capsids and envelopes: Structure and function," *eLS*, 2010.
- [14] T. Douglas and M. Young, "Virus particles as templates for materials synthesis," *Advanced Materials*, vol. 11, pp. 679-681, 1999.
- [15] N. M. Molino and S.-W. Wang, "Caged protein nanoparticles for drug delivery," *Current opinion in biotechnology*, vol. 28, pp. 75-82, 2014.
- [16] J. A. Speir, S. Munshi, G. Wang, T. S. Baker, and J. E. Johnson, "Structures of the native and swollen forms of cowpea chlorotic mottle virus determined by X-ray crystallography and cryo-electron microscopy," *Structure*, vol. 3, pp. 63-78, 1995.
- [17] T. Douglas and M. Young, "Host-guest encapsulation of materials by assembled virus protein cages," *Nature*, vol. 393, pp. 152-155, 1998.
- [18] E. Eanes and G. Glenner, "X-ray diffraction studies on amyloid filaments," *Journal of Histochemistry & Cytochemistry*, vol. 16, pp. 673-677, 1968.
- [19] R. N. Rambaran and L. C. Serpell, "Amyloid fibrils," *Prion*, 2008.

- [20] M. Pepys, "Pathogenesis, diagnosis and treatment of systemic amyloidosis," *Philosophical Transactions of the Royal Society B: Biological Sciences*, vol. 356, pp. 203-211, 2001.
- [21] M. Sunde, L. C. Serpell, M. Bartlam, P. E. Fraser, M. B. Pepys, and C. C. Blake, "Common core structure of amyloid fibrils by synchrotron X-ray diffraction," *Journal of molecular biology*, vol. 273, pp. 729-739, 1997.
- [22] L.-F. Lue, Y.-M. Kuo, A. E. Roher, L. Brachova, Y. Shen, L. Sue, *et al.*, "Soluble amyloid β peptide concentration as a predictor of synaptic change in Alzheimer's disease," *The American journal of pathology*, vol. 155, pp. 853-862, 1999.
- [23] J. Wang, D. W. Dickson, J. Q. Trojanowski, and V. M.-Y. Lee, "The levels of soluble versus insoluble brain A β distinguish Alzheimer's disease from normal and pathologic aging," *Experimental neurology*, vol. 158, pp. 328-337, 1999.
- [24] S. B. Prusiner, "Novel proteinaceous infectious particles cause scrapie," *Science*, vol. 216, pp. 136-144, 1982.
- [25] B. Caughey, K. Brown, G. Raymond, G. Katzenstein, and W. Thresher, "Binding of the protease-sensitive form of PrP (prion protein) to sulfated glycosaminoglycan and congo red [corrected]," *Journal of virology*, vol. 68, pp. 2135-2141, 1994.
- [26] K.-M. Pan, M. Baldwin, J. Nguyen, M. Gasset, A. Serban, D. Groth, *et al.*, "Conversion of alpha-helices into beta-sheets features in the formation of the scrapie prion proteins," *Proceedings of the National Academy of Sciences*, vol. 90, pp. 10962-10966, 1993.

- [27] C. M. Eakin, A. J. Berman, and A. D. Miranker, "A native to amyloidogenic transition regulated by a backbone trigger," *Nature structural & molecular biology*, vol. 13, pp. 202-208, 2006.
- [28] V. J. McParland, N. M. Kad, A. P. Kalverda, A. Brown, P. Kirwin-Jones, M. G. Hunter, *et al.*, "Partially unfolded states of β 2-microglobulin and amyloid formation in vitro," *Biochemistry*, vol. 39, pp. 8735-8746, 2000.
- [29] J. H. Come, P. E. Fraser, and P. T. Lansbury, "A kinetic model for amyloid formation in the prion diseases: importance of seeding," *Proceedings of the National Academy of Sciences*, vol. 90, pp. 5959-5963, 1993.
- [30] A. Lomakin, D. S. Chung, G. B. Benedek, D. A. Kirschner, and D. B. Teplow, "On the nucleation and growth of amyloid beta-protein fibrils: detection of nuclei and quantitation of rate constants," *Proceedings of the National Academy of Sciences*, vol. 93, pp. 1125-1129, 1996.
- [31] D. M. Walsh, D. M. Hartley, Y. Kusumoto, Y. Fezoui, M. M. Condron, A. Lomakin, *et al.*, "Amyloid β -protein fibrillogenesis Structure and biological activity of protofibrillar intermediates," *Journal of Biological Chemistry*, vol. 274, pp. 25945-25952, 1999.
- [32] A. Geddes, K. Parker, E. Atkins, and E. Beighton, "'Cross- β ' conformation in proteins," *Journal of molecular biology*, vol. 32, pp. 343-358, 1968.
- [33] O. S. Makin, E. Atkins, P. Sikorski, J. Johansson, and L. C. Serpell, "Molecular basis for amyloid fibril formation and stability," *Proceedings of the National Academy of Sciences of the United States of America*, vol. 102, pp. 315-320, 2005.

- [34] O. S. Makin and L. C. Serpell, "Structures for amyloid fibrils," *Febs Journal*, vol. 272, pp. 5950-5961, 2005.
- [35] R. Nelson and D. Eisenberg, "Recent atomic models of amyloid fibril structure," *Current opinion in structural biology*, vol. 16, pp. 260-265, 2006.
- [36] M. R. Sawaya, S. Sambashivan, R. Nelson, M. I. Ivanova, S. A. Sievers, M. I. Apostol, *et al.*, "Atomic structures of amyloid cross- β spines reveal varied steric zippers," *Nature*, vol. 447, pp. 453-457, 2007.
- [37] A. Naito, M. Kamihira, R. Inoue, and H. Saitô, "Structural diversity of amyloid fibril formed in human calcitonin as revealed by site-directed ^{13}C solid-state NMR spectroscopy," *Magnetic Resonance in Chemistry*, vol. 42, pp. 247-257, 2004.
- [38] R. M. Donlan, "Biofilms: microbial life on surfaces," *Emerg Infect Dis*, vol. 8, 2002.
- [39] J. W. Costerton, P. S. Stewart, and E. P. Greenberg, "Bacterial biofilms: a common cause of persistent infections," *Science*, vol. 284, pp. 1318-1322, 1999.
- [40] T. Rasamiravaka, Q. Labtani, P. Duez, and M. El Jaziri, "The formation of biofilms by *Pseudomonas aeruginosa*: a review of the natural and synthetic compounds interfering with control mechanisms," *BioMed research international*, vol. 2015, 2015.
- [41] H.-C. Flemming and J. Wingender, "The biofilm matrix," *Nature Reviews Microbiology*, vol. 8, pp. 623-633, 2010.
- [42] I. W. Sutherland, "Biofilm exopolysaccharides: a strong and sticky framework," *Microbiology*, vol. 147, pp. 3-9, 2001.

- [43] H. Levine, "Thioflavine T interaction with synthetic Alzheimer's disease β -amyloid peptides: Detection of amyloid aggregation in solution," *Protein Science*, vol. 2, pp. 404-410, 1993.
- [44] H. LeVine, "[18] Quantification of β -sheet amyloid fibril structures with thioflavin T," *Methods in enzymology*, vol. 309, pp. 274-284, 1999.
- [45] A. Lorenzo and B. A. Yankner, "Beta-amyloid neurotoxicity requires fibril formation and is inhibited by congo red," *Proceedings of the National Academy of Sciences*, vol. 91, pp. 12243-12247, 1994.
- [46] H. Puchtler, F. Sweat, and M. Levine, "On the binding of Congo red by amyloid," *Journal of Histochemistry & Cytochemistry*, vol. 10, pp. 355-364, 1962.
- [47] T. Seviour, S. H. Hansen, L. Yang, Y. H. Yau, V. B. Wang, M. R. Stenvang, *et al.*, "Functional amyloids keep quorum-sensing molecules in check," *Journal of Biological Chemistry*, vol. 290, pp. 6457-6469, 2015.
- [48] T. P. Knowles, A. W. Fitzpatrick, S. Meehan, H. R. Mott, M. Vendruscolo, C. M. Dobson, *et al.*, "Role of intermolecular forces in defining material properties of protein nanofibrils," *Science*, vol. 318, pp. 1900-1903, 2007.
- [49] G. Zeng, B. S. Vad, M. S. Dueholm, G. Christiansen, M. Nilsson, T. Tolker-Nielsen, *et al.*, "Functional bacterial amyloid increases *Pseudomonas* biofilm hydrophobicity and stiffness," *Frontiers in microbiology*, vol. 6, 2015.
- [50] T. Scheibel, R. Parthasarathy, G. Sawicki, X.-M. Lin, H. Jaeger, and S. L. Lindquist, "Conducting nanowires built by controlled self-assembly of amyloid fibers and selective metal deposition," *Proceedings of the National Academy of Sciences*, vol. 100, pp. 4527-4532, 2003.

- [51] J. P. Mackay, J. M. Matthews, R. D. Winefield, L. G. Mackay, R. G. Haverkamp, and M. D. Templeton, "The hydrophobin EAS is largely unstructured in solution and functions by forming amyloid-like structures," *Structure*, vol. 9, pp. 83-91, 2001.
- [52] V. Novitskaya, O. V. Bocharova, I. Bronstein, and I. V. Baskakov, "Amyloid fibrils of mammalian prion protein are highly toxic to cultured cells and primary neurons," *Journal of Biological Chemistry*, vol. 281, pp. 13828-13836, 2006.
- [53] M. S. Dueholm, S. V. Petersen, M. Sønderkær, P. Larsen, G. Christiansen, K. L. Hein, *et al.*, "Functional amyloid in *Pseudomonas*," *Molecular microbiology*, vol. 77, pp. 1009-1020, 2010.
- [54] M. S. Dueholm, M. T. Søndergaard, M. Nilsson, G. Christiansen, A. Stensballe, M. T. Overgaard, *et al.*, "Expression of Fap amyloids in *Pseudomonas aeruginosa*, *P. fluorescens*, and *P. putida* results in aggregation and increased biofilm formation," *Microbiologyopen*, vol. 2, pp. 365-382, 2013.
- [55] M. S. Dueholm, D. Otzen, and P. H. Nielsen, "Evolutionary insight into the functional amyloids of the pseudomonads," *PloS one*, vol. 8, p. e76630, 2013.
- [56] A. Taglialegna, S. Navarro, S. Ventura, J. A. Garnett, S. Matthews, J. R. Penades, *et al.*, "Staphylococcal Bap proteins build amyloid scaffold biofilm matrices in response to environmental signals," *PLoS Pathog*, vol. 12, p. e1005711, 2016.
- [57] I. Lasa and J. R. Penadés, "Bap: a family of surface proteins involved in biofilm formation," *Research in microbiology*, vol. 157, pp. 99-107, 2006.

- [58] C. Cucarella, M. Á. Tormo, C. Ubeda, M. P. Trotonda, M. Monzón, C. Peris, *et al.*, "Role of biofilm-associated protein bap in the pathogenesis of bovine *Staphylococcus aureus*," *Infection and immunity*, vol. 72, pp. 2177-2185, 2004.
- [59] J. Valle, C. Latasa, C. Gil, A. Toledo-Arana, C. Solano, J. R. Penadés, *et al.*, "Bap, a biofilm matrix protein of *Staphylococcus aureus* prevents cellular internalization through binding to GP96 host receptor," *PLoS pathogens*, vol. 8, p. e1002843, 2012.
- [60] K. Schwartz, A. K. Syed, R. E. Stephenson, A. H. Rickard, and B. R. Boles, "Functional amyloids composed of phenol soluble modulins stabilize *Staphylococcus aureus* biofilms," *PLoS Pathog*, vol. 8, p. e1002744, 2012.
- [61] A. Marchand, J. Verdon, C. Lacombe, S. Crapart, Y. Hechard, and J. Berjeaud, "Anti-*Legionella* activity of staphylococcal hemolytic peptides," *Peptides*, vol. 32, pp. 845-851, 2011.
- [62] S. Y. Queck, B. A. Khan, R. Wang, T.-H. L. Bach, D. Kretschmer, L. Chen, *et al.*, "Mobile genetic element-encoded cytolysin connects virulence to methicillin resistance in MRSA," *PLoS Pathog*, vol. 5, p. e1000533, 2009.
- [63] C. J. Alteri, J. Xicohténcatl-Cortes, S. Hess, G. Caballero-Olín, J. A. Girón, and R. L. Friedman, "*Mycobacterium tuberculosis* produces pili during human infection," *Proceedings of the National Academy of Sciences*, vol. 104, pp. 5145-5150, 2007.
- [64] S. Ramsugit, S. Guma, B. Pillay, P. Jain, M. H. Larsen, S. Danaviah, *et al.*, "Pili contribute to biofilm formation in vitro in *Mycobacterium tuberculosis*," *Antonie Van Leeuwenhoek*, vol. 104, pp. 725-735, 2013.

- [65] S. S. Branda, F. Chu, D. B. Kearns, R. Losick, and R. Kolter, "A major protein component of the *Bacillus subtilis* biofilm matrix," *Molecular microbiology*, vol. 59, pp. 1229-1238, 2006.
- [66] D. Romero, C. Aguilar, R. Losick, and R. Kolter, "Amyloid fibers provide structural integrity to *Bacillus subtilis* biofilms," *Proceedings of the National Academy of Sciences*, vol. 107, pp. 2230-2234, 2010.
- [67] R. Terra, N. R. Stanley-Wall, G. Cao, and B. A. Lazazzera, "Identification of *Bacillus subtilis* SipW as a bifunctional signal peptidase that controls surface-adhered biofilm formation," *Journal of bacteriology*, vol. 194, pp. 2781-2790, 2012.
- [68] M. Serrano, R. Zilhão, E. Ricca, A. J. Ozin, C. P. Moran, and A. O. Henriques, "A *Bacillus subtilis* secreted protein with a role in endospore coat assembly and function," *Journal of bacteriology*, vol. 181, pp. 3632-3643, 1999.
- [69] D. Romero, H. Vlamakis, R. Losick, and R. Kolter, "Functional analysis of the accessory protein TapA in *Bacillus subtilis* amyloid fiber assembly," *Journal of bacteriology*, vol. 196, pp. 1505-1513, 2014.
- [70] M. r. Hammar, A. Arnqvist, Z. Bian, A. Olsén, and S. Normark, "Expression of two *csg* operons is required for production of fibronectin-and Congo red-binding curli polymers in *Escherichia coli* K-12," *Molecular microbiology*, vol. 18, pp. 661-670, 1995.
- [71] U. Römling, Z. Bian, M. Hammar, W. D. Sierralta, and S. Normark, "Curli fibers are highly conserved between *Salmonella typhimurium* and

- Escherichia coli with respect to operon structure and regulation," *Journal of bacteriology*, vol. 180, pp. 722-731, 1998.
- [72] M. Landreh, A. Rising, J. Presto, H. Jörnvall, and J. Johansson, "Specific chaperones and regulatory domains in control of amyloid formation," *Journal of Biological Chemistry*, vol. 290, pp. 26430-26436, 2015.
- [73] M. Hammar, Z. Bian, and S. Normark, "Nucleator-dependent intercellular assembly of adhesive curli organelles in Escherichia coli," *Proceedings of the National Academy of Sciences*, vol. 93, pp. 6562-6566, 1996.
- [74] A. P. White, S. K. Collinson, P. A. Banser, D. L. Gibson, M. Paetzel, N. C. Strynadka, *et al.*, "Structure and characterization of AgfB from Salmonella enteritidis thin aggregative fimbriae," *Journal of molecular biology*, vol. 311, pp. 735-749, 2001.
- [75] U. Römling, M. Rohde, A. Olsen, S. Normark, and J. Reinköster, "AgfD, the checkpoint of multicellular and aggregative behaviour in Salmonella typhimurium regulates at least two independent pathways," *Molecular microbiology*, vol. 36, pp. 10-23, 2000.
- [76] M. R. Chapman, L. S. Robinson, J. S. Pinkner, R. Roth, J. Heuser, M. Hammar, *et al.*, "Role of Escherichia coli curli operons in directing amyloid fiber formation," *Science*, vol. 295, pp. 851-855, 2002.
- [77] H. Loferer, M. Hammar, and S. Normark, "Availability of the fibre subunit CsgA and the nucleator protein CsgB during assembly of fibronectin-binding curli is limited by the intracellular concentration of the novel lipoprotein CsgG," *Molecular microbiology*, vol. 26, pp. 11-23, 1997.

- [78] D. G. Thanassi and S. J. Hultgren, "Assembly of complex organelles: pilus biogenesis in gram-negative bacteria as a model system," *Methods*, vol. 20, pp. 111-126, 2000.
- [79] D. G. Thanassi, E. T. Saulino, M.-J. Lombardo, R. Roth, J. Heuser, and S. J. Hultgren, "The PapC usher forms an oligomeric channel: implications for pilus biogenesis across the outer membrane," *Proceedings of the National Academy of Sciences*, vol. 95, pp. 3146-3151, 1998.
- [80] L. S. Robinson, E. M. Ashman, S. J. Hultgren, and M. R. Chapman, "Secretion of curli fibre subunits is mediated by the outer membrane-localized CsgG protein," *Molecular microbiology*, vol. 59, pp. 870-881, 2006.
- [81] A. Arnqvist, A. Olsén, J. Pfeifer, D. G. Russell, and S. Normark, "The Crl protein activates cryptic genes for curli formation and fibronectin binding in *Escherichia coli* HB101," *Molecular microbiology*, vol. 6, pp. 2443-2452, 1992.
- [82] Z. Bian, A. Brauner, Y. Li, and S. Normark, "Expression of and Cytokine Activation by *Eschevichia coli* Curi Fibers in Human Sepsis," *Journal of Infectious Diseases*, vol. 181, pp. 602-612, 2000.
- [83] U. Römling, W. D. Sierralta, K. Eriksson, and S. Normark, "Multicellular and aggregative behaviour of *Salmonella typhimurium* strains is controlled by mutations in the *agfD* promoter," *Molecular microbiology*, vol. 28, pp. 249-264, 1998.
- [84] U. Gerstel and U. Römling, "Oxygen tension and nutrient starvation are major signals that regulate *agfD* promoter activity and expression of the

- multicellular morphotype in *Salmonella typhimurium*," *Environmental microbiology*, vol. 3, pp. 638-648, 2001.
- [85] A. Arnqvist, A. Olsén, and S. Normark, " σ S-dependent growth-phase induction of the *csgBA* promoter in *Escherichia coli* can be achieved in vivo by σ 70 in the absence of the nucleoid-associated protein H-NS," *Molecular microbiology*, vol. 13, pp. 1021-1032, 1994.
- [86] A. Olsén, A. Arnqvist, M. Hammar, S. Sukupolvi, and S. Normark, "The RpoS sigma factor relieves H-NS-mediated transcriptional repression of *csgA*, the subunit gene of fibronectin-binding curli in *Escherichia coli*," *Molecular microbiology*, vol. 7, pp. 523-536, 1993.
- [87] A. Bougdour, C. Lelong, and J. Geiselmann, "Crl, a low temperature-induced protein in *Escherichia coli* that binds directly to the stationary phase σ subunit of RNA polymerase," *Journal of Biological Chemistry*, vol. 279, pp. 19540-19550, 2004.
- [88] P. K. Brown, C. M. Dozois, C. A. Nickerson, A. Zuppardo, J. Terlonge, and R. Curtiss, "MlrA, a novel regulator of curli (AgF) and extracellular matrix synthesis by *Escherichia coli* and *Salmonella enterica* serovar Typhimurium," *Molecular microbiology*, vol. 41, pp. 349-363, 2001.
- [89] L. A. Pratt and T. J. Silhavy, "Crl stimulates RpoS activity during stationary phase," *Molecular microbiology*, vol. 29, pp. 1225-1236, 1998.
- [90] L. A. Pratt, W. Hsing, K. E. Gibson, and T. J. Silhavy, "From acids to *osmZ*: multiple factors influence synthesis of the OmpF and OmpC porins in *Escherichia coli*," *Molecular microbiology*, vol. 20, pp. 911-917, 1996.

- [91] D. L. Hung, T. L. Raivio, C. H. Jones, T. J. Silhavy, and S. J. Hultgren, "Cpx signaling pathway monitors biogenesis and affects assembly and expression of P pili," *The EMBO journal*, vol. 20, pp. 1508-1518, 2001.
- [92] C. Prigent-Combaret, E. Brombacher, O. Vidal, A. Ambert, P. Lejeune, P. Landini, *et al.*, "Complex regulatory network controls initial adhesion and biofilm formation in *Escherichia coli* via regulation of the *thecsgD* gene," *Journal of bacteriology*, vol. 183, pp. 7213-7223, 2001.
- [93] N. Ruiz and T. J. Silhavy, "Sensing external stress: watchdogs of the *Escherichia coli* cell envelope," *Current opinion in microbiology*, vol. 8, pp. 122-126, 2005.
- [94] C. Dorel, O. Vidal, C. Prigent-Combaret, I. Vallet, and P. Lejeune, "Involvement of the Cpx signal transduction pathway of *E. coli* in biofilm formation," *FEMS microbiology letters*, vol. 178, pp. 169-175, 1999.
- [95] L. Ferrières and D. J. Clarke, "The RcsC sensor kinase is required for normal biofilm formation in *Escherichia coli* K-12 and controls the expression of a regulon in response to growth on a solid surface," *Molecular microbiology*, vol. 50, pp. 1665-1682, 2003.
- [96] N. Majdalani and S. Gottesman, "The Rcs phosphorelay: a complex signal transduction system*," *Annu. Rev. Microbiol.*, vol. 59, pp. 379-405, 2005.
- [97] O. Vidal, R. Longin, C. Prigent-Combaret, C. Dorel, M. Hooreman, and P. Lejeune, "Isolation of an *Escherichia coli* K-12 mutant strain able to form biofilms on inert surfaces: involvement of a new *ompR* allele that increases curli expression," *Journal of bacteriology*, vol. 180, pp. 2442-2449, 1998.

- [98] T. Kikuchi, Y. Mizunoe, A. Takade, S. Naito, and S. i. Yoshida, "Curli fibers are required for development of biofilm architecture in Escherichia coli K-12 and enhance bacterial adherence to human uroepithelial cells," *Microbiology and immunology*, vol. 49, pp. 875-884, 2005.
- [99] A. Olsén, A. Jonsson, and S. Normark, "Fibronectin binding mediated by a novel class of surface organelles on Escherichia coli," 1989.
- [100] K. Lundmark, G. T. Westermark, A. Olsén, and P. Westermark, "Protein fibrils in nature can enhance amyloid protein A amyloidosis in mice: Cross-seeding as a disease mechanism," *Proceedings of the National Academy of Sciences*, vol. 102, pp. 6098-6102, 2005.
- [101] J. D. Barak, L. Gorski, P. Naraghi-Arani, and A. O. Charkowski, "Salmonella enterica virulence genes are required for bacterial attachment to plant tissue," *Applied and Environmental Microbiology*, vol. 71, pp. 5685-5691, 2005.
- [102] A. G. Torres, C. Jeter, W. Langley, and A. G. Matthyse, "Differential binding of Escherichia coli O157: H7 to alfalfa, human epithelial cells, and plastic is mediated by a variety of surface structures," *Applied and environmental microbiology*, vol. 71, pp. 8008-8015, 2005.
- [103] X. Wang, D. R. Smith, J. W. Jones, and M. R. Chapman, "In vitro polymerization of a functional Escherichia coli amyloid protein," *Journal of Biological Chemistry*, vol. 282, pp. 3713-3719, 2007.
- [104] X. Wang, N. D. Hammer, and M. R. Chapman, "The molecular basis of functional bacterial amyloid polymerization and nucleation," *Journal of Biological Chemistry*, vol. 283, pp. 21530-21539, 2008.

- [105] X. Wang and M. R. Chapman, "Sequence determinants of bacterial amyloid formation," *Journal of molecular biology*, vol. 380, pp. 570-580, 2008.
- [106] P. Tian, W. Boomsma, Y. Wang, D. E. Otzen, M. H. Jensen, and K. Lindorff-Larsen, "Structure of a functional amyloid protein subunit computed using sequence variation," *Journal of the American Chemical Society*, vol. 137, pp. 22-25, 2014.
- [107] M. Perutz, J. Finch, J. Berriman, and A. Lesk, "Amyloid fibers are water-filled nanotubes," *Proceedings of the National Academy of Sciences*, vol. 99, pp. 5591-5595, 2002.
- [108] A. Aggeli, M. Bell, N. Boden, J. Keen, P. Knowles, T. McLeish, *et al.*, "Responsive gels formed by the spontaneous self-assembly of peptides into polymeric β -sheet tapes," 1997.
- [109] A. Aggeli, M. Bell, L. M. Carrick, C. W. Fishwick, R. Harding, P. J. Mawer, *et al.*, "pH as a trigger of peptide β -sheet self-assembly and reversible switching between nematic and isotropic phases," *Journal of the American Chemical Society*, vol. 125, pp. 9619-9628, 2003.
- [110] M. F. Gebbink, D. Claessen, B. Bouma, L. Dijkhuizen, and H. A. Wösten, "Amyloids—a functional coat for microorganisms," *Nature reviews microbiology*, vol. 3, pp. 333-341, 2005.
- [111] X. Zhao and S. Zhang, "Designer Self-Assembling Peptide Materials," *Macromolecular bioscience*, vol. 7, pp. 13-22, 2007.
- [112] D. Li, E. M. Jones, M. R. Sawaya, H. Furukawa, F. Luo, M. Ivanova, *et al.*, "Structure-based design of functional amyloid materials," *Journal of the American Chemical Society*, vol. 136, pp. 18044-18051, 2014.

- [113] T. P. Knowles, T. W. Oppenheim, A. K. Buell, D. Y. Chirgadze, and M. E. Welland, "Nanostructured films from hierarchical self-assembly of amyloidogenic proteins," *Nature nanotechnology*, vol. 5, pp. 204-207, 2010.
- [114] I. Cherny and E. Gazit, "Amyloids: not only pathological agents but also ordered nanomaterials," *Angewandte Chemie International Edition*, vol. 47, pp. 4062-4069, 2008.
- [115] W.-J. Chung, J.-W. Oh, K. Kwak, B. Y. Lee, J. Meyer, E. Wang, *et al.*, "Biomimetic self-templating supramolecular structures," *Nature*, vol. 478, pp. 364-368, 2011.
- [116] T. P. Knowles and M. J. Buehler, "Nanomechanics of functional and pathological amyloid materials," *Nature nanotechnology*, vol. 6, pp. 469-479, 2011.
- [117] C. Zhong, T. Gurry, A. A. Cheng, J. Downey, Z. Deng, C. M. Stultz, *et al.*, "Strong underwater adhesives made by self-assembling multi-protein nanofibres," *Nature nanotechnology*, vol. 9, pp. 858-866, 2014.
- [118] Z. Botyanszki, P. K. R. Tay, P. Q. Nguyen, M. G. Nussbaumer, and N. S. Joshi, "Engineered catalytic biofilms: Site-specific enzyme immobilization onto E. coli curli nanofibers," *Biotechnology and bioengineering*, vol. 112, pp. 2016-2024, 2015.
- [119] A. Y. Chen, Z. Deng, A. N. Billings, U. O. Seker, M. Y. Lu, R. J. Citorik, *et al.*, "Synthesis and patterning of tunable multiscale materials with engineered cells," *Nature materials*, vol. 13, pp. 515-523, 2014.

- [120] P. Q. Nguyen, Z. Botyanszki, P. K. R. Tay, and N. S. Joshi, "Programmable biofilm-based materials from engineered curli nanofibres," *Nature communications*, vol. 5, 2014.
- [121] Y. Zhou, D. R. Smith, D. A. Hufnagel, and M. R. Chapman, "Experimental manipulation of the microbial functional amyloid called curli," in *Bacterial cell surfaces*, ed: Springer, 2013, pp. 53-75.
- [122] A. Micsonai, F. Wien, L. Kernya, Y.-H. Lee, Y. Goto, M. Réfrégiers, *et al.*, "Accurate secondary structure prediction and fold recognition for circular dichroism spectroscopy," *Proceedings of the National Academy of Sciences*, vol. 112, pp. E3095-E3103, 2015.
- [123] J. M. Walker, *The proteomics protocols handbook*: Springer, 2005.
- [124] N. D. Hammer, "Characterization of the curli nucleator CsgB," The University of Michigan, 2009.
- [125] M. S. Lord, C. Modin, M. Foss, M. Duch, A. Simmons, F. S. Pedersen, *et al.*, "Monitoring cell adhesion on tantalum and oxidised polystyrene using a quartz crystal microbalance with dissipation," *Biomaterials*, vol. 27, pp. 4529-4537, 2006.
- [126] C. Modin, A.-L. Stranne, M. Foss, M. Duch, J. Justesen, J. Chevallier, *et al.*, "QCM-D studies of attachment and differential spreading of pre-osteoblastic cells on Ta and Cr surfaces," *Biomaterials*, vol. 27, pp. 1346-1354, 2006.
- [127] E. Yuca, A. Y. Karatas, U. O. S. Seker, M. Gungormus, G. Dinler-Doganay, M. Sarikaya, *et al.*, "In vitro labeling of hydroxyapatite minerals by an engineered protein," *Biotechnology and bioengineering*, vol. 108, pp. 1021-1030, 2011.

- [128] M. Rodahl and B. Kasemo, "Frequency and dissipation-factor responses to localized liquid deposits on a QCM electrode," *Sensors and Actuators B: Chemical*, vol. 37, pp. 111-116, 1996.
- [129] A. Teo, S. Dimartino, S. J. Lee, K. K. Goh, J. Wen, I. Oey, *et al.*, "Interfacial structures of whey protein isolate (WPI) and lactoferrin on hydrophobic surfaces in a model system monitored by quartz crystal microbalance with dissipation (QCM-D) and their formation on nanoemulsions," *Food Hydrocolloids*, vol. 56, pp. 150-160, 2016.
- [130] R. H. Walters, K. H. Jacobson, J. A. Pedersen, and R. M. Murphy, "Elongation kinetics of polyglutamine peptide fibrils: a quartz crystal microbalance with dissipation study," *Journal of molecular biology*, vol. 421, pp. 329-347, 2012.
- [131] P. Goyal, P. V. Krasteva, N. Van Gerven, F. Gubellini, I. Van den Broeck, A. Trounopoulos-Tsailaki, *et al.*, "Structural and mechanistic insights into the bacterial amyloid secretion channel CsgG," *Nature*, vol. 516, pp. 250-253, 2014.
- [132] N. D. Hammer, J. C. Schmidt, and M. R. Chapman, "The curli nucleator protein, CsgB, contains an amyloidogenic domain that directs CsgA polymerization," *Proceedings of the National Academy of Sciences*, vol. 104, pp. 12494-12499, 2007.
- [133] C. Prigent-Combaret, G. Prensier, T. T. Le Thi, O. Vidal, P. Lejeune, and C. Dorel, "Developmental pathway for biofilm formation in curli-producing *Escherichia coli* strains: role of flagella, curli and colanic acid," *Environmental microbiology*, vol. 2, pp. 450-464, 2000.

- [134] A. J. de Kerchove and M. Elimelech, "Structural growth and viscoelastic properties of adsorbed alginate layers in monovalent and divalent salts," *Macromolecules*, vol. 39, pp. 6558-6564, 2006.
- [135] G. Lubarsky, M. Davidson, and R. Bradley, "Hydration–dehydration of adsorbed protein films studied by AFM and QCM-D," *Biosensors and Bioelectronics*, vol. 22, pp. 1275-1281, 2007.
- [136] E. Ostuni, L. Yan, and G. M. Whitesides, "The interaction of proteins and cells with self-assembled monolayers of alkanethiolates on gold and silver," *Colloids and Surfaces B: Biointerfaces*, vol. 15, pp. 3-30, 1999.
- [137] M. Vallet-Regí, "Ordered mesoporous materials in the context of drug delivery systems and bone tissue engineering," *Chemistry—A European Journal*, vol. 12, pp. 5934-5943, 2006.
- [138] G. Wei and P. X. Ma, "Structure and properties of nano-hydroxyapatite/polymer composite scaffolds for bone tissue engineering," *Biomaterials*, vol. 25, pp. 4749-4757, 2004.
- [139] Q. Wei, T. Becherer, S. Angioletti-Uberti, J. Dzubiella, C. Wischke, A. T. Neffe, *et al.*, "Protein interactions with polymer coatings and biomaterials," *Angewandte Chemie International Edition*, vol. 53, pp. 8004-8031, 2014.
- [140] H. Yoshimoto, Y. Shin, H. Terai, and J. Vacanti, "A biodegradable nanofiber scaffold by electrospinning and its potential for bone tissue engineering," *Biomaterials*, vol. 24, pp. 2077-2082, 2003.